Naval Research Laboratory
Washington, DC 20375-5320

NRL/MR/6793--92-7161

Final Report—The NRL Modified Betatron Accelerator Program

C. A. KAPETANAKOS
L. K. LEN
T. SMITH
S. J. MARSH
P. LOSCHIALPO
D. DIALETIS
J. MATHEW

Beam Physics Branch
Plasma Physics Division

December 31, 1992

REPORT DOCUMENTATION PAGE

Form Approved
OMB No. 0704-0188

1. AGENCY USE ONLY (*Leave Blank*)	2. REPORT DATE	3. REPORT TYPE AND DATES COVERED
	December 31, 1992	Final

4. TITLE AND SUBTITLE

Final Report—The NRL Modified Betatron Accelerator Program

5. FUNDING NUMBERS

WU - 1485
WU - 2835

6. AUTHOR(S)

C. A. Kapetanakos, L. K. Len,* T. Smith,* S. J. Marsh,† P. Loschialpo,
D. Dialetis,** and J. Mathew

7. PERFORMING ORGANIZATION NAME(S) AND ADDRESS(ES)

Naval Research Laboratory
Washington, DC 20375-5320

8. PERFORMING ORGANIZATION REPORT NUMBER

NRL/MR/6793—92-7161

9. SPONSORING/MONITORING AGENCY NAME(S) AND ADDRESS(ES)

SPAWAR
Washington, DC 20363

ONR
Arlington, VA 22217

10. SPONSORING/MONITORING AGENCY REPORT NUMBER

11. SUPPLEMENTARY NOTES

This report is supported by ONR and SPAWAR.
*FM Technologies, Inc., Fairfax, VA 22032
†SFA Inc., Landover, MD 20785
**Science Applications International Corp., 170 Goodridge Drive, McLean, VA 22102

12a. DISTRIBUTION/AVAILABILITY STATEMENT

Approved for public release; distribution is unlimited.

12b. DISTRIBUTION CODE

13. ABSTRACT (*Maximum 200 words*)

This final report summarizes the highlights of the NRL modified betatron accelerator program and documents the status at its termination of July 17, 1992. A substantial fraction of the results in this report has not been published previously.

14. SUBJECT TERMS

Final report
Modified betatron accelerator

15. NUMBER OF PAGES

152

16. PRICE CODE

17. SECURITY CLASSIFICATION OF REPORT	18. SECURITY CLASSIFICATION OF THIS PAGE	19. SECURITY CLASSIFICATION OF ABSTRACT	20. LIMITATION OF ABSTRACT
UNCLASSIFIED	UNCLASSIFIED	UNCLASSIFIED	SAR

Table of Contents

FINAL REPORT—THE NRL MODIFIED BETATRON ACCELERATOR PROGRAM

I. Introduction

This final report summarizes important experimental results from the NRL modified betatron program and documents its status at its termination on July 17, 1992. The objective of this program was to study the critical physics issues of the concept and to accelerate a 1 kA electron ring to 20 MeV with subsequent extraction of the ring. Critical physics issues associated with the concept are self field effects, image forces at the walls of the vacuum chamber, ring equilibrium, ring stability during acceleration, beam injection and finally extraction.

At the time of its termination the trapped current in the NRL device was in excess of 1 kA and the electron energy, as inferred from the main x-ray peak, above 20 MeV. Even more importantly, the NRL research effort furnished valuable information on the various critical physics issues of the concept. Twelve years ago i.e., at the commencement of the modified betatron program very little was known about the physics of high current, recirculating accelerators. Today, there is a solid, well documented, although incomplete data base.

During its life span, the NRL program addressed both theoretically and experimentally several important physical processes associated with the high current circular accelerators. Currently, the majority of these processes is reasonably well understood. However, there are some experimental observations, such as the toroidal distribution of the beam losses when the twelve resonant coils are activated, which, as of today, remain without a complete explanation. In addition, a critical physics issue, the extraction of the beam, has been addressed experimentally only temporarily and its data base is very limited.

Manuscript approved November 5, 1992.

Our experimental effort to develop a beam extraction scheme from the modified betatron accelerator proceeded at slower than expected pace, mainly because the technical approach had to be modified a few months before the termination of the program. In 1988, an extraction technique was reported by the NRL research staff that is easily realizable and has the potential to lead to high extraction efficiency. The hardware for this mainline extraction approach was designed and fabricated. However, it was never installed in the experiment because it requires a beam with low transverse velocity, since the aperture of the agitator is small. There is evidence that the beam in the NRL device has substantial transverse velocity caused by magnetic field disturbances. As a result of this difficulty, we had to pursue some alternate extraction approaches that do not require beams with low transverse velocity.

The alternate beam extraction approaches had to be terminated prematurely with the shutdown of the program. Still, these incomplete beam extraction studies have furnished some very interesting data on the toroidal beam loss distribution and the dependence of the beam loss rate on the amplitude and risetime of the current pulse that powers the twelve kicker coils. These results are discussed in Section IVe.

Although the conception and subsequent development of the modified betatron accelerator was motivated by defense oriented applications, it is likely that this device will be useful in some areas of civilian economy. As a result of its compactness, light weight and high-current carrying capability, the modified betatron can generate very intense electron beam that can provide high dose rates at reduced unit irradiation cost.

In this report, we have compiled several publications written by the NRL-MBA re-

search staff, which cover the highlights of the experimental effort. In addition, we have included recent unpublished experimental results. The bulk of the theoretical work is not included. This work is adequately documented in the published literature[1]. The Appendix provides a list of all the publications, both theoretical and experimental, written by the NRL research staff on the MBA and other similar accelerators.

II. Historical Background

The modified betatron accelerator was the major component of the Advanced Accelerator Program (AAP) that formally started in FY 81. However, preliminary work on the modified betatron concept[2] was done before FY 81. At its commencement, the AAP was a Special Focus Program (later it was renamed Accelerated Research Initiative) and it was jointly supported by ONR and by in-house funds.

During FY 81 the modified betatron concept went through intensive theoretical evaluation. The objective of this evaluation was to assess the viability of the modified betatron as a high current accelerator and to derive a set of scaling laws that can be used in the design of the device.

The extensive theoretical and numerical studies were reviewed by the Modified Betatron Review Panel that was convened at NRL by Dr. T. Coffey on November 19 and 20, 1981. The panel made several recommendations. Probably the most important was the conceptual design of a proof-of-principle experiment. A key excerpt from the Panel's report.

> **As a general remark, the panel was impressed by the very high quality of the NRL presentations and technical programs. The technical progress during the past 11 months has been substantial in all areas, and provides a strong basis for expecting continued steady progress in the equilibrium, stability, injection and extraction properties of the modified betatron. While virtually all aspects of the high current modified betatron provide a very difficult technical challenge, it is the**

strong recommendation of the panel that NRL proceed immediately with the conceptual design of a proof-of-principle experiment. The conceptual design should be completed no later than November 1982, with construction project approval to follow a design review at that time.

During the concept evaluation phase, it was brought to our attention that Donald Kerst[3] in the U.S.A. and John Lawson[3] in England have added weak toroidal fields to conventional betatrons[4] to increase their current carrying capabilities. However, these quick experiments produced inconclusive results. In addition, in 1968 a USA patent was obtained by P.J. Gratreau[5] for a betatron with a toroidal magnetic field and a radial electric field for deflecting the injected beam. The importance of the space charge effects is not addressed in Gratreau's patent. These effects have been included in an unpublished work by A.G. Bonch-Osmolovsky.[6]

A device similar to the modified betatron is the plasma betatron. In the modified betatron the high current circulating beam is generated by an external source and space charge effects and images on the wall play a dominant role in the confinement of the electron ring. In contrast, in plasma betatrons the circulating electrons are plasma runaway electrons and are produced from the plasma that fills the vacuum chamber. The space charge of the electron beam is neutralized by the background ions and thus does not play any role in the confinement of the beam. Suggested initially by Budker[7], the plasma betatron was investigated by several groups including J.C. Linhart[8] and C. Maisonnier, Reynold and Skarsgard[9] and more recently by Rostoker's group[10]. The MBA Preliminary

Design Review Panel met at NRL on December 7 and 8, 1982 and made several general and detailed recommendations and approved the construction of the apparatus as presented by the NRL research staff, but under two constraints.

At the time of the review the objective of the modified betatron program was the formation of multikiloampere (5-10 kA) electron rings with subsequent acceleration from 3 to 50 MeV and the study of critical physics issues of such rings.

The most pressing Physics issues of the modified betatron concept, at the time, were:

1. Is it possible to efficiently inject a high current beam in a toroidal device?

2. Do equilibrium states exist for a high current ring?

3. Are these equilibrium states stable on the time scale of interest?

4. Is the orbit displacement resulting from the energy mismatch manageable?

Since a high quality 3 MeV, 10 - 20 kA injector accelerator required substantial development and could not be obtained at an affordable cost and in order to reduce the risk and the cost of the program, the initial objective was modified on March 29, 1983. According to the reformulated program the development of the modified betatron should proceed in two phases, with the following objectives:

Phase A: Formation of 1 kA, 1 MeV electron ring in a modified betatron configuration using an inexpensive vacuum chamber. Without accelerating the ring (DC ring experiment) study the critical physics issues associated with the concept, such as injection, equilibrium and short time stability.

Phase B: After the installation of a new vacuum chamber accelerate the ring to 20 MeV and study the critical physics issues associated with the acceleration, such as long time ring stability and radiation losses.

The construction and assembly of the accelerator was completed on February 11, 1985, and the testing of the various power systems on April 20, 1985. The first injection experiments started on April 22, 1985.

Phase A, i.e., the DC ring experiment was completed on July 29, 1986. Specifically, electron rings were formed with circulating current between 1 - 3 kA. The DC ring experiment has provided some valuable information on the physics of high current rings.[11, 12]

In relation to Phase B, a substantial effort was made in the development of an inexpensive vacuum chamber. The novel chamber made of epoxy reinforced graphite fibers was installed in the experiment in the Summer of 1987. Attempts to accelerate the beam over a one year period, i.e., between the summer of 1987 and the summer of 1988, were unsuccessful. The ring confinement time was limited to a few microseconds, too short for imparting any measurable energy to the beam.

In August, 1988, the decision was made to proceed immediately with the design, fabrication and installation of strong focusing windings[13, 14] in the device. At the time, Omicron Technology, Inc. had completed the design of a strong focusing system for the MBA. However, the cost (~ $ 700k) and the time requested by the contractor to complete the fabrication and installation of the strong focusing system (~ 40 weeks) were

not compatible with the budget and time schedule of the MBA. Thus, we decided to develop the strong focusing system in-house. The installation of the stellarator windings was completed in December 1988. The next few months were invested to assemble the power supply for the SF windings and to carry out experiments with runaway electrons. The experiments with an injected beam were initiated in April 1989. Within approximately two months, i.e., when the Technical Review Panel convened at NRL by Dr. S. Ossakow on June 27-28, 1989, to review the program, the trapped current was $\sim$ 0.5 kA and the beam energy[15] $\sim$ 10 MeV.

The Technical Review Panel made the recommendation that NRL management continues the MBA program for two more years, as it becomes apparent from the following excerpt taken from the Panel's report.

> **The Committee was impressed by the significant technical progress made during the past several months with the addition of a helical strong focusing field in the NRL modified betatron experiment. Dr. Kapetanakos and the entire experimental team are to be commended for achieving the difficult milestone of 10 MeV at 0.5 kA. It is anticipated that the improved physics understanding associated with these experiments will be substantial.**
>
> **Needless to say, the recent experimental results had a favorable impact on the Committee's assessment. It is recommended that Laboratory management give high priority**

to continuation of the modified betatron program, at least through the concept demonstration phase (20 MeV at 1 kA, including extraction) over the next twenty-four months.

The spiky x-ray signals produced by the lost electrons in the NRL device could be explained either by the cyclotron resonances or the cyclotron instability.[15] However, measurements of the magnetic field components of the electromagnetic modes inside the toroidal chamber have shown[16] that the amplitude of these modes was too small to excite the cyclotron instability. Thus, the definite conclusion was reached that the cyclotron resonance was the dominant beam loss mechanism.

During the next several months that followed the June 1989 review a concerted effort was made to locate and eliminate the field disturbances that may excite the cyclotron resonances.[17] As a result of this effort and also by increasing the strong focusing and toroidal magnetic fields, the beam energy was raised above 20 MeV while the trapped current was in excess of 1 kA.

In late spring-early summer, 1991, while the beam dynamic stabilization experiments with twelve resonant coils were underway, we observed that the beam could be kicked out of the magnetic field of the device within a time interval that was comparable to the risetime of the current pulse that powered the resonant coils.[18, 19] Three current pulses with risetimes 12, 5 and 0.4 μsec were used. With the 12 μsec risetime current pulse the FWHM of the x-ray signal was reduced from approximately 900 μsec to only 8 μsec, i.e., by more than two orders of magnitude while its amplitude increased by a factor of thirty.

Extensive studies of the spatial distribution of beam losses when the resonant coils are energized with the 0.4 μsec current pulse have shown that the beam strikes the wall at six very well defined toroidal positions that are 60° apart. Rotation of the vacuum chamber and thus of the strong focusing windings that are attached to the chamber by 30° as well as an $\ell = 1$ small radial displacement of the chamber had no effect on the beam distribution.[19] However, in the absence of the strong focusing field when the resonant coils are energized, the experimental results show that the beam strikes the wall at a single toroidal position near $\theta = 70°$.

Although the fabrication of the hardware for the resonant extraction[20] approach that was the mainline extraction scheme for the NRL device was completed by the end of FY 91, the resonant extraction was never tested experimentally. The reason is that this extraction technique is based on a single agitator with a very small aperture. Therefore, it requires a beam with low transverse velocity. However, this was not the case in the NRL experiment. The amplitude of the various field imperfections never was reduced to a low enough level to make the transverse velocity of the beam compatible with the small aperture of the agitator. To avoid this difficulty we had to invent a new agitator with large aperture. Among the various kickers considered, magnetic cusps were found to be the most promising. Extensive numerical studies of several cusp configurations have shown that a single layer, 24.2 cm long cusp surrounded by a resistive shroud could provide sufficient displacement to the beam over a 20 nsec time period. Unfortunately such a cusp could not be fabricated on time and thus we had to proceed with an inferior agitator that is based on three double cusps that are located 120° apart in the toroidal direction. This agitating

system was fabricated in-house and tested in the experiment for a short period of time just before the termination of the MBA program. These incomplete results are discussed in Section IVe.

Table I lists most of the important dates in the history of the MBA program and Table II lists the names of the technical staff on November 15, 1991, i.e., the day NRL decided to terminate the MBA program.

Table I
MODIFIED BETATRON ACCELERATOR
IMPORTANT DATES

EVENT AND DATE	COMMENTS
Start Date: 1 October 1980.	
Concept Review: 19-20 Nov. 1981.	Modified Betatron Concept was reviewed by a national panel of experts at NRL.
Design Review: 7-8 Dec. 1982.	The design of the device was reviewed by a national panel of experts, which recommended construction of a proof-of-principle experiment.
Program Reformulation: 29 March 1983.	To reduce cost and risk program objectives were modified (from 10 kA, 50 MeV to 1 kA, 20 MeV).
Diagnostic Devel. - Workshop: 6-7 Oct. 1983.	Modified Betatron diagnostics were reviewed by a national group of experts.
Construction Completed: 11 Feb. 1985.	Construction and assembly of the accelerator was completed.
Testing Completed: April 1985.	All power systems in operation.
DC Ring Experiments Started: 22 April 1985.	First injection experiment.
DC Ring Experiments Completed: July 1986.	Interesting results were obtained, but were limited to a few microseconds.
ARI Termination: 30 Sep. 1986	

MODIFIED BETATRON ACCELERATOR
IMPORTANT DATES (Cont'd)

EVENT AND DATE	COMMENTS
Installation of strong focusing windings (SFW) completed: Dec 1988.	To reduce cost, the SFW were designed and fabriated in-house.
Commencement of experiments with SFW and injected beam: April 1989.	
First successful beam trapping exp: May 9, 1989.	
First successful acceleration: May 19, 1989.	By June, 1989, the trapped current was $\sim$ 0.5 kA and the beam energy $\sim$10 MeV.
Technical Review: 27-29 June 1989.	Progress was reviewed by a national panel of experts, which recommended that NRL management give high priority to the program.
Trapped current exceeds 1 kA and beam energy 20 MeV: June 1991.	

MODIFIED BETATRON ACCELERATOR
IMPORTANT DATES (Cont'd)

EVENT AND DATE	COMMENTS
Commencement of preliminary extraction experiments: Summer 1991.	Using twelve resonant kickers. Beam FWHM is comparable to risetime of the current pulse that drives the kickers.
CPB Accelerator Technology Review: 16-17 Oct., 1991.	Purpose of the review was to determine the strengths, potential shortcomings and weaponization potential of the various accelerator technologies.
NRL decided to terminate the MBA program before the end of FY 92: 15 Nov. 1991.	
The University of Crete (Greece) offers to buy the MBA intact: January 1992.	
MBA Program Terminated: 17 July 1992.	
NRL decided to loan the major components of the MBA to the University of Crete: Aug. 1992	

Table II

NRL MODIFIED BETATRON

RESEARCH STAFF

NOV. 15, 1991

C.A. Kapetanakos, P.I.

Experiment

L.K. Len (FMT)

T. Smith (FMT)

J. Mathew

P. Loschialpo

J.H. Chang

J. Golden (part-time) (BRA)

Consultant

D. Kerst (SFA)

Theory and Simulation

D. Dialetis(SAIC)

J. Marsh (SFA)

Engineering

K. Smith (SFA)

L. Seto (SFA)

Technicians

R. Covington (SFA)

D. Hardesty

S. Krafsig (SFA)

B. Lewis

III. Experimental Results Before the Installation of Strong Focusing (1985 - 1988).

This Section briefly describes the highlights of the experimental effort before the installation of the strong focusing windings. To make these results meaningful to the reader who is not familiar with the modified betatron, a short theoretical introduction has been included that addresses the transverse dynamics of the electron ring. Although the initial studies[21-23] of the transverse electron ring dynamics were based on the linearized equations of motion, here we have adopted a different approach that was developed later on and is based on the two constants of the motion.[24] The latter approach has several advantages; such as (i) It is easier and thus more transparent, (ii) allows the ring orbits to be determined over the entire minor cross section of the torus and not only near its minor axis, and (iii) the toroidal effects associated with the various fields can be included in a natural and straightforward way.

a. Beam Dynamics

Consider an electron ring inside a perfectly conducting torus of circular cross section as shown in Fig. 1. The center of the ring is located at a distance Δr, Δz from the minor axis of the torus. The kinetic energy γmc^2 of a reference electron that is located at the position r, z varies according to the equation

$$mc^2 \frac{d\gamma}{dt}(r,z) = -|e|\vec{v} \cdot \vec{E}(r,z), \tag{1}$$

where $\vec{E}$ (r,z) is the total electric field at the position of the reference electron. The electric field is related to the space charge Φ and magnetic vector potential $\vec{A}$ by

$$\vec{E}(r,z) = -\nabla\Phi - \frac{1}{c}\frac{\partial \vec{A}}{\partial t}, \tag{2}$$

where the total time derivative of Φ is given by

$$\frac{d\Phi}{dt} = \frac{\partial\Phi}{\partial t} + \vec{v}\cdot\nabla\Phi. \tag{3}$$

For the problem of interest, the accelerating and self fields vary slowly in time and thus it is a reasonable approximation to assume

$$\frac{\partial \vec{A}}{\partial t} = \frac{\partial\Phi}{\partial t} \approx 0. \tag{4}$$

Combining Eqs. (1) to (4), we obtain

$$\frac{d\gamma(r,z)}{dt} - \frac{|e|}{mc^2}\frac{d\Phi(r,z)}{dt} = 0$$

or, after integration

$$\gamma(r,z) - \frac{|e|}{mc^2}\Phi(r,z) = \text{constant}. \tag{5}$$

According to Eq. (5) the sum of the kinetic and potential energy of the reference electron is conserved. In a subsequent more accurate calculation[14] the approximation of Eq. (4) has been relaxed. It has been found that the partial time derivative of the potentials contributes a small term that is proportional to ν/γ^2.

Since the fields of the modified betatron configuration are independent of the toroidal angle θ, the canonical angular momentum P_θ is also a constant of the motion, i.e.,

$$P_\theta = \gamma m r v_\theta - \frac{|e|}{c} r A_\theta = \text{constant}, \tag{6}$$

where A_θ is the toroidal component of the total magnetic vector potential and v_θ is the toroidal velocity of the reference electron. Assuming that $v_\theta \approx v$ and eliminating γ from Eqs. (5) and (6), it is obtained

$$\left\{ \left[\frac{P_\theta}{mcr} + \frac{|e|}{mc^2} A_\theta(r,z) \right]^2 + 1 \right\}^{1/2} - \frac{|e|}{mc^2} \Phi(r,z) = \text{constant}, \tag{7a}$$

or, at the centroid of the ring

$$\left\{ \left[\frac{P_\theta}{mcR} + \frac{|e|}{mc^2} A_\theta(R,Z) \right]^2 + 1 \right\}^{1/2} - \frac{|e|}{mc^2} \Phi(R,Z) = \text{constant}. \tag{7b}$$

For very high energy beams, i.e., when $\gamma^2 \gg 1$, Eq. (7b) *is reduced to*

$$\frac{P_\theta}{mcR} + \frac{|e|}{mc^2} [A_\theta(R,Z) - \Phi(R,Z)] = \text{constant}. \tag{7c}.$$

This non-linear conservation law can furnish very useful information on the slow (drift) motion of the ring in the r,z plane, provided that the potentials A_θ and Φ at the center of the ring are known. It should be noticed that Eqs. (7) are independent of the toroidal magnetic field. This is a consequence of the assumption that $v \approx v_\theta$, i.e., to the omission of the fast motion of the electrons.

In Eq. (7), the total magnetic vector potential A_θ (r,z) is

$$A_\theta(r,z) = A_\theta^{ext}(r,z) + A_\theta^{self}(r,z),$$

where $A_\theta^{ext}(r,z)$ is the external and A_θ^{self}(r,z) is the self magnetic vector potential.

It is assumed that the betatron magnetic field is described by

$$A_\theta^{ext}(r,z) = B_{zo}\left[\left(\frac{r_o}{r}\right)^n\left(\frac{r}{2-n}\right) + \frac{r_o^2}{r}\frac{(1-n)}{(2-n)} + \frac{nz^2}{2r}\right], \tag{8}$$

where B_{zo} is the magnetic field at r=r_o, z=o and n is the external field index, i.e.,

$$n = -\frac{r_o}{B_{zo}}\left(\frac{\partial B_z}{\partial r}\right)_{r_o,\,o}.$$

For a cylindrical electron beam inside a straight, perfectly conducting cylindrical pipe, the self potentials can be computed exactly, even for large beam displacements from the minor axis. In the local coordinate system ρ,ϕ the self potentials inside the beam, i.e., for $|\vec{\rho}-\vec{\Delta}| \le r_b$ are given by

$$A_\theta^{self}(\rho,\phi) = -2|e|N_\ell\beta_\theta\left\{1/2 + \ell n\frac{a}{r_b} - \frac{[\rho^2+\Delta^2-2\rho\Delta cos(\phi-\alpha)]}{2r_b^2}\right.$$

$$\left. - \sum_{\ell=1}^{\infty}(\frac{\rho}{a})^\ell\left(\frac{\Delta}{a}\right)^\ell \ell^{-1}cos\,(\phi-a)\right\}, \tag{9a}$$

and

$$\Phi(\rho,\phi) = -2|e|N_\ell\left\{1/2 + \ell n\frac{a}{r_b} - \frac{[\rho^2+\Delta^2-2\rho\Delta cos(\phi-\alpha)]}{2r_b}\right.$$

$$\left. - \sum_{\ell=1}^{\infty}\left(\frac{\rho}{a}\right)^\ell\left(\frac{\Delta}{a}\right)^\ell \ell^{-1}cos(\phi-\alpha)\right\}. \tag{9b}$$

At the beam center, i.e., for $\rho = \Delta$ and $\phi = \alpha$, Eqs. (9a) and (9b) become

$$A_\theta^{self}(R,Z) = -2|e|N_\ell\beta_\theta\left\{1/2 + \ell n\frac{a}{r_b} + \ell n[1 - \frac{(R-r_o)^2+Z^2}{a^2}]\right\}, \tag{10a}$$

and

$$\Phi(R,Z) = -2|e|N_\ell \left\{ 1/2 + \ell n \frac{a}{r_b} + \ell n[1 - \frac{(R-r_o)^2 + Z^2}{a^2}] \right\}, \qquad (10b)$$

where N_ℓ is the linear electron density, r_b is the minor radius of the beam, a is the minor radius of the conducting pipe and $\beta_\theta = v_\theta/c$.

To obtain a better understanding of the potentials inside a perfectly conducting torus, we solved the differential equations for Φ and $\vec{A}$ to first order in the ratio a/R, but to any order[25] in the normalized displacement Δ/a. For a constant particle density n_o ring and to second order in Δ/a, the electrostatic potential at the center of the ring is given by

$$\Phi(R,Z) \approx -2N_\ell|e| \left[1/2 + \ell n(a/r_b) - \frac{(R-r_o)^2 + Z^2}{a^2} \right.$$

$$\left. - \frac{r_b^2}{8a^2} \frac{(R-r_o)}{R} \right], \qquad (11a)$$

and for J_θ= constant, the stream function ψ is

$$\psi(R,Z) \simeq -2N_\ell|e|R\beta_\theta \left[1/2 + \ell n(a/r_b) - \frac{(R-r_o)^2 + Z^2}{a^2} - \frac{r_b^2}{8a^2} \frac{(R-r_o)}{R} \right]. \qquad (11b)$$

Similarly, the image fields at the centroid of the ring are given by

$$E_r = -\frac{2|e|N_\ell}{a} \left[\frac{(R-r_o)}{a} + \left(\frac{a}{2R} \right) \ell n \frac{a}{r_b} + \frac{r_b^2}{8Ra} \right], \qquad (12a)$$

$$E_z = -\frac{2|e|N_\ell}{a} \left(\frac{Z}{a} \right), \qquad (12b)$$

$$B_r^{self} = -\frac{2|e|N_\ell \beta_\theta}{a}\left(\frac{Z}{a}\right), \tag{12c}$$

and

$$B_z^{self} = \frac{2|e|N_\ell \beta_\theta}{a}\left[\frac{(R-r_o)}{a} - \left(\frac{a}{2R}\right)\left(\ell n\frac{a}{r_b}+1\right) + \left(\frac{r_b^2}{8Ra}\right)\right], \qquad \text{for } J_\theta = \text{constant}. \tag{12d}$$

The toroidal term in Eq. (11) is very small for the parameters of interest and therefore the potentials at the center of the ring are approximately cylindrical.[24] For low energy rings the small toroidal term could be important and may have a profound effect on the shape of the orbits. However, when $\gamma \gg 1$, the potentials for n_o = constant and J_θ = constant become approximately equal and hence they do not contribute substantially in Eq. (7c).

Equation (7b) has been solved numerically, using the potentials of Eqs. (8) and (11). Typical macroscopic beam orbits in the r,z plane are shown in Fig. 2. The various parameters for those runs are listed in Table III. Only orbits that are at least one beam minor radius away from the wall are shown. Each orbit corresponds to a different value of the constant in Eq. (7b). A striking feature of the results is the sensitivity of the orbits to the value of the constant.

The number marked in every fourth orbit is equal to $10^4 \cdot$ [constant - < constant >], where the average value of the constant, i.e. < constant> for each run is shown at the top of the figure. For all the cases tested, less than 3% change in the constant of the motion was sufficient to generate orbits that extend over the entire minor cross-section of the torus. Orbits shown with solid lines correspond to a constant that is greater than

<constant> and those shown with a dashed line correspond to a constant that is less than <constant >. All the orbits close inside the vacuum chamber. However, a fraction of them lie inside the annular region that extends from the dotted-dashed line to the wall. This region has a width that is less than the beam radius and hence part of the beam will strike and wall.

In the general case, it is difficult to derive an explicit expression for the ring orbits in the transverse plane from Eqs. (7b) and (11). However, in the limit $\gamma^2 \gg 1, \beta_\theta/\beta \simeq 1$ and $\nu/\gamma \ll 1$, such an expression can be obtained near the minor axis of the torus.

Assuming that $\beta_\theta \simeq \beta$ and since $\gamma\beta \simeq \gamma$ - 1/2 γ, Eqs. (5) and (6) give

$$\frac{P_\theta}{mcR} + \frac{|e|}{mc^2} A_\theta^{ext} + \frac{|e|}{mc^2}(A_\theta^{self} - \Phi) + \frac{1}{2\gamma} = \text{constant} = G. \tag{13}$$

Expanding γ near r_o and using Eq. (5), it is obtained

$$\delta\gamma = \gamma - \gamma_o = \frac{|e|}{mc^2} \frac{\partial \Phi}{\partial r}\bigg|_{r_o} \Delta r + \frac{\partial G}{\partial r}\bigg|_{r_o} \Delta r,$$

where $\Delta r = R - r_o$. It is shown later on that $\frac{\partial G}{\partial r}\big|_{r_o} = 0$ and thus the above equation becomes

$$\delta\gamma = \gamma - \gamma_o = \frac{|e|}{mc^2} \frac{\partial \Phi}{\partial r}\bigg|_{r_o} \Delta r. \tag{14}$$

From Eqs. (11a) and (11b), the difference in the self potentials can be written as

$$A_\theta^{self} - \Phi = 2N_\ell |e| \left\{ 1/2 + \ell n \frac{a}{r_b} - \frac{(\Delta r^2 + \Delta z^2)}{a^2} - \frac{r_b^2}{8a^2} \frac{\Delta r}{R} \right\} (1 - \beta_\theta). \tag{15}$$

Since

$1-\beta_\theta \simeq 1-\beta \simeq 1/2\gamma^2$ and substituting $\delta\gamma$ from Eq. (14) in the expansion for $1/\gamma^2$, it is obtained

$$1-\beta_\theta \simeq \frac{1}{2\gamma_o^2}[1-\frac{2}{\gamma_o}\frac{|e|}{mc^2}\frac{\partial\Phi}{\partial r}\Big|_{r_o}\Delta r]. \tag{16}$$

Similarly, expanding $1/2\ \gamma$ as

$$\frac{1}{2\gamma} \approx \frac{1}{2\gamma_o} - \frac{|e|}{2\gamma_o^2 mc^2}\frac{\partial\Phi}{\partial r}\Big|_{r_o}\Delta r, \tag{17}$$

and 1/R as

$$\frac{1}{R} \approx (\frac{1}{r_o})[1-\frac{\Delta r}{r_o}+\left(\frac{\Delta r}{r_o}\right)^2], \tag{18}$$

and using a linear expression for the external vector potential

$$A_\theta^{ext} \simeq B_{zo}r_o[1+\frac{\Delta r^2(1-n)}{2r_o^2}+\frac{\Delta z^2 n}{2r_o^2}], \tag{19}$$

Eqs. (13) to (19) give

$$[\frac{P_\theta}{mcr_o}+\frac{\Omega_{zo}^{ext}r_o}{2c}(1-n)-\frac{\nu r_o^2}{\gamma_o^2 a^2}]\left(\frac{\Delta r}{r_o}\right)^2+[\frac{\Omega_{zo}^{ext}r_o}{2c}n-\frac{\nu r_o^2}{\gamma_o^2 a^2}]\left(\frac{\Delta z^2}{r_o}\right)$$

$$-[\frac{P_\theta}{mcr_o}+\frac{\nu}{2\gamma_o^2}(\frac{r_b^2}{2a^2}+\ell n\frac{a}{r_b})]\left(\frac{\Delta r}{r_o}\right)=\tilde{G}, \tag{20}$$

where $\Delta r = R-r_o, \Delta z = Z, \tilde{G}$ is a constant that is determined from the initial conditions and ν is the Budker's parameter.

Equation (20) describes the ring orbits near the minor axis, when $\gamma_o^2 \gg 1$. These orbits are centered around the minor axis of the torus when the coefficient of the $(\frac{\Delta r}{r_o})$ term is zero, i.e., when

$$\frac{P_{\theta o}}{mcr_o} + \frac{\nu}{2\gamma_o^2}\left[\left(\frac{r_b}{2a}\right)^2 + \ell n\frac{a}{r_b}\right] \approx \frac{\delta P_\theta}{mcr_o} \approx 0. \tag{21}$$

For $(r_b/a)^2 \ll 1$ and $\gamma_o \gg 1$, Eq. (21) predicts that $\frac{P_\theta}{mcr_o} \approx 0$. Therefore, the orbits are circular when the external field index is approximately equal to 0.5, in agreement with the computer results shown in Fig. 2.

Equation (20) can be writtern as:

$$q_1\left(\frac{\Delta r}{r_o}\right)^2 + q_2\left(\frac{\Delta z}{r_o}\right)^2 - (2\delta P_\theta/mr_o^2\Omega_{zo}^{ext})\left(\frac{\Delta r}{r_o}\right) = \frac{2\tilde{G}c}{\Omega_{zo}^{ext}r_o}, \tag{22}$$

where

$$q_1 = 1 - n - n^* + 2P_\theta/mr_o^2\Omega_{zo}^{ext}$$

$$q_2 = n - n^*,$$

and

$$n^* = 2\nu r_o c/\gamma_o^2 a^2 \Omega_{zo}^{ext}.$$

According to Eq. (22), the macroscopic beam orbits are stable, provided $q_1\ q_2 > 0$. Figure 3 shows the product $q_1 q_2$ as a function of n^*. Since $n^* \sim I_b/\gamma_o^3$, the parameter n^*

decreases rapidly during acceleration. Therefore, in order to avoid crossing the unstable region ($q_1 q_2 < o$) when γ_o increases, it is necessary to select the beam parameters during injection so that n^* is located to the left of the unstable region.

The extreme of Eq. (5) furnishes useful information on the dynamics of the ring in the r-z plane. First, we will show that this extreme is the radial balance equation of motion for the reference electron.

Setting the partial derivative of Eq. (5) with respect to r equal to zero

$$\frac{\partial \gamma}{\partial r} - \frac{|e|}{mc^2}\frac{\partial \Phi}{\partial r} = 0, \tag{23}$$

and using the relation $\gamma = (1 + \beta^2\gamma^2)^{1/2}$ and Eq. (6), we obtain

$$\frac{\partial \gamma}{\partial r} = \beta[-\frac{P_\theta}{mcr^2} + \frac{|e|}{mc^2}\frac{\partial A_\theta^{ext}}{\partial r} + \frac{|e|}{mc^2}\frac{\partial A_\theta^{self}}{\partial r}], \tag{24}$$

where we have assumed that $\beta = v/c$ is approximately equal to $\beta_\theta = v_\theta/c$.

Substituting Eq. (6) into Eq. (24) and using the equations

$$B_z^{ext} = \frac{A_\theta^{ext}}{r} + \frac{\partial A_\theta^{ext}}{\partial r}, \tag{25a}$$

$$B_z^{self} = \frac{A_\theta^{self}}{r} + \frac{\partial A_\theta^{self}}{\partial r},$$

and

$$E_r = -\frac{\partial \Phi}{\partial r}, \tag{25c}$$

it is obtained

$$-\gamma m\frac{v_\theta^2}{r} = -|e|[E_r + \frac{v_\theta}{c}(B_z^{ext} + B_z^{self})], \tag{26}$$

i.e., the radial balance equation. This equation gives the equilibrium position of the ring, which is located along the $\hat{e}_r$ axis. At this position the reference electron at the centroid of the ring moves only along the toroidal direction, i.e., $v_r = v_z = 0$.

When the equilibrium position is at $r = r_o$, the toroidal velocity of the reference electron can be determined from Eqs. (6) and (21) and is

$$v_{\theta o} = \frac{r_o\Omega_{zo}^{ext}/\gamma_o - \frac{\nu}{2\gamma_o^3}[(\frac{r_b}{2a})^2 + \ell n\frac{a}{r_b}]}{[1 + \frac{2\nu}{\gamma_o}(1/2 + \ell n\frac{a}{r_b})]}. \tag{27}$$

With the exception of the very small term on the numerator, Eq. (27) is the same with the expression reported previously[21, 22] for beams with square current density profile.

The external magnetic field B_{zo}^{ext} required to confine the ring at $r = r_o$ and be readily found from Eq. (27). Omitting the small term in the numerator of Eq. (27), we obtain

$$B_{zo}^{ext} = B_{zo}^{sp}[1 + \frac{2\nu}{\gamma_o}(1/2 + \ell n\frac{a}{r_b})], \tag{28}$$

where the single particle magnetic field is $B_{zo}^{sp} = \frac{\gamma_o\beta_{\theta 0}}{r_o}\frac{mc^2}{|e|}$.

The magnetic field required to maintain the beam at an equilibrium position that is different than r_o can also be determined from the radial balance equation. Substituting E_r and B_z^{self} from Eqs. (12a) and (12d) into Eq. (26), it is obtained

$$B_z^{ext} = B_z^{ep}\left\{1+\frac{2\nu}{\gamma}[1/2+\ell n\frac{a}{r_b}+\frac{R(R-r_o)}{a^2(\gamma\beta)^2}+\frac{r_b^2}{8a^2(\gamma\beta)^2}]\right\}. \tag{29}$$

Equation (29) has been derived under the assumption that ν is not a function of R.

As a consequence of the assumption that $\beta_\theta = \beta$ and $\gamma_\theta = \gamma$, the fast motion of the electrons has been neglected. This effect can be taken into account either by using the exact equations of motion or the relativistic guiding center equations of motion. It can be shown from the guiding center equations with linear external fields but non-linear image fields that for symmetric orbits with their center on the minor axis, the square of the bounce frequency ω_B^2 is given by

$$\omega_B^2 = \left(\frac{\Omega_{zo}}{\Omega_{\theta o}}\right)^2\left(\frac{\beta_\theta c}{r_o}\right)^2 * \left[\left(n-\frac{2\nu}{\beta^2\gamma^3}\frac{1+\alpha^2\gamma^2}{\frac{\Omega_{zo}r_o}{\gamma\beta_\theta c}}\frac{1}{1-(\frac{\ell}{a})^2}(\frac{r_o}{a})^2\right)\right.$$

$$\left.*\left(1-n-\frac{2\nu}{\beta^2\gamma^3}\frac{1+\alpha^2\gamma^2}{\frac{\Omega_{zo}r_o}{\gamma\beta_\theta c}}\frac{1}{1-(\frac{\ell}{a})^2}(\frac{r_o}{a})^2\right)\right], \tag{30}$$

with

$$\frac{\Omega_{zo}r_o}{\gamma\beta_\theta c} = \left(1+\frac{1}{2}\alpha^2\right)+\frac{2\nu}{\gamma}\left[\frac{1}{2}+\frac{1}{2}\left(1+\frac{1+\alpha^2}{\beta^2}\right)\ell n\frac{a}{r_b}+\ell n\left(1-\frac{\rho^2}{a^2}\right)\right]. \tag{31}$$

In Eqs. (30) and (31)

$$\beta_\theta^2 = \frac{\beta^2}{1+\alpha^2}, \quad \frac{1}{\beta_\theta^2\gamma_\theta^2} = \frac{1+\alpha^2\gamma^2}{\beta^2\gamma^2}, \quad \nu = \frac{I_b(kA)}{17.045\beta_\theta},$$

$\beta^2 = 1-\frac{1}{\gamma^2}$ and $\alpha = v_\perp/v_\theta$, where $v_\perp$ is the transverse velocity component that is due to the fast motion.

b. Description of the Experiment and Results

In its initial form, i.e., before the installation of the strong focusing windings, the NRL modified betatron comprised two different external magnetic fields; the betatron field that is a function of time and is responsible for the acceleration of the electrons and the toroidal magnetic field that varies only slightly during acceleration[27]. Figure 4 shows a photograph of the experiment.

The NRL modified betatron is an air-core device. Both the local field and the magnetic flux are produced by eighteen circular coils that are connected in series. Their total inductance is approximately $530\mu H$. The coils are powered by an 8.64 mF capacitor bank (48 capacitors each having 172 μF nominal capacitance) that can be charged up to 17 kV. At full charge, the bank delivers to the coils a peak current of about 65 kA. The current flowing through the coils produces a field that varies sinusoidally with a quarter period risetime of 2.6 msec and an amplitude on the minor axis at peak charging voltage equal to 2.1 kG. Immediately after the peak the field is crowbarred with a 4.5 msec decay time.

The flux condition and field index are adjusted by two sets of trimmer coils that are connected in parallel to the main coils. The current through the trimmers is adjusted with series inductors. Typically $\sim 10\% - 15\%$ of the total current flows throught the trimmers.

The toroidal magnetic field controls mainly the minor cross section of the electron ring and the growth rate of several unstable collective modes. This field is generated by twelve air-core, rectangular coils that are connected in series. The coils are made of aluminum squ[illegible]oing and have a 150 cm height and 135 cm width. The total inductance of the twelve coils is $\sim$ 85 μH and are powered by a 34-mF capacitor bank (85 capacitors each

having 400 μF nominal capicitance) that can be charged to a peak voltage of 10.6 kV. At peak voltage, the bank delivers to the coils $\sim$ 214 kA. This current produces a field that varies sinusoidally with a quarter period risetime of 2.3 msec and an amplitude on the minor axis in excess of 5.0 kG.

Demountable, high current joints allow removal of the outer legs of the coils. The high current density, low bolting force joints are attainable with multilam. The number and size of the coils has been selected in order to attain tolerable field errors. The discreteness of the coils produces a periodic field error that has all three components, i.e., $\Delta B_\theta, \Delta B_z$ and ΔB_r. Recent measurement of the ΔB_r component with an accurate probe[26] have shown that its average value over a 30° span at r=105 cm is $\sim$ 0.2 % of the toroidal field. Thus, when $B_\theta = 5$ kG, $< \Delta B_r > \simeq 25G$.

The coils are supported by a stiff structure that consists of two triangular decks, three aluminum legs, a central tension rod and a central spline. The decks are made of polytruded epoxy-glass beams and stainless steel plates that are not electrically continuous. The gaps in the stainless steel plates are necessary to avoid circulating currents from the changing magnetic flux.

Nested among the vertical field coils is the vacuum chamber. The 100 cm major radius, 15.2 cm-inside minor radius chamber has been constructed using epoxy-reinforced carbon fibers and has been briefly described previously. The diode that emits the injected beam is located inside the vacuum chamber and ~8.7 cm from the minor axis. Both the diode and the generator that powers the diode have been briefly discussed in previous publications.[15, 28]

During the first few microseconds following injection, the macroscopic beam motion in the transverse plane is studied by monitoring the light emitted from a thin (2-10μm) polycarbonate foil that is stretched across the minor cross section of the vacuum chamber. The foil is carbon coated on the upstream side to avoid electrostatic charging. Figure 5 shows open-shutter photographs of the light emitted as the electron beam passes through the foil for various values of the vertical magnetic field. As the vertical magnetic field decreases, the equilibrium position of the beam, located approximately at the geometric center of the transverse orbit, also decreases. At $B_{zo} \approx 42$ G the center of the orbit is located very near the minor axis.

Figure 6 shows the vertical magnetic field B_{zo} required to keep the beam at its equilibrium position R_{eq} for five beam currents 3, 2.5, 2.0, 1.0 and 0 kA. These results have been obtained from Eq. (26) using the fields shown in Eqs. (12). Although the beam current varies from shot to shot and there is uncertainty in both the energy and radius of the beam, the qualitative agreement between experiment and theory is satisfactory. It is apparent that the image forces from the induced charge and current on the wall of the vacuum chamber play a very important role and dramatically change the shape of the B_{zo} vs. R_{eq} curve.

The bounce frequency[22] ω_B, i.e., the angular frequency with which the beam moves on the macroscopic orbits of Fig. 2 has been measured in the NRL modified betatron accelerator under a wide range of experimental conditions. Figure 7 shows the bounce frequency squared vs. the circulating electron ring current. The solid lines have been computed from Eqs. (30) and (31) for $n = 0.5$ and for three values of the normalized

transverse velocity $\beta_\perp$. The solid circles are from the experiment. It is apparent that the measured ω_B^2 is substantially greater than that predicted by the theory for $\beta_\perp/\beta = 0$. A reasonable agreement between theory and experiment is obtained only under the assumption that $\beta_\perp/\beta \simeq 0.5$. As a rule, the measured ω_B is several times greater than that predicted by the cold beam theory. A satisfactory explanation of this discrepancy has been, so far, elusive.

Before the installation of the strong focusing windings, the operating point[12] in the NRL-MBA was to the right of the instability gap (see Fig. 3), i.e., in the high current regime. The low current regime was inaccessible because the beam could not drift enough over the first revolution to avoid the injector. It has been shown that an electron beam inside a resistive wave guide is drag instability unstable [29] when its current I_b exceed the critical current I_{crit}, i.e., when the beam is in the high current regime. The drag instability is due to the poloidal displacement of the electric and magnetic images that is caused by the finite resistivity of the chamber wall.

The growth rate Γ predicted by the linear theory[29], for (b-a)$< \delta < \sqrt{b(b-a)}$, is

$$(r_o\Gamma/c) = \frac{c(\gamma_o^2-1)}{2\pi}\left(\frac{r_o}{b}\right)\frac{\rho}{(b-a)}\frac{x}{(x-1)}, \tag{32}$$

where δ is the skin depth, ρ is the wall resistivity, b-a is the wall thickness, $x = I_b/I_{crit}$ and $I_{crit} = 4.26(\gamma_o^2-1)^{3/2}(a/r_o)^2(kA)$. The rest of the parameters have been defined previously. The beam lifetime is computed from

$$t_o = \ell n(a/\Delta_o)/\Gamma, \tag{33}$$

where Δ_o is the injection position.

Figure 8 shows the normalized ring lifetime c $t_o/2\pi r_o$ as a function of the electron ring current for several value of γ_o. In effect, $ct_o/2\pi r_o$ is the number of revolutions around the major axis performed by the beam before it strikes the wall. The dashed line shows the number of revolution over a bounce period. When no attempt is made to trap the beam, only the portion of the solid curves to the left of the dashed curve are meaningful. According to Fig. 8, the maximum number of revolutions the beam could perform before striking the wall is limited to about 40. However, we have routinely observed in the experiment beam lifetimes that were five times longer.

The solid curves in Fig. 8 have been plotted under the assumption that on each curve the beam electrons have the same kinetic energy, independently of the beam current. This implies that the voltage on the diode of the injector V_d increases as the beam current increases. Figure 9 shows the normalized beam lifetime as a function of beam current for fixed voltage on the diode. This represents a realistic simulation of the experiment. The dramatic increase in the beam lifetime with beam current is due to the lower growth rate at lower γ_o and also to the reduction of I_{crit}.

Several trapping techniques have been used to trap the beam in the modified betatron before the installation of the strong focusing windings. All these techniques required that the beam drifts a sufficient distance during the first revolution around the major axis that the beam misses the diode. In the three initial techniques, sufficient drift could be attained only when the beam current was high, i.e., when the beam was in the high current regime. However, in the high current regime the beam lifetime was limited by the drag instability.

To avoid this difficulty a technique was invented to enhance the drift motion of the beam during its first revolution around the major axis[12]. This technique was based on the generation of a pulsed radial magnetic field that would drift the beam radially inward. In general, all four techniques were not very reliable and introduced additional complications.

In summary, the studies in the MBA before the installation of the strong focusing windings led to the formation of electron rings with circulating current [12] as high as 3 kA. In addition, these studies furnished important information on the critical physics issues of the concept, such as

- demonstrated the beneficial effect of B_θ on the expansion of the ring's minor radius,
- unambiguously confirmed the bounce motion of the ring,
- verified the pronounced effect of image forces on the ring equilibrium,
- confirmed the existence of the macroscopic instability gap and the transformation of ring orbits from diamagnetic to paramagnetic,
- revealed, for symmetric orbits, that the bounce frequency is several times higher than the theoretical prediction, and
- shown that, at least for the drift trapping techniques, the low current regime is unaccessible.

Finally, these studies revealed that over a wide range of parameters the ring lifetime was limited to a few μsec which is comparable to the magnetic field diffusion time through the vacuum chamber. Thus, it became apparent from these results that the modified betatron had to be modified in order to increase the beam lifetime and thus to achieve

acceleration. In August 1988 the decision was made to proceed rapidly with the design, fabrication and installation of strong focusing windings.

Table III

Parameters for the results shown in Fig. 2

	Fig. 2a	Fig. 2b	Fig. 2c
External field index	0.35	0.5	0.65
Torus major radius (m)	100	100	100
Torus minor radius (cm)	16	16	16
Ring minor radius (cm)	3	3	3
Ring current (kA)	5	5	5
Electron energy (MeV)	3.123	3.123	3.123
Betatron field B_{zo} (G)	138.4	138.4	138.4
P_θ/mcr_o	-0.0018	- 0.0020	- 0.0023

IV. Results After the Installation of Strong Focusing Windings (SFW)

a. Background on the SFW

The beneficial effect of the SFW on the confinement of charged particles has been known for some time. There are two basic configurations: The stellarator[13] shown in Fig. 10 and the torsatron[14] shown in Fig. 11. The stability properties of the stellarator windings for high current beams have been studied initially by Gluckstern[30] in linear geometry and by Roberson[13] et al. in toroidal geometry. The beneficial effect of torsatron windings on high current electron beams has been addressed by Kapetanakos[14, 31] et al.

To improve the confining properties of the MBA we considered both configurations. The stellarator configuration was selected not only because of the small net vertical field and the lower current per winding, but also because it is compatible with our contemplated extraction scheme.[32]

Figure 12 shows the orbital stability diagram[13] in the rotating frame for an external field index n=0.5. The two axes are:

$$U = \frac{b^2 + 2 - 4n_s r_b^2/a^2}{(m+b)^2}, \tag{34}$$

and

$$V = \frac{|\mu|}{(m+b)^2}, \tag{35}$$

where

$b = B_{\theta 0}/B_{z0}$, $m = -2\alpha r_o$, $n_s = \omega_b^2/2\gamma_0^2\Omega_{z0}^2$,

$\mu = B_s^{ex}\epsilon_{st}\alpha r_0/B_{x0}$,

$\Omega_s^{ex}\epsilon_{st} = 4\alpha\Omega_0\rho_0 K_2'(2\alpha\rho_0), \alpha = 2\pi/L, B_0 = \frac{8\pi I_{St}}{cL}, \omega_b$ is the beam plasma frequency ρ_0 is the winding radius, L is the axial pitch, I_{St} is the winding current, r_0 is the major radius and r_b is the beam minor radius.

We have decided to select the parameters of the windings in such a way that the experiment will operate in region 2, because it has been shown that the electron ring will be stable during acceleration if it is located in this region at injection.[31]

When $B_\theta > 0$ and $v_\theta > 0$, operation in region 2 requires that

$$0 < U \leq 1 - 4V, \tag{36}$$

or

$$|\mu| \leq \left(\frac{m}{4}\right)^2 + \frac{mb}{8} + \frac{1}{4}\left(\frac{n_s r_b^2}{a^2} - \frac{1}{2}\right), \tag{37}$$

and

$$\left(\frac{b}{2}\right)^2 + \frac{1}{2} \geq \frac{n_s r_b^2}{a^2}. \tag{38}$$

It can be shown from (37) that $m > 0$ or $m < -2b$. For $m > 0$ and since $m = -2\alpha r_o$, $\alpha < 0$ or the windings should be left-handed.

When $n \neq 1/2$, the entire region 2 is not stable. The parameters of the injected beam should be selected to the right of the dashed line of region 2 (shown in Fig. 13). Along this line the bounce frequency in the laboratory frame $\omega_B = \omega_{--} = 0$ (instability gap).

During the acceleration phase this dashed line moves to the left and eventually coincides with the vertical axis. The parameter V of injection goes to $2/\mathrm{m}^2$ and thus never crosses the $\omega_{--} = 0$ line.

The exact stallarator field index[13] is defined by

$$n_{st} = \frac{\mu^2}{m^2 + mb - \frac{1}{2} + \eta_s r_b^2/a^2}. \tag{39}$$

When $mb \gg m^2 - \frac{1}{2} + n_s r_b^2/a^2$, n_{st} becomes

$$n_{st} \simeq \frac{\mu^2}{mb} = -\frac{(\Omega_s^{ex}\epsilon_{st})^2 \alpha r_0}{2\Omega_{z0}\Omega_{\theta 0}}. \tag{40}$$

Figure (14) shows n_{st}, n_s, $n_s(r_b/a)^2$ and $\tilde{n}_s(r_b/a)^2$ for typical parameters of the NRL modified betatron accelerator. The index $\tilde{n}_s(r_b/a)^2$ scales as γ_o^{-1} and is applicable after the wall current induced by the injected beam has decayed. Figure (15) shows the same indices for $r_b = 2\ cm$. It is apparent from these figures that $n_s > n_{st}$ at injection.

It can be shown that in the presence of strong focusing the linearized electron ring centroid orbit equation in the transverse plane is[14]

$$\left\{\frac{< P_\theta >}{mcr_0} - \frac{\nu r_0^2}{a^2\beta_{\theta i}\gamma_i^2} + \frac{\Omega_{z0}r_0}{2c}(1-n) - \frac{(\Omega_s^{ex}\epsilon_{St})^2\alpha r_0^2}{4c\Omega_{\theta 0}}\right\}\left(\frac{X}{r_0}\right)^2$$

$$+\left\{-\frac{\nu r_0^2}{a^2\beta_{\theta i}\gamma_i^2} + \frac{\Omega_{z0}r0}{2c}n - \frac{(\Omega_s^{ex}\epsilon_{St})^2\alpha r_0^2}{4c\Omega_{\theta 0}}\right\}\left(\frac{Z}{r_0}\right)^2 - \frac{\delta P_\theta}{mcr_0}\left(\frac{X}{r_0}\right) = \Lambda, \tag{41}$$

where:

$\frac{\delta P_\theta}{mcr_0} = \frac{< P_\theta >}{mcr_0} + \frac{\nu}{\beta_{\theta i}\gamma_i^2}\left(\ell n\frac{a}{r_b} + \frac{r_b^2}{4a^2}\right)$, $< P_\theta >$ is the averaged, canonical angular momentum over the intermediate frequency,

$$\Lambda \equiv \beta_{\theta i}\gamma_i - \frac{< P_\theta >}{mcr_o} - \frac{\Omega_{zo}r_o}{c} + 2\nu\beta_{\theta i}\left[\frac{1}{2} + \ell n\frac{a}{r_b} - \frac{1}{\beta_{\theta i}^2}\left(1 - \frac{1}{2\gamma_i^2}\right)\left(\frac{X_i}{a}\right)^2\right],$$

γ_i is the normalized beam energy at injection, $\beta_{\theta i}$ is the normalized beam velocity at injection and X_i is the injection position. In contrast with Eq. (20), Eq. (41) is not based on the assumption that $\gamma^2 \gg 1$ and $\frac{\partial \Phi}{\partial t} = \frac{\partial A_\theta}{\partial t} = 0$. The factor of two difference in the $\ell n\frac{a}{r_b}$ in the $\delta P_\theta/mcr_0$ term of Eqs. (20) and (41) could be traced to this approximation.

According the Eq. (41), a beam injected on the minor axis, i.e., $X_i = Z_i = 0$ will remain on the minor axis provided its energy is selected to satisfy the condition

$$\beta_{\theta i}\gamma_i = \beta_{\theta 0}\gamma_0 = \frac{\nu}{\beta_{\theta 0}\gamma_0^2}\left(\ell n\frac{a}{r_b} + \frac{r_b^2}{4a^2}\right)$$

$$+\frac{\Omega_{z0}r_o}{c} - 2\nu\beta_{\theta 0}\left(\frac{1}{2} + \ell n\frac{a}{r_b}\right).$$

In the NRL device the strong focusing field[15] is generated by four twisted windings carrying current in alternate directions. The left-handed windings are located 23.4 cm from the minor axis and have a 209.4-cm period, i.e., there are three periods over the circumference of the torus. They are supported by epoxy-reinforced graphite jackets and have been designed to carry up to 30 kA. The windings are connected in series and the current temporal profile is controlled by a ballast inductor. Since I_{st}, $\Omega_{\theta 0}$ and Ω_{z0}/γ remain approximately constant during acceleration, n_{st} scales inversely proportional to the relativistic factor γ.

b. Injection and Trapping

A challenging physics issue of the modified betatron concept was the capture of the injected beam into the closed magnetic field configuration of the device. For successful trapping the beam has to drift fast enough during the first revolution to avoid the injector and also its poloidal orbit has to be modified in such a way that the beam will not return to the injector after a bounce period. Modification of the beam's poloidal orbit can be achieved by either changing the equilibrium position of the gyrating electrons or by reducing the radius of the poloidal orbit.

At the time the decision was made to install strong focusing windings to the device, the NRL research staff was considering three different trapping schemes. The first was based on the resistivity of the vacuum chamber's wall[33], the second on a localized toroidal electric field[34] that is produced by a coaxial pulseline and the third on a pulsed vertical magnetic field that is generated by conductors[14] located inside the vacuum chamber. According to the linear theory, the resistivity of the wall in the NRL device was not high enough to provide the required inward shift to the beam over a bounce period. Thus, the first trapping scheme was ignored. The second, i.e., the toroidal pulseline[34] was adopted as the mainline trapping scheme with the third as a backup.

The toroidal pulseline was constructed and tested. However, it was never installed in the experiment, because when the current of the strong focusing windings was raised to a high enough level and the direction of the poloidal orbit was changed from diamagnetic to paramagnetic the beam spiraled near the minor axis and was trapped. This interesting phenomenon has been observed over several thousands of shots and for a wide range of

parameters. However, its explanation remained elusive until February 1991.

At the beginning of 1991, a series of detailed experiments[35] were carried out to measure with accuracy the various parameters associated with the trapping of the beam. As a result of these experiments a revised model of resistive trapping was developed that is in agreement with the experimental results.

The predicted decay rate Γ^{-1} from the initial linear theory for the parameters of the experiment was between 15 and 20 μsec, i.e., too long to explain the experimental results. Two modifications were introduced to the original model. First, the analysis is not restricted to beam motion near the minor axis[36] and therefore nonlinear effects and the fast diffusion times that scale as $\mu_0(b-a)^2/\pi^2\rho$, where $(b-a)$ is the thickness of the chamber and ρ is the wall resistivity, become important. Second, in order to take into account the intermediate motion of the beam that has been omitted in the calculation of the image fields of the beam, the wall surface resistivity was computed using the skin depth that corresponds to the frequency of the intermediate mode and not the actual thickness of the chamber.

Results from the revised resistive model are shown[35] in Fig. 16. The various parameters for the run are listed in Table IV. Figure 16 (a) shows the projection of the centroid's orbit on the $\theta = 0$ plane. Both the intermediate and slow (bounce) modes are apparent. Since there are six field periods for $0 \leq \theta \leq 2\pi$, the electrons perform six oscillations during one revolution around the major axis. To take into account the intermediate motion that has been neglected in the calculation of the image fields, the surface resistivity in the code was computed using the skin depth that corresponds to the intermediate frequency and

not the actual thickness of the wall.

The solid circles in Fig. 16 (b) show the positions the beam crosses the $\theta = 240°$ plane. This is a realistic simulation of the experimental situation. The time difference between two circles is equal to the period around the major axis, i.e., $\sim$ 23 nsec. The parameters of this run are similar to those in Fig. 16 (c) and the similarity of the two orbits is quite apparent. When the crossing plane is moved from $\theta = 240°$ to a different azimuthal position θ, the beam orbit rotates around the minor axis. The rotation predicted by the theory is very similar to that observed in the experiment.

In most of the experiments the center of the circular opening of the conical anode was located at the midplane and 8.7 cm from the minor axis of the toroidal chamber. In a series of experiments the diode moved to progressively larger radial positions from the minor axis. Successful trapping of the beam was observed as long as the radial distance was less than 10 cm.

Table IV

Parameters of the run shown in Fig. 16

Torus major radius r_o	100 cm
Torus minor radius a	15.2 cm
Relativistic factor γ	1.5
Winding radius ρ_0	23.4 cm
Winding current I_{st}	24 kA
Vertical field at injection B_{z0}	26 G
Toroidal field $B_{\theta 0}$	4 kG
Beam minor radius r_b	3 mm
Beam current I_b	1.2 kA
Wall resistivity	8 mΩ-cm
Intermediate frequency, ω_w	1.8×10^9 sec^{-1}

c. Beam Dynamics During Acceleration

Following trapping the beam settles at the radial distance of 98.5 - 99.0 cm and not on the minor axis, which is located at $r_0 = 100$ cm. Since the stellerator windings have been wound using a simple winding law $\varphi = 3\theta$, where φ is the poloidal and θ is the toroidal coordinate, the magnetic axis of the windings is located at r=98.87 cm as shown in Fig. 17. Therefore, this result is not surprising.

The x-ray traces indicate that the beam losses are negligibly small between injection and approximately 200 μsec. Three different diagnostics, magnetic probes, x-rays from localized targets and fibers, have shown that the beam electrons strike the inner surface of the vacuum chamber slightly above the midplane.

Due to the finite resistivity of the vacuum chamber wall the return current induced by the beam at injection decays within two to three magnetic field loop times $\tau_{00} = \frac{4\pi a \Delta a}{\rho c^2}[\ell n \frac{8r_0}{a} - 2]$, where a is the minor radius of the torus and Δa its thickness, r_0 is the major radius and ρ is the combined resistivity of the wall. As a consequence of the current decay, the magnetic field of the beam diffuses into the hole of the torus.

For a beam of minor radius r_b that is located on the minor axis of a torus of major radius r_0 and minor radius a, the magnetic flux ϕ that links the beam axis is related to the vector potential $A^{in}_{\theta 0}$ at the centroid of the beam by the relation

$$\phi = 2\pi r_0 A^{in}_{\theta 0}(r = r_0, z = 0), \tag{42}$$

where[36]

$$A^{in}_{\theta 0}(r = r_0, z = 0) = \frac{I_b}{c}\left[2\left(\ell n \frac{8r_0}{r_b} - \frac{3}{2}\right) - 2\left(\ell n \frac{8r_0}{a} - 2\right) e^{-t/\tau_{00}}\right]. \tag{43}$$

The loop voltage can be computed from Eqs. (42) and (43) and is

$$V_{loop} = \frac{4\pi r_0 I_b}{\tau_{00} c^2} \left[\ell n \left(\frac{8r_0}{a} \right) - 2 \right] e^{-t/\tau_{00}}. \tag{44}$$

For I_b = 1 kA, r_0 = 1 m, τ_{00} = 40 μsec and a=15.2 cm, Eq. (44) gives V_{loop} = $61.6e^{-t/\tau_{00}}$ (volts), and the total energy loss within 5 τ_{00}, i.e., when the first beam losses are observed is 120 keV.

The energy gained by the beam during 5 τ_{00}, when the acceleration rate is 0.8 kV/turn, is 8.0 MeV. Since at injection the beam energy is approximately 0.5 MeV, its total energy is 8.5 MeV and thus the energy mismatch is $\Delta\gamma/\gamma$ = 1.4%. At γ = 18, Fig.14 gives $n_{st} \simeq 1.55$ and $n_e(r_b/a)^2 \simeq 0$, thus the expected shift Δr in the beam centroid is

$$\Delta r = \frac{(\Delta\gamma/\gamma) r_0}{0.5 - n_e(r_b/a)^2 + n_{st}} \simeq 0.9\ cm$$

In addition to the reduction of the beam energy to build up the fields inside the loop, some beam energy is also lost to the heating of the wall. However, this loss is typically an order of magnitude smaller than the energy loss associated with the build up of the fields.

The Larmor radius of the fast motion in the toroidal magnetic field $B_{\theta 0}$ of 5 kG at t = 200 μsec is only 3 cm, even when $\beta_\perp$ = 0.5, which is an upper limit. For $\beta_\perp > 0.5$ the beam equilibrium will be lost and the entire beam will strike the wall in a short period of time. Therefore, the diffusion of the self field and the finite Larmor radius cannot provide sufficient radial displacement to the electrons to reach the wall at t=200 μsec.

Figure 18 shown a typical x-ray signal. This signal lasts for several hundred microseconds. The slow loss rate is a manifestation that individual particles strike the wall rather

than the entire beam. Figure 14 shows that the individual particle self index of 1 kA, 1 cm radius beam becomes equal to n_{st} ($I_{st} = 30\ kA$), when $\gamma_0 = 6.5$. At this energy the individual particle orbital stability is lost, at least temporarily and theory[22, 37] and computer simulations[38] predict a substantial increase in the beam radius, when the beam electrons have even a small axial energy spread. This crossing of the individual particle instability gap is consistent with several features of the experimental results. However, the time τ_x the x-ray signal initially appears is independent of the trapped current, which is inconsistent with the fact that n_s is proportional to the beam current.

The dependence of τ_x on the toroidal magnetic field is shown in Fig. 19. In all the shots shown in Fig. 19 the peak B_z field was kept constant. However, the current in the strong focusing windings had to be raised with rising B_θ in order to provide sufficient drift to the beam and thus to reduce beam losses at the diode during the first revolution. For fixed B_θ, τ_x varies inversely proportional to the acceleration rate dB_z/dt. Figure 20 shows τ_x as a function of the peak B_z field that occurs at about 2.6 msec. This quantity is proportional to dB_z/dt. It appears that τ_x varies with B_θ and dB_z/dt the same way as the peaks of the x-ray signal.

It has been shown theoretically and confirmed with extensive numerical work that the equilibrium position of the beam is not sensitive to the transverse velocity, provided that $\beta_\perp/\beta < 0.5$. In the absence of strong focusing and space charge, the radial change of the equilibrium position Δr with $\beta_\perp$ is given by

$$\frac{\Delta r}{r_0} = 2\left[1 - (1-\alpha^2)^{-\frac{1}{2}} + \alpha^2/2(1-\alpha^2)\right], \tag{45}$$

where $\alpha = \beta_\perp/\beta$.

Equation (45) is plotted in Fig. 21. It is apparent from these results that the equilibrium position of the beam will not change noticeably, even though the beam will acquire some transverse velocity as it crosses a large number of higher ℓ resonances.

It has been determined experimentally that a betatron flux condition of 2.3 provides the best confinement to the beam*. For the same parameters TRIDIF predicts a $\langle B_z \rangle / B_{z0}$ that is in good agreement with the experiment as shown in Fig. 22a. The vacuum chamber has small effect on the betatron flux condition and only for the first 200 μsec. EFFI, a static code predicts a slightly lower flux condition. The radial profile of the normalized flux is shown in Fig. 22b. The solid solid line gives the normalized flux at t=50 μsec for a sinusoidally varrying current with a peak value of 40 kA. The rest of the parameters are listed in the figure. The dashed line shows the total rA_θ immediately after the injection of a 1 kA hollow electron beam. The beam is injected at 100 cm and has a radius of 1 cm. When the missing flux inside the hollow beam is taken into account, Eq. (43) is in very good agreement with the results of Fig. 22b.

---

*It has been reported[28] previously that the best results have been obtained for $\langle B_z \rangle / B_{z0} \simeq 2.0$.. Since then an error was found in the calibration of B_z probe that raised this value to 2.3.

d. Studies of the Cyclotron Resonances

In a modified betatron with strong focusing there are four characteristic transverse modes. In the laboratory frame these four modes $\omega_{\pm\pm}$ are given by[39]

$$[\omega_{\pm\pm}/(\Omega_{z0}/\gamma)] = \pm\frac{(m+b)}{2}\left[U+1\pm 2(U+4V^2)\right]^{1/2}+\frac{m}{2}, \tag{46}$$

where U and V have been defined in Eqs. (34) and (35), m is the number of field periods, b=$B_{\theta 0}/B_{z0}$ and Ω_{z0} is the cyclotron frequency of the vertical field.

When $n_s \ll (b/2)^2$, $b^2 \gg 1$ and for modest winding current, as that in the NRL device, the four modes become

$$\begin{aligned}
&\omega_{++} \approx m\Omega_z/\gamma + \Omega_\theta/\gamma \qquad \text{(High Freq. Cyclotron),} && (a)\\
&\omega_{--} \approx \omega_B \qquad\qquad\quad \text{(Bounce),} && (b)\\
&\omega_{-+} \approx -\Omega_\theta/\gamma \qquad\quad \text{(Cyclotron),} && (c)\\
&\omega_{+-} \approx m\Omega_z/\gamma - \omega_B \qquad \text{(S.F.mode).} && (d)
\end{aligned} \tag{47}$$

and

Integer resonances occur when

$$\omega_{\pm\pm}/(\Omega_{z0}/\gamma) = k,\ k = \pm 1, \pm 2, \pm 3, \ldots \tag{48}$$

Equations (46) and (48) are plotted in Figs. 23 to 26. Figure 23 shows the centroid integer resonances associated with ω_{--} (bounce) and ω_{+-} (SF field mode) for typical parameters

of the NRL device and before the self magnetic field of the beam diffuses out of the vacuum chamber. Figure 24 shows the same resonances as Fig. 23 but after the self magnetic field of the beam has diffused out of the chamber. The individual particle integer resonances of the bounce and SF mode are shown in Fig. 25. Finally, Fig. 26 shows the centroid integer resonances associated with the cyclotron mode ω_{-+}. When Eq. (47) is valid, the cyclotron resonance condition takes the very simple form[40] $B_{\theta 0}/B_{x0} \approx \ell$, where ℓ is an integer $\gg 1$. Therefore, the cyclotron resonance is due to the coupling, caused by a field error(s) of the cyclotron motion associated with the toroidal and vertical fields.

It is apparent from Fig. 26 that for $I_{et} < 30\ kA$ and $\ell > 7$, the strong focusing field does not have a noticeable effect on the cyclotron resonance condition. Thus, the resonance condition is simplified to

$$\frac{r_0 \Omega_{\theta 0}}{c\gamma\beta_\theta} = \frac{(2\ell^2 - 1)}{2\ell}, \qquad \ell = 1, 2, 3 \ldots, \tag{49}$$

and it is valid even when the beam is off the minor axis.

The x-rays are monitored by three collimated x-ray detectors (scintillator-photomultiplier tube) that are housed inside lead boxes. In the results shown in Fig. 27, the x-rays enter the scintillator through a 1.94 cm-dia. tube and the detector is located 10.8 m from the vacuum chamber. As a rule, the shape of the x-ray signal recorded by all three detectors is spiky and the peaks always occur at the same value of $B_{\theta 0}/B_{x0}$, independent of the current flowing in the stellarator windings. In addition to the x-ray pulse, Fig. 27 shows the values of ℓ on the minor axis. These values have been computed from Eq. (49) by substituting $c\gamma\beta_\theta$ for $\Omega_{x0} r_0$. The ratio $B_{\theta 0}/B_{x0}$ is computed from the measured values of

fields. A perfect match between theory and experiment requires that the peaks occur at integer values of ℓ.

It is apparent from the resonant condition that when $B_{\theta 0}/B_{zo}$ = constant $\neq$ integer, the cyclotron resonance is not excited. To test this supposition, we installed 24 single-turn coils on the outside of the vacuum chamber, as shown in Fig. 28. These coils are powered by a capacitor bank and have a risetime of approximately 100 μsec. During this time period the coils generate a toroidal field ramp that increases linearly with time and the total toroidal field increases in synchronism with the betatron field. Results from the experiment are shown in Fig. 29, when the coils are energized at 800 μsec. Beam losses are suppressed for 100 μsec, i.e., as long as the condition $B_{\theta 0}/B_{z0} \neq$ integer is satisfied.

The damage done to the beam at each resonance depends on the speed with which the resonance is crossed. By increasing the acceleration rate the resonance is crossed faster and thus the damage inflicted to the beam is reduced. To achieve higher acceleration rate, the vertical field coils were divided into two halves with midplane symmetry and powered in parallel. Figure 30 shows the x-ray signal for three acceleration rates, (dB_{zo}/dt) peak = 0.69, 1.69 and 1.93 $G/\mu sec$, for a constant $B_{\theta 0} = 4kG$. At the lowest acceleration rate the x-ray peak that corresponds to $\ell = 12$ has the largest amplitude. At the intermediate acceleration rate the amplitude of $\ell = 12$ has been reduced by a factor of two and the $\ell = 8$ becomes the dominant peak. At the highest acceleration rate the amplitude of the $\ell = 12$ peak was further reduced while the amplitude of the lower ℓ value peaks has been substantially increased.

The crossing of the resonance can be speeded up by modulating the toroidal magnetic

field with a rapidly varying ripple. This is the dynamic stabilization or tune jumping technique and requires a carefully tailored pulse to be effective over many resonances. This stabilization technique has been tested experimentally using the 24 coils that are shown in Fig. 28. These results have been reported previously[19] and in general they are in agreement with the theoretical predictions and the computer calculations.

The dynamic behavior of the electron beam as it crosses the various ℓ number resonances depends on the nature and the amplitude of the field error.[41] The field error(s) that excites the resonance can be either vertical ΔB_z or axial (toroidal) ΔB_θ. In the case of a vertical field error and in the absence of acceleration and strong focusing field, the normalized transverse velocity $\beta_\perp$ and thus the Larmor radius of the transverse motion of the gyrating particles grows linearly with time,[40] provided that nonlinear effects associated with the particle velocity are neglected. When nonlinear effects are taken into account, $\beta_\perp$ is a periodic function of time.

In the presence of an accelerating field and a large vertical field error, [41] $\beta_\perp$ increases proportionally to the square root of time, while $\gamma\beta_\theta$ saturates, i.e., the electrons lock-in to a specific resonance (lock-in regime). When the amplitude of ΔB_z is below a threshold, $\beta_\perp$ exhibits Fresnel behavior, i.e., $\beta_\perp$ grows quickly for approximately 1 μsec and then saturates until the beam reaches the next resonance. The threshold value of ΔB_z can be made larger either by increasing the acceleration rate or by adding a low amplitude ripple to the main toroidal field.

In the case of an axial field error and in the absence of acceleration, $\beta_\perp$ grows exponentially with the time only for a very short period. Since $\beta_\perp$ increases at the expense of

β_θ the particles are kicked off resonance. Thus, $\beta_\perp$ varies periodically with time. Similarly, in the presence of an accelerating field $\beta_\perp$ behaves as in the case of the vertical field error.

The previous discussion is based on the assumption that the space charge is low and the strong focusing field is zero. In addition to introducing new characteristic modes, the strong focusing field makes the expression for the regular cyclotron mode more complicated. However, it can be shown that for the parameters of the NRL device and provided $\ell \gg 1$, the strong focusing has only minor effect on the cyclotron resonance. This is also supported by extensive computer calculations.

A typical example of this behavior is shown in Fig. 31. These results have been obtained from the numerical integration of exact equations of motion for the parameters listed in Table V. The threshold value of ΔB_z in the minor axis is approximately 0.2 G for the $\ell = 9$ mode. Figures 31a and 31c show $\beta_\perp$ vs. time below and above threshold, while Figs. 31b and 31d shows the corresponding $\gamma\beta_\theta$ vs. time. Since in Fig. 31d $\gamma\beta_\theta$ remains constant the resonance is never corssed [see Eq. (49)], i.e., the entire beam is lost at the same ℓ mode.

The temporal behavior of the x-ray signal (see Fig. 27) clearly indicates that only a fraction of the beam electrons may be in the lock-in regime, since we observe several ℓ modes. However, we carried out extensive experimental studies[19] with several, externally applied field errors of variable amplitude. These results indicate that the entire beam was lost in a single ℓ mode whenever the amplitude of the magnetic perturbation was above a threshold value. Details about these results are given in the next section.

In addition to the nature and amplitude of the field error, the dynamic behavior of

the beam depends on the initial conditions.[41] Results from the theoretical predictions are shown in Fig. 32, for the parameters listed in Table VI. Figure 32 shows contour plots of the final $\beta_\perp$ in the $\beta_\perp^{(0)}$, φ_0 plane, where $\beta_\perp^{(0)}$ and φ_0 are the amplitude and phase of the asymptotic initial value of transverse velocity and its phase. In Fig. 32a the amplitude of the field error has been chosen equal to $\sim$ 0.2 G. By increasing the field error amplitude from 0.2 G to 0.3 G, the lock-in regime has expanded for low $\beta_\perp^{(0)}$ over the entire range of initial phase angles as shown in Fig. 32b. When the electrons in the beam are uniformly distributed over the initial phase angle, the resonance diagram of Fig. 32 gives, for each initial $\beta_\perp^{(0)}$, the percentage of the beam that crosses the resonance and the percentage that locks into it. Therefore, it is not surprising that only a fraction of the electrons in the experiment are in the lock-in regime.

Following the successful demonstration of acceleration a concerted effort was made[17] to locate and eliminate or reduce the field disturbances that may excite the cyclotron resonances. The sources of field errors investigated included: 1. coil misalignment, 2. coil discreteness, 3. eddy currents induced in the modified betatron support structure and nearby components, 4. errors produced from the various portholes in the vacuum chamber, and 5. two contributions from the feeds of the vertical field coils. Reduction in many of these errors together with the operation at higher B_θ and strong focusing fields led to beam energies in excess of 20 MeV, while the trapped current was above 1 kA.

Although the cyclotron resonance is a potent mechanism that has the potential to disturb the beam at low acceleration rate and when the various fields are not carefully designed, it also may provide a powerful technique[20] for extracting the beam from the

magnetic field configuration of the modified betatron. Results from such initial and incomplete studies are presented in the next section.

Table V

Parameters of the runs shown in Figs. 31

Torus major radius r_o	100 cm
Toroidal magnetic field $B_{\theta o}$	2771 Gauss
Vertical magnetic field B_{zo}	305 Gauss
Field index n	0.5
Rate of change of vertical field $\dot{B}_{zo}$	2 Gauss/μsec
Resonance mode ℓ	9
Amplitude of VF-error ΔB_{zo}	0.190, 0.195 Gauss
Initial normalized toroidal momentum $\gamma\beta_\theta$	17.922
Initial normalized vertical velocity $\beta_\perp$	0.0
Initial radial displacement $r - r_o$	0.0 cm
Initial vertical displacement z	0.0 cm

Table VI

Parameters for the results shown in Fig. 32

Torus major radius r_o	100 cm
Toroidal magnetic field $B_{\theta o}$	2771 Gauss
Field index n	0.5
Rate of change of vertical field $\dot{B}_{zo}$	2 Gauss/μsec
Resonance mode ℓ	9
Amplitude of VF-error ΔB_{zo}	0.2, 0.3 Gauss
Initial normalized toroidal momentum $\gamma\beta_\theta$	17.922

e. Preliminary Beam Extraction Studies

The results of the NRL modified betatron accelerator have unambiguously demonstrated that the toroidal and strong focusing fields improve the current carrying capability of the device. However, these field also make the extraction of the beam from the magnetic field configuration substantially more involved.

In 1988, an extraction scheme was reported[20] by the NRL research staff that is easily realizable and has the potential to lead to high extraction efficiency. Briefly, this extraction scheme is based on the transformation of the circulating electron ring into a stationary helix, in the toroidal direction, by excitation of the resonance that naturally exists for some specific values of the ratio of the vertical to toroidal magnetic field. Transformation of the ring into a helix is achieved with a localized vertical magnetic field disturbance that is generated by an agitator coil. As the minor radius of the helix increases with each passage through the gap of the agitator coil, the electrons eventually reach the extractor, which has the property that all the magnetic field components transverse to its axis are equal to zero. Thus, the electron ring unwinds into a straight beam.

The hardware for this mainline extraction approach was designed and fabricated. However, it never was installed in the experiment. The reason is that it requires a beam with low transverse velocity because the aperture of the agitator is small. There is evidence that the beam in the NRL device has substantial transverse velocity. As a consequence of this difficulty we pursued some alternate extraction approaches that do not require beams with low transverse velocity.

At the beginning of summer in 1991, while the beam dynamic stabilization experiments[19]

with twelve external coils were underway, we observed that the beam could be kicked out[18, 19] of the magnetic field within a time that is comparable to the risetime of the current pulse, whenever the twelve coils were initiated while the beam was crossing the $\ell = 12$ resonance. Figure 33a shows the x-ray pulse when the resonant coils are off and Fig. 33b when the coils are on. The amplitude of the current pulse is 9 kA and its full risetime 12 μsec. The measured amplitude of the axial field disturbance ΔB_θ at the center of the coil is $\sim$ 240 G and its risetime 32 μsec. It is apparent from these results that the full width at half maximum (FWHM) of the x-ray signal has been reduced from approximately 900 μsec to 8 μsec (Fig 33c), i.e., by more than two orders of magnitude while its amplitude has increased by a factor of thirty. In the results shown in both Figs. 33a and 33b the toroidal magnetic field on the minor axis $B_{\theta 0}$, at injection, is 4.2 kG, the current flowing through the strong focusing windings is approximately 26.5 kA and the trapped beam current about 1 kA.

In a series of experiments with the twelve external coils the current flowing through them was changed by more than a factor of two. The results show that the FWHM of the x-ray signal varies inversely with the current in the coils as shown in Fig. 34.

In the results described so far, the twelve coils were divided into two groups that were connected in parallel while the six coils of each group were connected in series. By connecting all the twelve coils in parallel the current pulse risetime was reduced to 5 μsec, while the field risetime was reduced to approximately 6 μsec. Even shorter risetime pulses have been obtained with a set of internal coils. These coils are wound on blue nylon forms and encapsulated with epoxy. The 21 cm radius, single turn coils were mounted at the

joints of the vacuum chamber sectors. Six new drivers that produced a current pulse with risetime of 0.4 μsec powered the twelve coils. Each driver powered a pair of coils connected in parallel, with a combined inductance of 270 nH. All the drivers were triggered by the same trigger generator. The circuit of a driver and the multiple trigger generator are shown in Fig. 35.

Figure 36 shows the axial component of the field in free space and also in the presence of lateral walls. The geometry and the parameters used in the TRIDIF Code are given as inserts in the figure. As expected, the walls substantially reduce the amplitude of the field even at the radial distance of 12 cm. On the minor axis the reduction is even greater.

The width of the x-ray pulse depends on the risetime of the current pulse. The results are shown in Fig. 37. In addition, the results indicate that for the twelve coil configuration, the amplitude of ΔB_θ field pulse required to extract the entire beam during the risetime of the field pulse is approximately 80 G.

To determine the toroidal distribution of the beam losses when the internal coils are energized a 400-μm diameter optical fiber was mounted on the outside of the vacuum chamber. By the time the ℓ=12 resonance is crossed, the electrons have acquired sufficient energy to penetrate the chamber. The light generated when the electrons strike the fiber is monitored with a PM tube. Initially, a small section of the fiber was placed in different poloidal positions at a fixed toroidal angle. These measurements confirmed our previous conclusion that the electrons strike the wall of the vacuum chamber at its inner radius. In all the subsequent measurements the active length of the fiber was selected equal to half the poloidal (minor) circumference of the chamber and was placed symmetrically around

the midplanes at the inner radius of the torus.

The results from scanning around the torus at 10° intervals are shown in Fig. 38. There are six distinct peaks, separated by 60°. The three dominant peaks have approximately the same amplitude.

Figure 39 shows results from the numerical integration of orbit equations for the beam centroid near the ℓ=12 cyclotron resonance. The values of the various parameters for the run are listed in Table VII. Figure 39a shows the projection of the beam centroid orbit in the transverse plane and Fig. 39b shows the same orbit on an expanded scale. The arrows indicate the direction of motion. Since the ratio of the toroidal cyclotron frequency $\Omega_\theta/_\gamma$ to the intermediate frequency ω_w is equal to $\ell/m = 2$, the beam centroid performs two revolutions (fast motion) around its quiding center during a single revolution in the strong focusing fields of the windings. The projection of the orbit in the $(r,\ \theta)$ plane is shown in Fig. 39c. There are six radial minima that occur at approximately the same toroidal angle as those of Fig. 38. However, in contrast with Fig. 38, all the peaks have the same amplitude. Figure 40 shows similar results from the crossing of $\ell = 9$ resonance. In this case $\frac{\Omega_\theta/\gamma}{\omega_w} = \frac{3}{2}$. This ratio is also manifested in the results of Fig 40c. For every three peaks, two are the same.

Under normal operating conditions the current that produces the strong focusing field is passively crowbarred and the fields decay with a long time constant L/R, where L is mainly the inductance of a ballast inductor that is in series with the windings. To test the effect of the strong focusing field on the distribution of beam loss, the ballast inductor was removed and the circuit was actively crowbarred. The shape of the current pulse

is a half sine with a half period of $\sim$ 650 μsec. The beam is injected near the peak of the pulse. Thus, the strong focusing field is practically zero when the resonant coils are energized. Under these conditions most of the beam is lost at a single toroidal position near θ=70°. Both the amplitude and the toroidal position of the peak remained intact when the vacuum chamber and thus the strong focusing windings that are permantly attached to it were rotated clockwise 30°. This result implies that neither field errors associated with the stellarator winding nor the return current are responsible for the formation of the peak. In addition, we have not observed any noticeable modification in the peak by shifting the vacuum chamber radially inward by $\sim$ 0.3 cm along the radial line that passes through the θ=90° and 270° toroidal positions.

However, we have observed a substantial modification in the loss spectrum when the feeds of the vertical coils that are located just above and *below the midplane* were rotated from θ=60° to θ=270°. It has been determined using a very accurate, figure eight magnetic probe that the feeds of this coil pair produce a substantial radial field error.

To test the feasibility of driving the beam to the wall on the time scale of one revolution around the major axis, the risetime of the current pulse had to be shortened and a new low inductance agitator with large aperture to be invented. The low inductance, small aperture agitator of the mainline extraction approach was not suitable, because it requires beams with low transverse velocity. Unfortunately, the amplitude of the various field imperfections in the NRL device was never reduced to low enough level and thus the beam acquired substantial transverse velocity during its long confinement time.

Among the various concepts considered, magnetic cusps were found to be the most

promising. Extensive numerical studies of several cusp configurations have shown that a single layer, 24.2 cm long cusp surrounded by a resistive (σ=60 mho/cm) shroud could provide sufficient displacement to the beam over a 20 nsec time period. This wide, 12 coil cusp system is shown in Fig. 41. Unfortunately such a cusp could not be fabricated on time and thus we had to proceed with an inferior agitator that is based on three double cusps that are located 120° apart in the toroidal direction. This agitating system was fabricated in-house and tested in the experiment for a short period of time just before the termination of the MBA program.

Each of the three double cusps consists of four coils. The first pair of coils is located ±3.73 cm from the symmetry plane of the cusp and the second ±5.92 cm. The coils are wound on thin toroidal forms made of epoxy reinforced graphite fibers and are encapsulated with epoxy. An axial slot in the coil form allows fast penetration of the fields. The double cusps are mounted inside the vacuum chamber and are fed with demountable copper electrodes that enter the vacuum chamber at the ports. A photograph of one of the double cusps is shown in Fig. 42.

Figure 43 shows the axial profiles of radial and axial fields. The solid line is from the TRIDIF code. The code assumes that the temporal profile of the current I_c in the four coils is given by

$$I_c = 1000 \sin\left[\frac{\pi}{2}\frac{t(\text{nsec})}{400}\right] \quad (A),$$

and the wall of the vacuum chamber consists of two materials with conductivity

$$\sigma = \begin{cases} 160 \text{ mho/cm, for } & 15.2 \leq \rho \leq 15.45 \text{ cm,} \\ 800 \text{ mho/cm, for } & 15.45 \leq \rho \leq 15.55 \text{ cm,} \end{cases} \tag{50}$$

where ρ is the radial distance from the minor axis. The conductivity and thickness have been selected to give the same surface conductivity as in the experiment. The peak magnetic energy is 0.77 joules that corresponds to a coil inductance of 1.54 μH. The solid circles in Fig. 43 are the measured values of the fields at ρ=10.8 cm. It is apparent that there is good agreement between the experiment and the code. All three double cusps were not identical. In two of them the coil minor cross section was a semi-circle with the flat surface of the copper away from the minor axis and at the radial distance of 14.7 cm.

Figure 44 gives the axial profiles of the fields for a double cusp when the coil radius is 14.7 cm, the compound wall has a conductivity as that given in Eq. (50), the peak current in the coils is 3 kA and its risetime (quarter period) 20 nsec. These fields have been used in the beam centroid code to determine the displacement of the centroid in three revolutions (60 nsec). Results are shown in Fig. 45 for the parameters listed in Table VIII. Figure 45a shows the projection of the beam centroid orbit in the transverse plane. At t=0 the centroid is located 10.0 cm away from the minor axis. During the last 20 nsec of the run, i.e., during one revolution around the major axis the centroid is displaced by 0.9 cm. This radial displacement is almost sufficient for a small radius beam to avoid hitting the septum of the extractor. Obviously, larger radial displacements can be obtained either by increasing the current of the cusps or by tapering the radii of the cusp coils to reduce the positive component of B_ρ. A top view of the orbit is shown in Fig. 45b.

Figure 46a shows the projection of the beam centroid orbit in the transverse plane for

the same parameters as the run of Fig. 45 but artificially setting the positive component of $B_\rho = 0$. Comparison of the two figures clearly demonstrates the advantage of using a single polarity cusp. The radial displacement of the beam centroid in one revolution has increased by $\sim 30\%$. Figure 46b shows a top view of the orbit.

In the runs of Figs. 45 and 46 the various parameters of the beam centroid have been carefully selected to satisfy the $\ell = 12$ resonance condition. During the initial phase, i.e., for about 10-20 nsec the centroid transverse velocity is low and the orbit projection in the transverse plane is a triangle as shown in Fig. 47a. This figure shows the projection of the orbit for 20 nsec. The values of the various parameters are the same as in the run shown in Fig. 45, except for the initial radial position that is 10.5 cm instead of 10.0 cm and the cusp current, which is zero. With the cusps off, the beam remains in resonance for a long time and the orbit precession is small. With the cusps on, the centroid acquires transverse velocity, falls off resonance and start to precess rapidly. Figure 47b shows the three component of the magnetic field seeing by the centroid. As a result of the proximity of the orbit to the windings, the magnetic field components at the orbit are substantially different than those listed in Table VIII.

It became apparent in the Spring of 1992 that because of severe time and several other contraints the experiment was operating under, the only realistic approach to obtain short risetime current pulses to drive the double cusps was the sharpening of the pulse of the existing drivers using ferrites. The sharpening results from the change of permeability that occurs when a ferrite matierial is driven into saturation. Ferrite pulse sharpeners have been built and tested by earlier workers and their results have been documented in

the published literature.[42]

The ferrite loaded transmission line consists of a 5/32″- diameter inner conductor and a braided outer conductor slipped over an acrylic insulating tube. A cross sectional view of the line is shown in Fig. 48a. The inner diameter of the acrylic tube is 1/2″ and its outer diameter is 5/8″. The ferrites used were Krystinel K01 toroids with dimensions 3/16″ ID, 3/8″ OD and 1/8″ thick. All intervening spaces were filled with epoxy or oil. The potted ferrite line was found to give results almost identical to those obtained from an oil immersed line.

Figure 48b shows a schematic diagram of the experiments setup used to develop the ferrite pulse sharpeners. An 80-nF capacitor charged to voltages ranging from 35 kV to 60 kV DC, delivers a voltage pulse into a 45-foot-long, 50 Ω cable. A Rogowski coil monitors the current delivered to the cable. A 3-foot long ferrite loaded line sharpens the pulse from the 50 Ω cable, and transmits the sharpened pulse to another 25-foot-long 50-Ω cable short-circuited at one end. A Rogowski coil placed between the ferrite line and the 25-foot line, measured the waveshape of the sharpened current pulse.

At 50-kV charge voltage the amplitude of the first current step in the 45-foot, 50Ω cable is 1 kA. The ferrites saturate even before the current reaches 0.1 kA. The risetime of the current pulse, as measured by ROG1 is ~ 25 ns. The risetime of the sharpened pulse measured by ROG2 is ~ 3 ns. The presence of the Rogowski coil introduces added inductance in the cable connections. Since, the Rogowski coil has a response time of ~ 1 ns, the intrinsic risetime of the pulse is therefore ~ 2 ns. For optimum performance, the saturated characteristic impedance of the ferrite line needs to be the same as the impedance

of the cables on either end of the line. The impedance of the ferrite line shown in Fig. 48a appears to be 50 Ω. However, this requires a relative permeability of ~3 after saturation, as opposed to the ideal value of unity.

The cables on either side of the ferrite line isolate it from reflections from the load (short-circuit, here) and the spark gap switch, for the duration of the round trip transit time in each cable. If the ferrite line is made longer than the length needed to erode the injected current risetime, then the flattop is also eroded and the 45-foot cable needs to be made longer to compensate for this effect.

Figure 48c shows the layout of the drivers that powered the double cusps. Two 50 Ω ferrite sharpeners drive each coil. At 40 kV charge voltage the average amplitude of the first current step is 2.6 kA and the risetime is approximately 50 nsec and is solely determined by the effective inductance of the coil.

Typical results from the experiment are shown in Fig. 49. The important parameters are listed in Table IV. Figure 49a shows the x-ray signal with the cusps off and Fig. 49b shows the x-ray signal when the three cusps are energized at 480 μsec, i.e., when the ℓ=12 resonance is crossed. As in Fig. 33, most of the beam exits the magnetic field configuration in a single ℓ mode, although the current through the coils is substantially lower. The high frequency noise that is observed in Fig. 49b is a consequence of the fact that the 1.5 μsec integrator that has been used in the input of the digitizer in Fig. 49a was removed to avoid possible reduction of the sharp x-ray pulse when the cusps are activated.

A difficulty experienced during these studies was the substantial jitter of the drivers. Apparently, the cause of this difficulty was the roughness of the electrodes in the switches

of the drivers. Unfortunately, the overhauling of the spark gaps could not be fitted into the time schedule of the experiment.

Table VII

Parameters	Fig. 39	Fig. 40
Major radius r_o	100 cm	100 cm
Torus minor radius a	15.2 cm	15.2 cm
Winding radius ρ_o	23.4 cm	23.4 cm
α	0.03 cm^{-1}	0.03 cm^{-1}
Winding current I_{st}	20 kA	20 kA
Toroidal field $B_{\theta 0}$	3400 G	3400 G
Vertical field B_{z0}	308 G	410 G
Ext. field index n	0.5	0.5
dB_z/dt	0.85 G/μsec	0.85 G/μsec
Initial γ	16.555B	22.389
Initial radial position	-8.26 cm	-7.789
Initial vertical position	1.83 cm	0.283
Mode number ℓ	12	9

Table VIII

Major radius r_o	=	105 cm
Torus minor radius a	=	15.2 cm
Winding radius ρ_o	=	23.4 cm
α	=	0.029 cm^{-1}
Field periods m	=	6
Toroidal field $B_{\theta 0}$	=	3910 G
Vertical field B_{z0}	=	391 G
External field index	=	0.5
dB_z/dt	=	0.656 G/μsec
Cusp radius	=	14.7 cm
Cusp current	=	3 kA
Initial position	=	-10 cm
Initial γ	=	20.25
Run duration	=	60 nsec
Initial $\beta_\perp$	=	0
Mode number ℓ	=	12

Table IX

Toroidal magnetic field at injection	4 kG
SF windings current at injection	28 kA
Driver voltage	35 kV
Average amplitude of the first current step	2.2 kA
Pressure	4×10^{-6} torr
Trapped beam current	1.2 kA

V. Assessement of results

The purpose of this section is to assess the results of the experimental effort. In addition to briefly addressing the major successes and failures of the project, we discuss the level of understanding of the various physical processes that dominate the beam dynamics in the device and we make a few recommendations about the direction of future research in this area.

In the absence of strong focusing, we were able to trap a large number of electron in the device. Although the trapped electron current was as high as 3 kA, the lifetime of the electron ring was limited to a few microseconds. With the exception of the high current rings ($\sim$ 3 kA), the beam was centroid unstable, i.e., the entire beam drifted quickly to the wall of the vacuum chamber. The high current rings were suffering initially individual particle losses, i.e., slow decay of their current. Eventually, after their current was reduced to a low level the loss became catastrophic.

Probably without exception all the electron rings formed were in the high current regime. Attempts to form rings in the low current regime have been unsuccessful. The reason is that the reduced beam current could not provide enough drift to the beam during the first revolution for the electrons to clear the diode of the injector.

There is convincing evidence, but no actual proof, that the catastrophic beam loss was due to the drag instability. There is a large amount of experimental results which supports this conclusion. If we had succeeded to form stable rings in the low current regime, such a conclusion would be more definite.

A quantity that can be measured accurately in the device is the bounce frequency. As

a rule, the bounce frequency measured in the experiment was higher than that predicted by the theory and the codes. It is likely that the beam energy used to compute the bounce frequency is not known with sufficient accuracy.

The addition of the strong focusing windings made a dramatic improvement in the confining properties of the device and established the modified betatron as the first and, as of today, the only successful recirculating high current accelerator. And this, in spite of the fact that the windings have not been carefully fabricated or accurately positioned in the device.

Needless to say that this was the outcome of a necessity rather of a choice and it is contrary to the accepted practice in the technology of particle accelerators. To improve the accuracy of the strong focusing windings a new vacuum chamber was designed with embedded modular windings. It incorporates a new winding law that has a highly desirable feature. The magnetic and geometric axes coincide. Before potting, the windings were positioned on the surface to the vacuum chamber with an estimated accuracy of $\sim \pm$ 0.5 mm, using a winding machine. Unfortunately, the fabrication of the new vacuum chamber was not completed on time and thus the chamber never installed and tested in the experiment.

This is regretable, because there are strong indications that the random spatial fluctuations of the stellarator windings are responsible for the excitation of the cyclotron resonance. Figure 50 shows β_- and $\gamma\beta_\theta$ of the beam centroid in the fields of the modified betatron. The model assumes that the stellarator windings are made of 10 cm long segments that are randomly positioned at each end, within a cube of $\pm$ 2mm. The reference

particle is injected with $\gamma = 8.864$, just before it reaches the ℓ=24 resonance. At t=50 μsec, the centroid locks in the ℓ=19 mode and its $\gamma\beta_\theta$ remains constant. At t=60 μsec $\beta_\perp$ is approximately 30% and the diameter of its fast orbit $\sim$ 7 cm. The efficiency of transfering energy from the axial to the transverse direction by the random fluctuation of the strong focusing winding is remarkable.

The trapping of the injected beam into the closed magnetic field configuration of the device was one of the most challenging physics issues of the modified betatron program. For this reason a large fraction of the program's resources was invested to develop several injection schemes. Ironically, none of these trapping schemes was used in the device after the installation of strong focusing windings. The reason is that when the current of the strong focusing windings was raised to high enough level and the direction of the poloidal orbit was changed from diamagnetic to paramagnetic the beam spiraled from the injection position to the vicinity of the minor axis and was trapped.

This interesting phenomenon has been observed over several thousands of shots and for a wide range of parameters. However, its explanation remained elusive until the beginning of 1991. During January and February, 1991, a series of detailed experiments were performed that provided accurate data on the various processes associated with the trapping of the beam. As a result of these measurements, a revised model of resistive trapping was developed that is in agreement with the experimental results. The fact that the revised model explains not only the main features but also esoteric details of the experimental results, such as the rotation of the peaks of the poloidal orbit with the poloidal angle, makes us believe that the model is correct.

In most of the experiments the center of the circular opening of the conical node was located at the midplane and 8.7 cm from the minor axis of the toroidal chamber. In a series of experiments the diode moved to progressively larger radial positions from the minor axis. Successful trapping of the beam was observed as long as the radial distance was less than 10 cm. At this radial distance the stellarator fields are nonlinear and increase rapidly as the distance from the minor axis increases. Since the radius of the intermediate orbit is proportional to the strong focusing field, it is possible that the beam strikes the wall. Therefore, in order to successfully trap the beam the injection position should be carefully selected.

The slow electron loss rate during acceleration is a manifestation that individual particles, rather than the entire beam, strike the wall. The x-ray signal initially appears at approximately t=τ_x =200 μsec and lasts for as long as 1 msec. Following trapping the beam settles on the magnetic axis of the strong focusing system, which is located about 1 cm off the minor axis. If the guiding center of the beam centroid had remained on the magnetic axis during acceleration, the Larmor radius of the fast motion could not bring the electrons to the wall of the vacuum chamber. Only sufficient axial energy spread in the beam can provide appreciable displacement to the electrons in order to reach the wall. This axial energy spread cannot be due to scattering of beam electrons with the background gas, because τ_x would be a function of the pressure, which is not the case. Random field fluctuations produced by random displacement of say the strong focusing windings have the potential to introduce large axial energy spread to the beam. This conclusion is supported by computer calculations but it has not been confirmed experimentally.

A beam radial drift in combination with the fast motion provide a second mechanism for the electrons to reach the wall. The diffusion of the self magnetic field of the beam cannot provide sufficient radial displacement to the electrons to reach the wall of the chamber. Random spatial fluctuations in the strong focusing windings can provide a potent mechanism for transferring energy to the transverse direction and also a radial inward drift to the beam.

Figure 51 shows very recent results from a 261 μsec long run for randomly positioned stellarator windings. The cube dimensions have increased from $\pm$ 2 mm to $\pm$ 4 mm. The rest of the parameters are listed in Table X. The column in the left shows the positions the beam centroid crosses the $\theta = 0$ plane in the time internal indicated in each frame. The column in the right shows the temporal profile of $\beta_\perp$ and $\gamma\beta_\theta$. At $t \approx 8\mu$sec, the beam locks in the $\ell = 24$ mode and shortly thereafter $\gamma\beta_\theta$ remains constant up to 150 μsec. At this time and while $\beta_\perp$ has reached 78%, the beam unlocks from the $\ell = 24$ resonance and its $\beta_\perp$ starts to decrease. Simultaneously, the centroid starts to drift radially inward with a speed which is approximately 1 mm /μsec. At 261 μsec the beam centroid hits the wall just above the midplane. The similarity between these results and the experiment is striking. Several additional runs have shown that a substantial fraction of electrons inside the beam are not unstable to this kind of perturbations.

Although the mechanism that drives the electrons to the wall during acceleration has probably been identified, a definite proof is still missing. A diagnostic that can provide information on the beam position during acceleration would be very useful. The experimental results from the NRL device have unambiguously demonstrated that the electron

loss is reduced and the beam lifetime is prologued with increasing toroidal field. The beneficial effect of B_θ is not limited to the confinement of the beam during acceleration. As a rule, the trapped electron current is enhanced with increasing B_θ field.

Since the initial successful acceleration of electrons in the modified betatron, the x-ray signal is spiky and the peaks always occur at the same value of $B_{\theta 0}/B_{z0}$, independently of the current flowing in the stellarator windings. There is extensive experimental evidence that support the hypothesis that the spiky x-ray signal is caused by the excitation of the cyclotron resonances. During the last few years a large amount of work, both experimental and theoretical, has been done, mainly by the NRL research staff, on the crossing of cyclotron resonances and the subject appears to be well understood.

The cyclotron resonance is due to coupling, caused by field disturbances, between the cyclotron motions in the vertical and toroidal fields. Since the actual accelerating gradient in the present device is low, the electrons have to perform a large number of revolutions around the major axis in order to obtain large energies. Thus, cyclotron resonances are of special importance for the existing device, that has low tolerance to field errors.

Following the successful demonstration of acceleration a concerted effort was made to locate and eliminate, or at least reduce, the field distrubances that may excite the cyclotron resonances. Most of the errors detected were reduced to a level that was limited by the sensitivity of the magnetic field monitors ($\sim 2\%$). To reduce the errors produced by the mispositioned strong focusing windings a new vacuum chamber with very accurately positioned windings was constructed and partially fabricated. The large amplitude errors at the feeds of the vertical field coils were never corrected, mainly because the cost of

repair was beyond the limits of the project's budget.

Three different cyclotron resonance stabilization techniques were tested in the experiment. Among these techniques, acceleration of the beam at higher acceleration rate appears to have the highest practical potential. By increasing the acceleration rate the resonance is crossed faster and thus the damage inflicted to the beam is reduced. To achieve higher acceleration rate, the vertical field coils were divided into two halves with midplane symmetry and powered in parallel. The experimental results indicate that an increase in the acceleration rate by approximately a factor of 2.5 has a profound effect on the cyclotron resonances.

Although the cyclotron resonance is a potent mechanism that has the potential to disturb the beam at low acceleration rate and when the various fields are not carefully designed, it also may provide a powerful technique for extracting the beam from the magnetic field configuration of the modified betatron. As a matter of fact, this was realized well before the cyclotron resonances were observed in the NRL device.

Although the fabrication of the hardware for the resonant extraction approach that was the mainline extraction scheme for the NRL device was completed by the end of FY 91, the resonant extraction was never tested experimentally. The reason that this extraction technique is based on a low inductance ($\sim$ 4 nH) agitator with a very small aperture ($\sim$ 2 cm). Therefore, it requires a beam with low transverse velocity. However, this was not the case in the NRL experiment. The amplitude of the various field imperfections was never reduced to a low enough level to make the transverse velocity of the beam compatible with the small aperture of the agitator. Thus, we had to explore alternate extraction approaches

that are based on large aperture agitators.

Initially, twelve single turn coils were used either on the outside of the vacuum chamber or at the joints of twelve sectors. The coils were activated at the time the beam was crossing the ℓ=12 mode. These resonant coils were powered with 12, 5 and 0.4 μsec risetime current pulses. The beam could be kicked out of the magnetic field of the device within a time that was comparable to the risetime of the current pulse. The required amplitude of axial field disturbances ΔB_θ to extract the entire beam during the risetime of the field pulse is approximately 80 G.

Extensive studies of the spatial distribution of beam losses when the twelve internal resonant coils are energized with the 0.4 μsec current pulse have shown that the beam strikes the wall at six very well defined toroidal positions that are 60° apart. In the absence of the strong focusing field (when the resonant coils are energized) the beam strikes the wall at a single toroidal position near θ=70°. Although the results with the twelve resonant coils are very interesting and provided a valuable insight in the physics of extraction, this approach cannot lead to a practical extraction scheme, since it cannot form a single head in the beam. In addition to being capable of forming a single, well defined head in the beam, a practical agitator should have low inductance, large aperture and the capability to produce the required magnetic field disturbances at manageable voltages. Among the various agitator concepts considered, magnetic cusps were found to be the most promising.

Extensive numerical studies of several cusp configurations have shown that a single layer, 24.2 cm long cusp surrounded by a resistive shroud with a 21 cm radius could provide $\sim$ 1.4 cm radial displacement to the beam over a 20 nsec time period, when the current

through the coil is 2.5 kA. Unfortunately such a cusp could not be fabricated on time and thus we had to proceed with an inferior agitator that is based on three double cusps that are located 120° apart in the toroidal direction. This agitating system was fabricated in-house and tested in the experiment for a short period of time just before the termination of the MBA program.

The numerical results indicate that the 14.7 cm radius double cusps could provide 0.9 cm radial displacement during the last 20 nsec of a 60 nsec wide, 3 kA height rectangular current pulse. These cusps have been powered with 2-3 nsec risetime current pulses produced from the existing drivers with ferrite sharpeners. At 40 kV charge voltages the amplitude of the current step was 2.6 kA and its risetime $\sim$ 50 nsec and was solely determined by the inductance of the coil. Activation of these double cusps at 480 μsec, i.e., when the ℓ=12 resonance is crossed forced most of the beam to exit the magnetic field configuration in a single ℓ mode, as it is apparent from Fig. 49.

In contrast with the conventional accelerators that operate in the single-particle regime, the high current modified betatron operates in an uncharted territory, in which space charge effects from the self and image fields are as important as externally applied fields. Virtually, every aspect of the modified betatron has been a challenging technical task. As a result, the pace of progress has been slower than initially anticipated. However, the results have been very rewarding.

The extraction of the beam is presently the most important unresolved technical issue. Although some interesting results were obtained during the last few month with the NRL device, there are several fundamental questions that remain. Developing a large aperture

agitator with 1-2 nsec risetime that provides enough field to kick the beam radially by $\sim$ 2-3 cm at a reasonable voltage is not, in principle, a difficult task. However, when the integration of such an agitator into the device is considered, the task becomes considerably more complex. Specifically, the penetration of the fast fields requires the agitator to be located inside the chamber. To avoid any interference with the circulating beam the agitator should be near the wall of the chamber. This wall has to be continuous to avoid disruption of the return currents. The induced current on the wall by the rapidly changing field of the cusp substantially reduces its various field components. However, the proximity of the coils to the wall diminishes the inductance of the kicker. Although the voltage required to produce a specific field amplitude within a specific time is smaller with an internal cusp, introducing the high voltage into the chamber without adding substantial inductance to the system is a challenging engineering task.

Our diagnostics that probe the beam dynamics during the first few microseconds following injection, have been found both reliable and sufficient. However, our diagnostics that provide information on the beam current, position, size, axial energy spread and emittance during the acceleration phase have been found very inadequate. The development of such diagnostics that provide reliable information on the millisecond time scale will be both diffucult and expensive. Such a task, however, will be necessary in any serious future effort on the modified betatron or any other high current recirculating accelerator.

Our results have unambiguously demonstrated that the strong focusing windings improve the confining properties of the device at least in the intermediate time scale, i.e, during the first 100-200 μsec. In addition, these windings have increased substantially the

complexity of the accelerator. The loss of toroidal symmetry with the incorporation of the stellarator windings in the NRL initial system made our two dimensional particle simulation computer codes obsolete. The absence of a reliable 3-D computer simulation code to provide information on the dynamics of the individual particles inside the beam has inhibited our ability to completely understand the x-ray spectra. Any future investment in the modified betatron technology should include funds for either the development or the acquisition of a 3-D particle simulation code.

Undoubtedly, the modified betatron has several important advantages, in relation to other approaches, in the generation of high current beams. Among its shortcomings, its sensitivity to field errors is of concern. The port in the wall of the vacuum chamber that is required for any internal injection could be the source of a serious field error. By its nature, the injector porthole error cannot be eliminated as long as the diode is located inside the chamber. Therefore, it is advisable that an external injection scheme be developed that will eliminate or at least substantially reduce the size of the diode porthole. An additional advantage of the external injection is its compatibility with higher diode voltages. Such higher voltages will be necessary whenever the current of the device will be required to be raised well above the 1 kA level.

As a consequence of its sensitivity to field errors, any future device should be carefully designed to keep the field errors as low as possible but not much higher than 0.1%. Furtheremore, it will be very advantageous to select the acceleration rate ten times higher than in the present device, i.e., about 8-10 G/μsec.

Table X

Major radius r_o	= 100 cm
Torus minor radius a	= 15.2 cm
Toroidal magn. field $B_{\theta o}$	= 3 kG
Vertical magn. field B_{zo}	= 120 G
Relativistic factor γ at inj.	= 7.02
α	= 0.03 cm $^{-1}$
Minor radius of windings ρ_o	= 23.4 cm
Current in the St. windings	= 25 kA
dB_z/dt	= 0.69 G/μsec
Initial radial position (r-r_o)	= - 0.14 cm
Initial vertical position Z	= 0.0 cm
Initial transverse velocities $v_r = v_z$	= 0

References

* FM Technologies, Inc., 10529-B Braddock Road, Fairfax, Virginia

† SFA, Inc., Landover, Maryland 20785

** Science Applications International Corp., 170 Goodridge Drive, McLean, Virginia 22102

1. R. C. Davidson, *An Introduction to the Physics of Nonneutral Plasmas,* Addison-Wesley Publ. Co (1990). Chapter 4 of this book contains a comprehensive list of theoretical papers on the modified betatron.

2. P. Sprangle and C.A. Kapetanakos, *J. Appl. Phys.* **49**, 1 (1978).

3. D. Kerst and J. Lawson, private communication.

4. D. Kerst, *Phys. Rev.* **60**, 47 (1941); also Encycl. of Appl. Phys.**2**, 347 (1991).

5. P. J. Gratreau, U. S. Patent Number 3, 377, 563 (1968).

6. A. G. Bonch - Osmolovsky, Joint Institute for Nuclear Research, Dubua, USSR, Preprint No. P9-5299 (1970). Translated by G. Brodell and L. Jackson Laslett, UCRL- Trans. -1446 (1971).

7. G. I. Budker, *Proc. of the CERN Symposium on High Energy Accel. and Pion. Phys.*, Geneva, Switzerland (1956).

8. J. G. Linhart, *Proc. of the 4th Conf. on Ion. Phen. in Gases, Uppsala* (1959); Also *Plasma Phys.* (1960).

9. P. Reynolds and H.M. Skarsgard, *J. Nucl. Energy Part.* C1, **36** (1959).

10. H. Ishizuka, R. Prohasko, A. Fisher, and N. Rostoker, in *Proceedings of the 7th International Conference on High-Power Particle Beams* (Kernforschungszentrum Karlsruhe GmbH, Karlsruhe, Germany, 1988), Vol II, p. 857; Also H. Ishizuka, G. Leslie, B. Mandelbaum, A. Fisher and N. Rostoker, *IEEE Trans. Nucl Sci.* NS-32, 2727 (1985).

11. J. Golden, F. Mako, L. Floyd, K. McDonald, T. Smith, D. Dialetis, S. J. Marsh and C.A. Kapetanakos, *Proc. of the 6th Intern. Conf. on High-Power Particle Beams*, Kobe, Japan, P. 709 (1986).

12. J. Golden, L. K. Len, A. V. Deniz, J. Mathew, T. J. Smith, P. Loschialpo, J. H. Chang, D. Dialetis, S. J. Marsh and C. A. Kapetanakos, *Proc. of the 7th Intern. Conf. on High Power Particle Beams,* 88 Karlsruhe, FRG, Vol. I, 221 (1988).

13. C. Roberson, A. Mondelli, and D. Chernin, *Phys. Rev. Lett.* **50**, 507 (1983).

14. C. A. Kapetanakos, D. Dialetis and S. J. Marsh, *Part. Accel.* **21**, 1 (1987).

15. C. A. Kapetanakos, L. K. Len, T. Smith, J. Golden, K. Smith, S. J. Marsh, D. Dialetis, J. Mathew, P. Loschialpo, and J. H. Chang, *Phys. Rev. Lett.* **64**, 2374 (1990).

16. C.A. Kapetanakos, L. K. Len, T. Smith, D. Dialetis, S. J. Marsh, P. Loschialpo, J. Golden, J. Mathew and J. H. Chang, *Phys. Fluids B,* **3**, 2396 (1991).

17. J. Golden, L. K. Len, T. J. Smith, J. Mathew, P. Loschialpo, L. Seto, J. H. Chang and C. A. Kapetanakos, *Proc. of SPIE,* Vol. **1407**, p. 418 (1991).

18. L. K. Len, T. Smith, P. Loschialpo, J. Mathew, S. J. Marsh, D. Dialetis, J. Golden, J. H. Chang and C. A. Kapetanakos, *Proc. of the SPIE Conf.* Vol. 1629, p. 521 (1992).

19. C. A. Kapetanakos, L. K. Len, T. Smith, P. Loschialpo, J. Mathew, S. J. Marsh, D. Dialetis, J. Golden and J. H. Chang, NRL Memo Report NRL/MR/4795-92-6988 (1992).

20. C. A. Kapetanakos, S. J. Marsh, and D. Dialetis, *Phys. Rev. Lett.* **61**, 86 (1986).

21. P. Sprangle, C. A. Kapetanakos and S. J. Marsh *Proc. of the 4th Intern. Conf. on High Power Electron and Ion Beam Research and Tech.*, Vol. **2**, p. 803 (1981).

22. C. A. Kapetanakos, P. Sprangle, D. P. Chernin, S. J. Marsh and I. Haber, *Phys. Fluids*, **26**, 1634 (1983).

23. D. P. Chernin and P. Sprangle, *Part. Accel.* **12**, 85 (1982).

24. C. A. Kapetanakos and S. J. Marsh, *Phys. Fluids* **28**, 2263 (1985).

25. C. A. Kapetanakos and P. Sprangle, NRL Memo Report No. 5388 (1984).

26. P. Loschialpo, S. J. Marsh, L. K. Len, T. Smith and C. A. Kapetanakos, Subm. to *Rev. Sc. Inst.* (1992).

27. C. A. Kapetanakos and P. Sprangle, U. S. Patent Number 4, 481, 475 (1984).

28. L. K. Len, T. Smith, J. Golden, K. Smith, S. J. Marsh, D. Dialetis, J. Mathew, P. Loschialpo, J. H. Chang, and C. A. Kapetanakos, *Proceedings of International Society for Optical Engineers (SPIE)* (SPIE, Bellingham, WA, 1990), Vol. 1226, p. 382.

29. P. Sprangle and C. A. Kapetanakos, **14**, 15 (1983).

30. R. L. Gluckstern, in *Proceedings of Linear Accelerator Conference* (Brookhaven Laboratory, Upton, NY, 1979), p. 245

31. C. A. Kapetanakos, P. Sprangle, S. J. Marsh, D. Dialetis and C. Agritellis, *Part. Accel.* **18**, 73 (1985).

32. S. J. Marsh, J. Golden, C. A. Kapetanakos and D. Anderson, *J. Appl. Phys.* **64**, 6138 (1988).

33. P. Sprangle and C. A. Kapetanakos, *Part. Accel.* **18**, 203 (1986).

34. J. Mathew, S. J. Marsh, D. Dialetis and C. A. Kapetanakos, NRL Memo Report No. NRL/MR/4795-92-7114 (1992).

35. C. A. Kapetanakos, D. Dialetis, S. J. Marsh, L. K. Len and T. Smith, *Phys. Rev. A* **44**, 3900 (1991).

36. D. Dialetis, S. J. Marsh and C. A. Kapetanakos, NRL Memo Report No. NRL/MR/4795-92-6985 (1992).

37. W. M. Manheimer and J. Finn, Part. Accel. **14**, 29 (1983).

38. I. Haber, S. J. Marsh and P. Sprangle, *Proc. of the 5th Intern. Conf. on High Power Particle Beams*, p. 485 (1983).

39. C. W. Roberson, A. Mondelli, and D. Chernin, *Part. Accel.* **17**, 79 (1985).

40. D. Chernin and P. Sprangle, *Part. Accel.* **12**, 101 (1982).

41. D. Dialetis, S. J. Marsh and C. A. Kapetanakos, Subm. to *Phys. Rev. A* (1992).

42. M. Weiner, *IEEE Trans. on Magnetics*, Vol. Mag.-17, 1472 (1981).

Appendix

Publications by the NRL

research staff.

Publications by the NRL researh staff

I. MODIFIED BETATRON ACCELERATOR (MBA)

(With and Without Strong Focusing)

A. THEORY

INJECTION

Injection of a High-Current Beam into a Modified Betatron Accelerator, C. A. Kapetanakos, P. Sprangle, and S. J. Marsh, Phys. Rev. Letts. 49, 741 (1982); Also, NRL Memo Report No. 4835 (1982).

External Injection into a High Current Modified Betatron, F. Mako, W. M. Manheimer, D. P. Chernin, F. Sandel, and C. A. Kapetanakos, Phys. Fluids 27, 2211 (1984); Also, NRL Memo Report No. 5196 (1983).

Simulation Studies on a Novel Modified Betatron Injection Scheme, W. Peter, R. J. Faehl, and F. Mako, Beams 83, 458, Proc. of the 5th Intl. Conf. on High Power Particle Beams (1983).

Beam Trapping in High Current Cyclic Accelerators with Strong Focusing Fields, P. Sprangle and C. A. Kapetanakos, Part. Accel. 18, 203 (1986); Also, NRL Memo Report No. 5458 (1985).

Beam Trapping in a Modified Betatron with Torsatron Windings, C. A. Kapetanakos, D. Dialetis and S. J. Marsh, Part. Accel., 21, 1 (1987); Also, NRL Memo Report No. 5619 (1985).

Beam Trapping in a Modified Betatron with Torsatron Windings, C. A. Kapetanakos, D. Dialetis, and S. J. Marsh, Proc. of the Compact Accelerators Technology Conference (Secret) Special Publication BRL-SP-52, p. 127 (1986).

A passive method to Trap an Electron Beam in a Stellatron Accelerator, A. V. Deniz, J. Appl. Phys. 69, 1151 (1991).

Dissipative Beam Trapping in a Modified Betatron with Strong Focusing, Y. Seo and P. Sprangle, Part. Accel. (1992).

Diffusion of the Self Magnetic Fields of an Electron Beam through a Resistive Toroidal Chamber, D. Dialetis, S. J. Marsh, and C. A. Kapetanakos, Sumbitted to J. of Th. Physics, (1992); Also, NRL Memo Report No. NRL/MR/4795-92-6985 (1992).

EQUILIBRIUM

Constant Radius Magnetic Acceleration of a Strong Non-neutral Proton Ring, P. Sprangle and C.A. Kapetanakos, J. Appl. Phys. 49, 1 (1978).

Dynamics of an Intense Electron Ring in a Modified Betatron Field, P. Sprangle, C. A. Kapetanakos, and S. J. Marsh, Proc. of the 4th Intl. Top. Conf. on High Power Electron and Ion Beam Research and Technology, Vol. 2, page 803 (1981); Also, NRL Memo Report No. 4666 (1981).

Equilibrium of a High Current Electron Ring in a Modified Betatron Accelerator, C. A. Kapetanakos, P. Sprangle, D. P. Chernin, S. J. Marsh, and I. Haber, Phys. Fluids, 26, 1634 (1983); Also, NRL Memo Report No. 4905 (1982).

Transverse Beam Dynamics in a Modified Betatron, D. P. Chernin and P. Sprangle, Part. Accel. 12, 85, (1982).

Self Consistent Theory of Equilibrium and Acceleration of a High Current Electron Ring in a Modified Betatron, W. M. Manheimer and J. Finn, Part. Accel. 14, 29 (1983).

The Stellatron - A high Current Betatron with Stellerator Fields, C. W. Roberson, A. Mondelli, and D. Chernin, Phys. Rev. Letters, 50, 507 (1983).

The Effect of Field Index Fluctuation on the Dynamics of a High Current Ring, C. Agritellis, S. J. Marsh, and C. A. Kapetanakos, Part. Accel. 16, 155 (1985); Also, NRL Memo Report No. 5141 (1983).

Self Potentials of an Electron Ring in a Torus for Large Displacement from the Minor Axis, C. A. Kapetanakos and P. Sprangle, NRL Memo Report No. 5388 (1984).

Non-linear Transverse Electron Beam Dynamics in a Modified Betatron Accelerator, C. A. Kapetanakos and S. J. Marsh, Phys. Fluids 28, 2263 (1985); Also, NRL Memo Report No. 5387 (1984).

Acceleration of an Electron Ring in a Modified Betatron with Transverse Pressure, J. M. Grossman, J. M. Finn, and W. M. Manheimer, Phys. Fluids 28, 695 (1985); Also, NRL Memo Report No. 5444 (1984).

Flux Diffusion and Acceleration in a High Current Modified Betatron, J. M. Grossman and W. M. Manheimer, Part. Accel. 16, 185 (1985).

The Plasma Assisted Modified Betatron, W. M. Manheimer, Part. Accel. 17, 157 (1985); Also, NRL Memo Report No. 5459 (1984)

Improving the Current-Carrying Capability of the Modified Betatron, C. A. Kapetanakos, D. Dialetis, and S. J. Marsh, Nucl. Inst. and Methods in Physics Research B24/25, 805 (1987).

Self Consistent Theory of Equilibrium and Adiabatic Evolution of a High Current Electron Ring in a Modified Betatron, J. M. Finn and W. M. Manheimer, Phys. Fluids 26, 3400 (1983).

Studies of the Electron-Ring Dynamics in a Modified Betatron for Large Ring Displacement from the Minor Axis, S. J. Marsh and C. A. Kapetanakos, Part. Accel. 23, (1988). Also, NRL Memo Report No. 5933 (1987).

STABILITY

Longitudinal and Transverse Instabilities in a High Current Modified Betatron Electron Accelerator, P. Sprangle and J. L. Vomroridis, Part. Accel. 18, 1 (1985); Also, NRL Memo Report No. 4688 (1984).

Electron-Ion Instabilities in a High Current Modified Betatron, W. M. Manheimer, Part. Accel. 13, 209 (1983).

Drag Instability in a Modified Betatron, P. Sprangle and C. A. Kapetanakos, Part. Accel. 14, 15 (1983); Also, NRL Memo Report No. 4950 (1983).

Integer Resonances in a Modified Betatron, D. Chernin and P. Sprangle, Part. Accel. **12**, 101 (1982).

Beam Current Limitations Due to Instabilities in Modified and Conventional Betatrons, P. Sprangle and D. Chernin, Part. Accel. **15**, 35 (1984); Also, NRL Memo Report No. 5176 (1983).

Emittance Growth in a Modified Betatron Crossing the Orbital-Turning-Point Transition, I. Haber, S. J. Marsh, and P. Sprangle, Proc. of the 5th Intl. Conf. on High Power Particle Beams, Page 485 (1983).

Self-Consistent Modified Betatron Equilibria and their Adiabatic Evolution, J. Grossman, W. M. Manheimer, and J. Finn, Proc. of the 5th Intl. Conf. on High Particle Beams, page 489 (1983).

Stabilization of the Negative Mass Instability in a Rotating Relativistic Electron Beam, Y. Y. Lau and D. Chernin, Phys. Rev. Letts. **52**, 1425 (1984).

Mode Coupling in the Modified Betatron, D. P. Chernin, Part Accel. **14**, 139 (1984); Also, NRL Report No. 5061 (1984).

Dynamic Behavior of an Electron Ring Close to a Cyclotron Resonance in a Modified Betatron Accelerator, D. Dialetis, S. J. Marsh, and C. A. Kapetanakos. Submitted to Phys. Rev. (1992).

Current Loss in Modified Betatrons Due to Field Error Resonances, E. Esarey, P. Sprangle, S. J. Marsh, and Y. H. Seo, NRL Memo Report No. 6694 (1992).

EXTRACTION

Injection and Extraction of a Relativistic Electron Beam in a Modified Betatron, B. Hui and Y. Y. Lau, Phys. Rev. Lett. 53 2024 (1984).

High Midplane Accessibility Stellarator Windings for High Current Toroidal Accelerators, S. J. Marsh, J. Golden, and C. A. Kapetanakos, J. Appl. Phys. 64, 6138 (1988); Also, NRL Memo Report No. 6025 (1987).

Beam Extraction Scheme from the Modified Betatron Accelerator, C. A. Kapetanakos, S. J. Marsh, and D. Dialetis, Phys. Rev. Lett. 61, 86 (1988); Also, NRL Memo Report No. 6214 (1988).

B. EXPERIMENT

Preliminary Design of the NRL Modified Betatron, J. Golden, J. A. Pasour, D. E. Pershing, K. Smith, F. Mako, S. Slinker, F. Mora, N. Orrick, R. Altes, A. Flifiet, P. Champney, and C. A. Kapetanakos, Proc. of IEEE Trans. Nucl. Science, NS-30, 2114 (1983).

Pulsed, Low-Error, High Current TF and VF Coils with Demountable Joints, F. Mako, K. Smith, J. A. Pasour, D. E. Pershing, K. McDonald, R. Altes, J. Golden, and C. A. Kapetanakos, Proc. of 10th Symp. on Fusion Eng., Philadelphia, PA. (1983).

The NRL Modified Betatron, J. Golden, F. Mako, L. Floyd, K. McDonald, T. Smith, P. Sprangle, and C. A. Kapetanakos, Proc. of the Compact Accelerators Technology Conference (Secret) Special Publication BRL-SP-52, p. 121 (1986).

Measurements of Fuse and Resistor Characteristics for Multimagajoule Capacitor Bank Applications, K. F. McDonald, T. Smith, J. Golden, L. Floyd, and B. Conley, Rev. Sci. Instrum. 58, 1287 (1987).

Internal Injection into the NRL Modified Betatron, F. Mako, J. Golden, L. Floyd, K. McDonald, T. Smith, and C. A. Kapetanakos, IEEE Trans. on Nucl. Sci., Vol. NS-32, 3027 (1985).

Modified Betatron Data Acquisition and Control System, L. Floyd, J. Golden, T. Smith, E. Day and S. J. Marsh, IEEE Trans. Nucl. Sci. NS-32 #5, 2092 (1985).

Controls and Data Acquisition for the NRL Modified Betatron Accelerator, L. Floyd, J. Golden, T. Smith, E. Day and S. J. Marsh, LANL Accelerator Control Workshop Proc., Nucl. Methods and Instrum., A247, 68, (1986).

Progress in the Development of the NRL Modified Betatron Accelerator, J. Golden, F. Mako, L. Floyd, K. McDonald, T. Smith, D. Dialetis, S. J. Marsh, and C. A. Kapetanakos, Proc. of the 6th Intl. Conf. on High Power Beams, 709 (1986).

Beam "Self-Trapping" in the NRL Modified Betatron Accelerator, F. Mako, J. Golden, D. Dialetis, L. Floyd, N. King, and C. A. Kapetanakos, Proceedings of the High Brightness Accelerators 773 (1988).

The NRL Modified Betatron Accelerator Pulsed Power System, K. F. McDonald, F. Mako, T. Smith, L. Floyd, J. Golden and C. A. Kapetanakos, Proc. of the 5th Pulsed Power Conf. (1986).

A Novel Trapping Scheme in the Modified Betatron Accelerator, J. Golden, F. Mako, L. Floyd, T. Smith, D. Dialetis, S. J. Marsh, and C. A. Kapetanakos, IEEE Part. Accel. Conf. Vol. 2, 936 (1987).

Studies of a Multikiloamphere Electron Ring Confined in a Modified Betatron Accelerator, J. Golden, L. K. Len, A. Deniz, J. Mathew, T. J. Smith, P. Loschialpo, J. H. Chang, D. Dialetis, S. J. Marsh, and C. A. Kapetanakos, Proc. of the 7th International Conference on High Power Particle Beams-Beams '88, Karlsruhe FRG, Vol. I, 221 (1988).

Progress in the Development of the NRL Modified Betatron Accelerator, L. K. Len, T. Smith, J. Golden, K. Smith, S. J. Marsh, D. Dialetis, J. Mathew, P. Loschialpo, J. H. Chang, and C. A Kapetanakos, Proc. of SPIE Vol. 1226, p. 382 (1990).

Improved Beam Confinement in the Modified Betatron with Strong Focusing, C. A. Kapetanak s, L. K. Len, T. Smith, J. Golden, K. Smith, S. J. Marsh, D. Dialetis, J. Mathew, P. Loschialpo, and J. H. Chang, Phys. Rev. Lett. 64 2374 (1990).

Diffusion of magnetic Fields in a Toroidal Conducting Shell of Circular Cross Section, D. Dialetis, L. K. Len, J. Golden, and C. A. Kapetanakos, J. Appl. Phys., 69, 1813 (1991); Also, NRL Memo Report No. 6719 (1990).

Compact, High Current Accelerators and their Prospective Application, C. A. Kapetanakos, L. K. Len, T. Smith, D. Dialetis, S. J. Marsh, P. Loschialpo, J. Golden, J. Mathew, and J. H. Chang, Phys. Fluids B3 2396 (1991).

Studies of Synchrotron Radiation Emission from the NRL Modified Betatron, T. Smith,

J. Golden, and C. A. Kapetanakos, J. Appl. Phys. 69, 6836 (1991); Also, NRL Memo Report No. 6774 (1991).

The NRL Modified Betatron Accelerator, L. K. Len, T. Smith, J. Golden, S. J. Marsh, D. Dialetis, J. Mathew, P. Loschialpo, J. H. Chang and C. A. Kapetanakos, Proc. of Eur. Part. Accel. Conf. Vol. 1, p. 446 (1991).

Studies of the Integer Cyclotron Resonances in a Modified Betatron Accelerator, C. A. Kapetanakos, L. K. Len, T. Smith, P. Loschialpo, J. Mathew, S. J. Marsh, D. Dialetis, J. Golden, and J. H. Chang; To be published in the Proceedings of the DARPA/Services Conference (1992); Also, NRL Memo Report No. 6988 (1992).

Excitation of the $\ell = 12$ Cyclotron Resonance in the NRL Modified Betatron Accelerator, L. K. Len, T. Smith, P. Loschialpo, J. Mathew, S. J. Marsh, D. Dialetis, J. Golden, J. H. Chang, and C. A. Kapetanakos, Proc. of the SPIE Conf. Vol. 1629, p. 521 (1992).

Identification of Toroidal Field Errors in a Modified Betatron Accelerator, P. Loschialpo, S. J. Marsh, L. K. Len, T. Smith, and C. A. Kapetanakos, Submitted to Rev. of Sci. Inst., (1992).

Beam Trapping in a Modified Betatron Accelerator, C. A. Kapetanakos, D. Dialetis, S. J. Marsh, L. K. Len, and T. Smith, Phys. Rev. A 44, 3900 (1991); Also, NRL Memo Report No. 6808 (1991).

Recent Developments on the NRL Modified Betatron Accelerator, J. Golden, L. K. Len, T. J. Smith, J. Mathew, P. Loschialpo, L. Seto, J. H. Chang, and C. A. Kapetanakos, Proc. of SPIE Vol. 1407, p. 418 (1991).

Beam Trapping in a Modified Betatron with a Localized Bipolar Electric Field Pulse, J. Mathew, S. J. Marsh, D. Dialetis, and C. A. Kapetanakos, Submitted to J. Appl. Physics; Also, NRL Memo Report No. NRL/MR/4795-92-7114 (1992).

Output Switch for a Megavolt Electron Beam Generator, J. Mathew and J. Golden, Rev. Sci. Instrum. **62**, 1514 (1991).

II. OTHER HIGH CURRENT ACCELERATORS

High Current, High Voltage Accelerators as Free electron Lasers Drivers, C. W. Roberson, J. A. Pasour, C. A. Kapetanakos, P Sprangle, J. Golden, F. Mako, and R. Lucey, Proc. of Free Electron Laser Conference in Sun Valley, ID, September (1981).

Energy Scaling Laws for the Racetrack Induction Accelerator, A. A. Mondelli, and C. W. Roberson, Part. Accel. **15**, 221 (1984); Also, NRL Report No. 5008 (1982).

Dynamics of a High-Current Electron Ring in a Conventional Betatron Accelerator, C. A. Kapetanakos, S. J. Marsh, and P. Sprangle, Part. Accel. **14**, 261 (1984); Also, NRL Memo Report 5108 (1983).

Recent Developments in Ultra-High Current Electron Induction Accelerators, C. A. Kapetanakos, and P. Sprangle. Phys. Today, February (1985); Also, NRL Memo Report No. 5259 (1984).

Studies of a Rapid Electron Beam Accelerator (REBATRON), C. A. Kapetanakos, P. Sprangle, S. J. Marsh, D. Dialetis, and C. Agritellis, Part. Accel. **18**, 73 (1985); Also, NRL Memo Report No. 5503 (1985).

The REBATRON as a High Energy Accelerator, D. Dialetis, S. J. Marsh, and C. A. Kapetanakos, NRL Memo Report No. 5655 (1986).

Recent Rebatron Studies, A. Prakash, S. J. Marsh, D. Dialetis, C. Agritellis, P. Sprangle, and C. A. Kapetanakos, IEEE Trans. on Nucl. Sci., Vol. NS-32, 3265 (1986).

Analysis of the Acceleration Process in a Rebatron, D. Dialetis, S. J. Marsh, and C. A. Kapetanakos, Part Accel. 21, 227 (1987).

Ultra-High Current Accelerators, C. A. Kapetanakos, McGraw-Hill Yearbook of Science and Technology 348-350 (1987).

The Fast Modified Betatron Accelerator, C. A. Kapetanakos, J. of Defense Res. 21, 541 (1992). (SECRET).

Ph.D Thesis

Study of the Synchrotron Radiation Emission from the NRL Modified Betatron Accelerator, Tab Smith, Doctor of Philosophy, Univ. of Maryland, 1990.

Patents

Betatron Accelerator having High Ration of Budker Parameter to Relativistic Factor, C. A. Kapetanakos and P. Sprangle, U.S. Patent No. 4, 481, 475 (1984).

Low Perturbation Electron Injector for Cyclic Accelerators, F. Mako, W. Manheimer, C. A. Kapetanakos and F. Sandel, U.S. Patent No. 4, 608, 537 (1986).

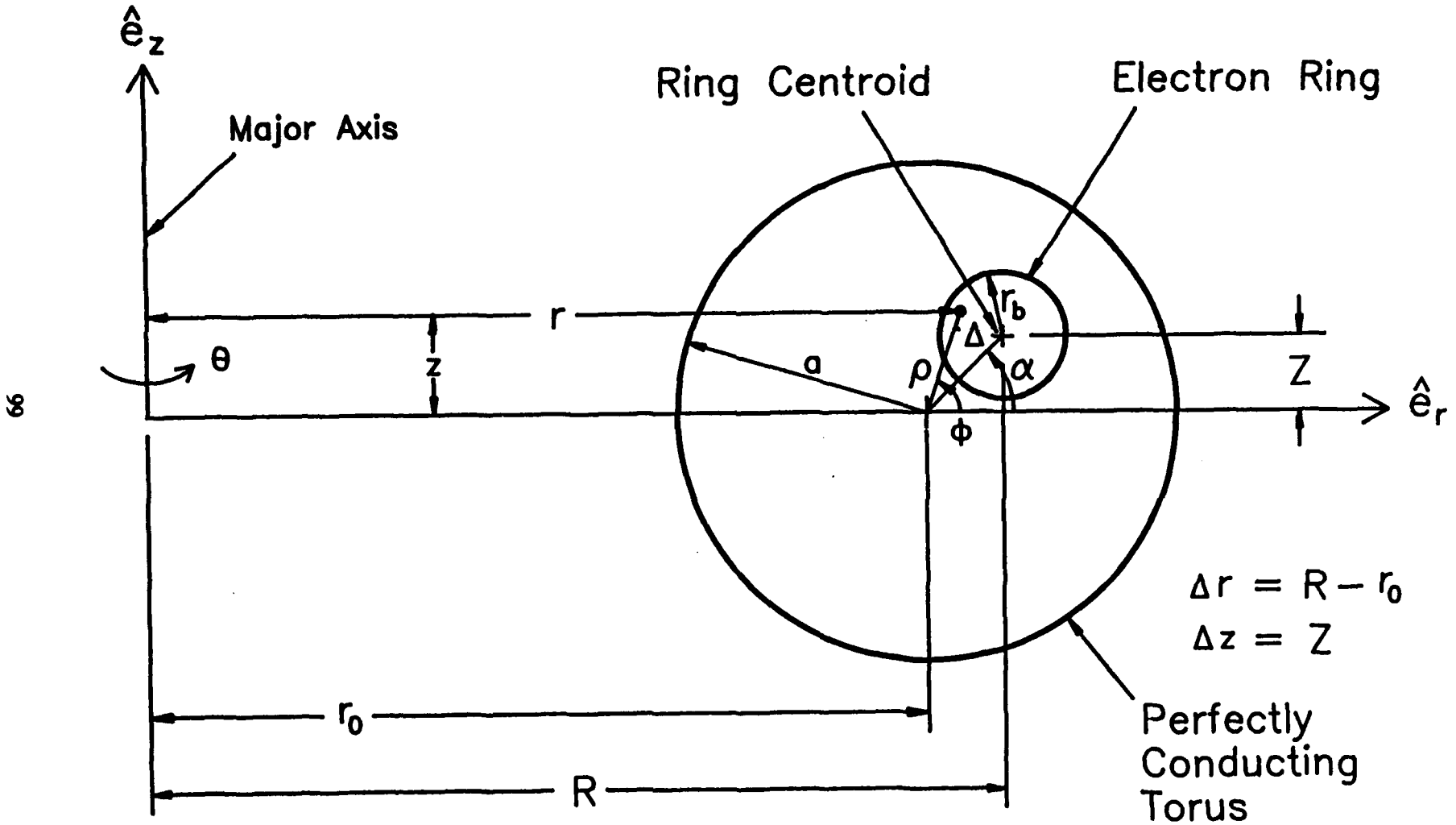

Fig. 1. System of coordinates.

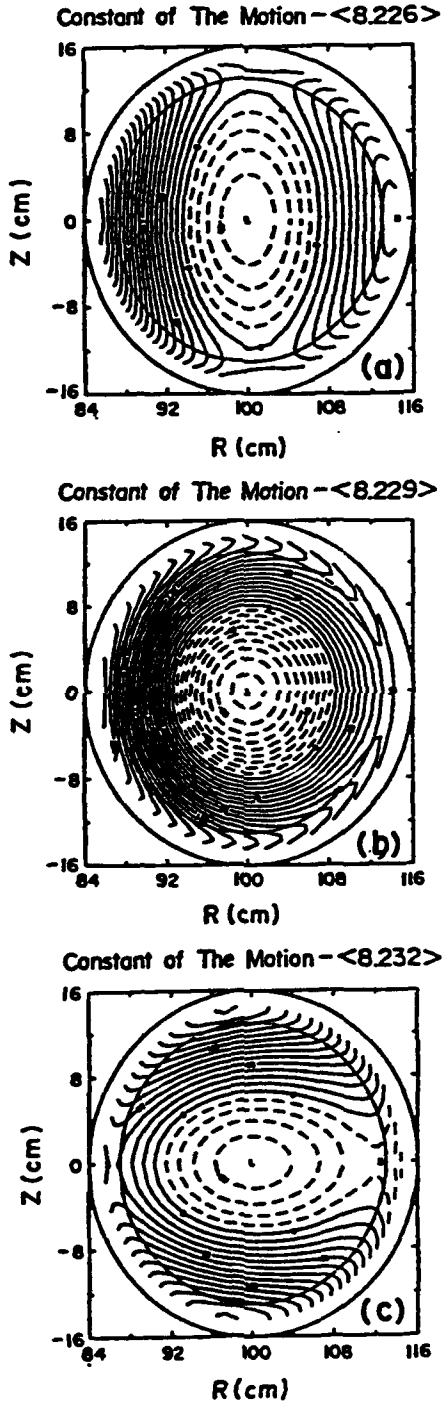

Fig. 2. Orbits of ring centroid in the transverse plane from Eq. (7b) and the potentials of Eq. (11). In (a) the external field index is 0.35, in (b) 0.5 and in (c) 0.65.

Modified Betatron without Strong Focusing
Ring Centroid Orbital Stability Diagram

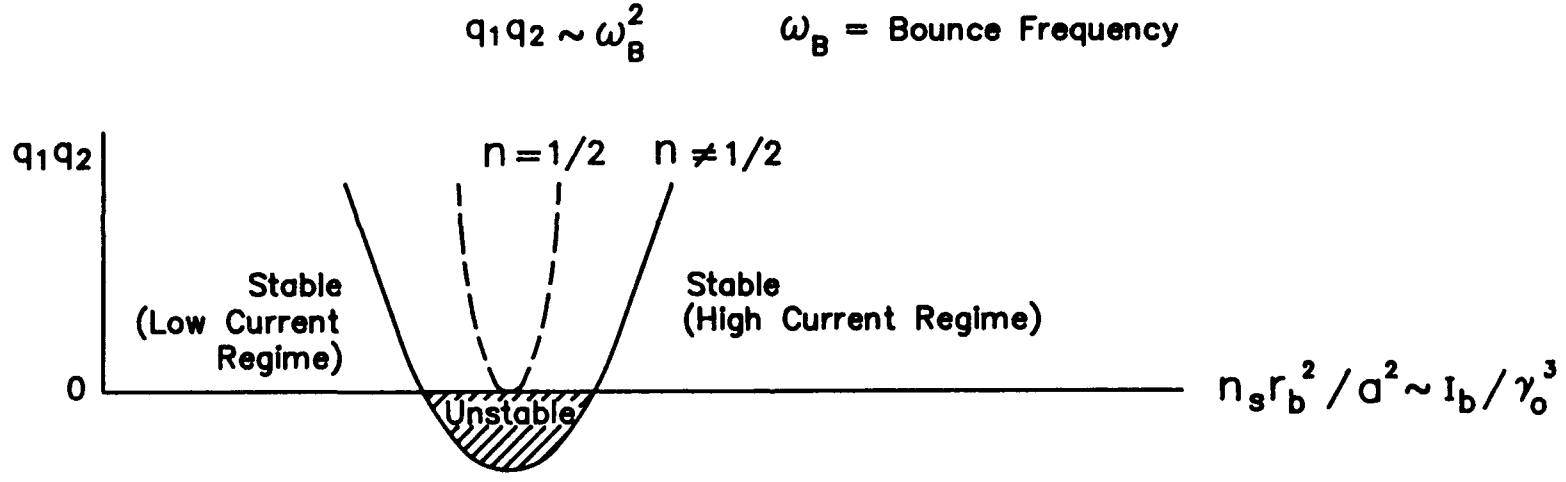

Fig. 3. Schemetic of the ring centroid orbital stability diagram for a modified betatron without strong focusing.

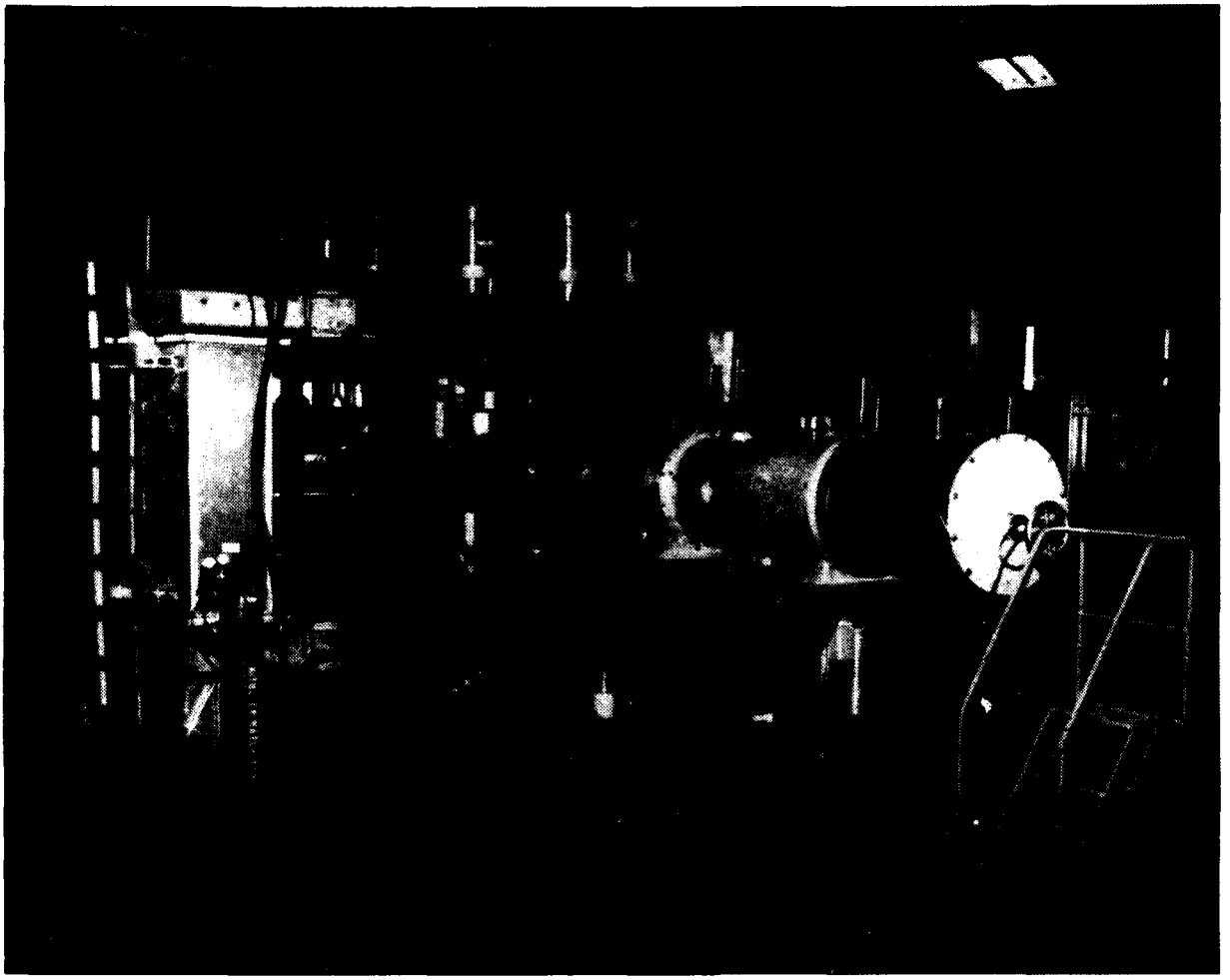

Fig. 4. Photograph of the NRL modified betatron accelerator.

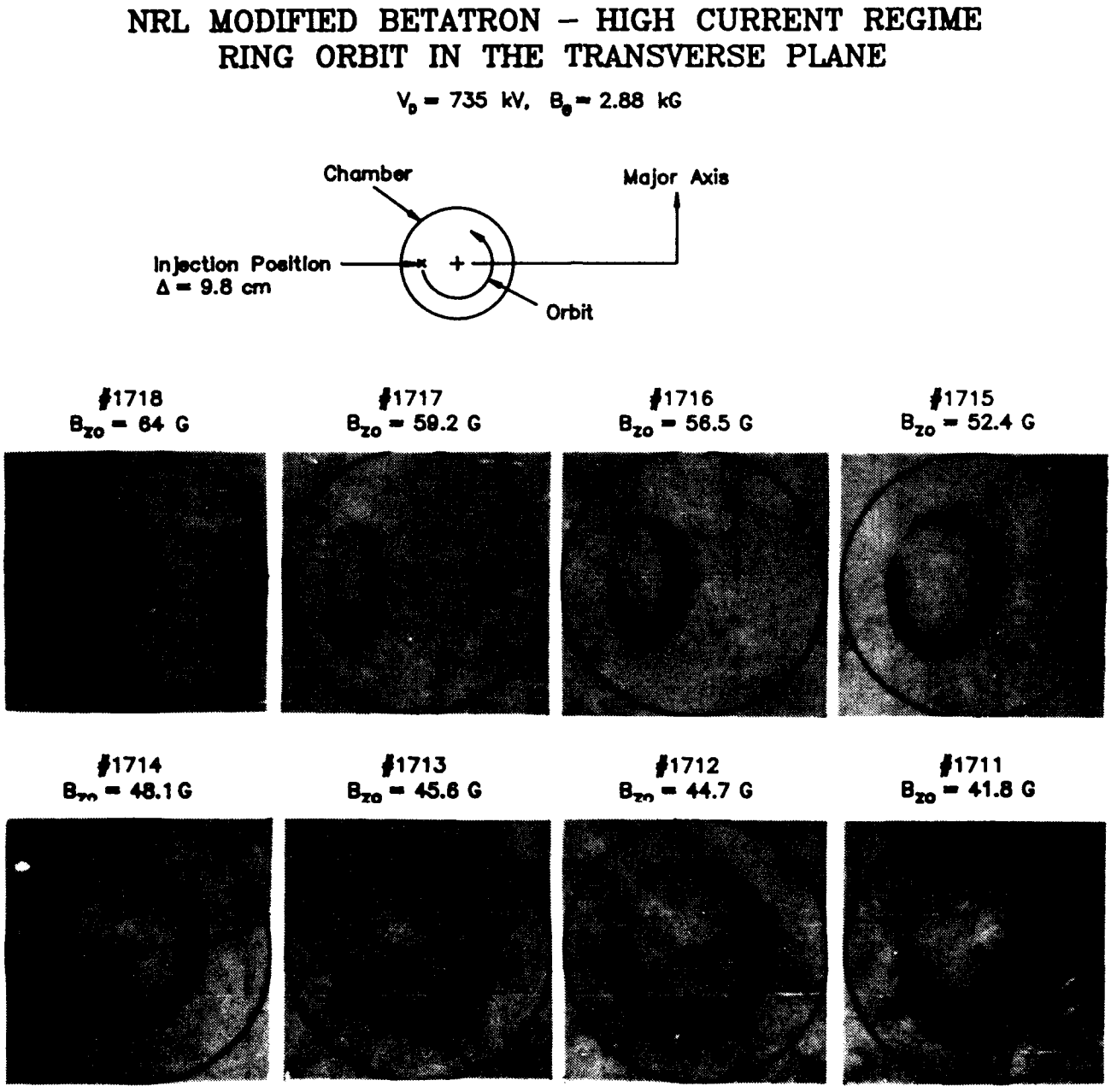

Fig. 5. Ring orbits in the transverse plane for several values of vertical magnetic field.

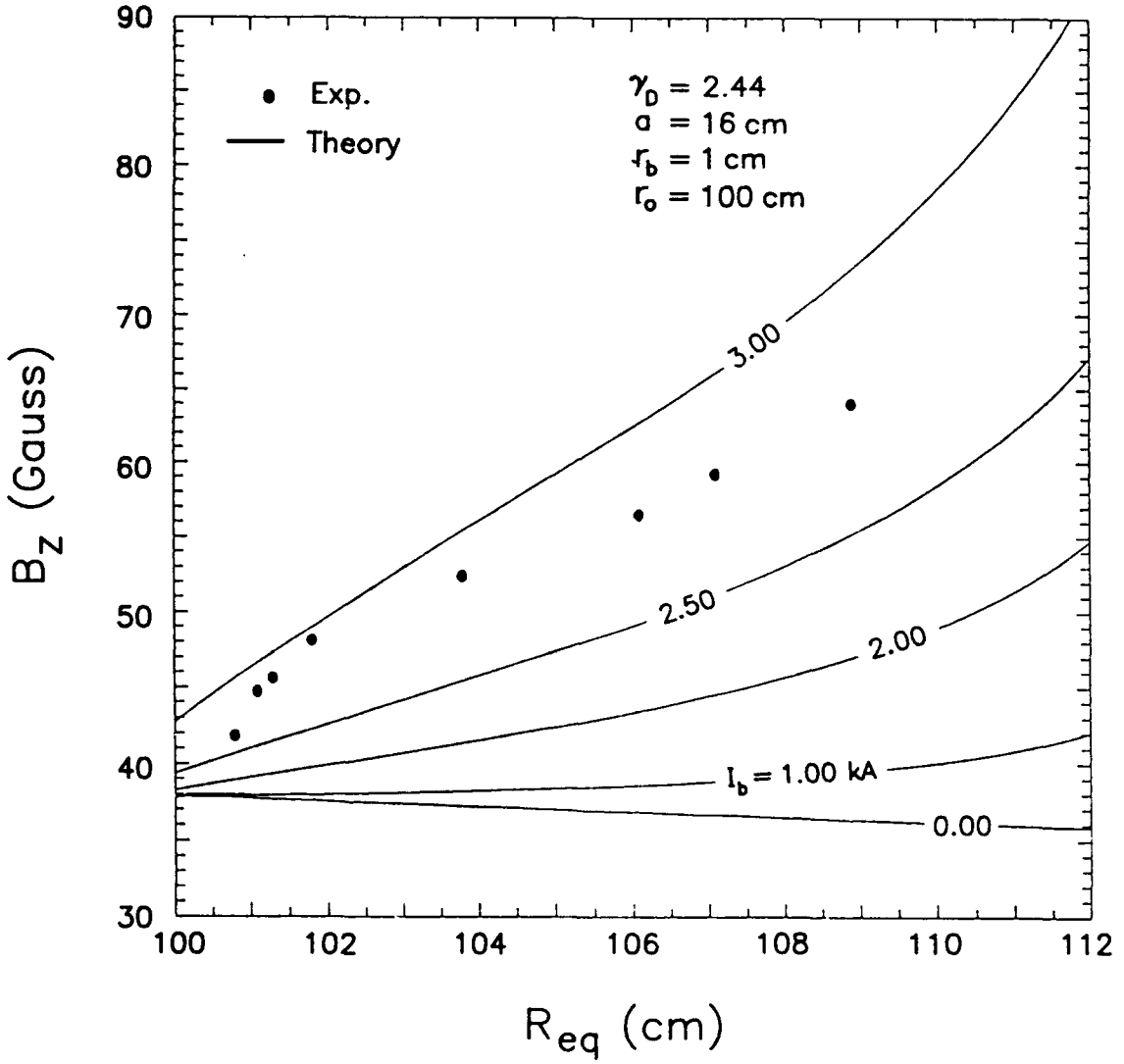

Fig. 6. Vertical magnetic field required to hold the electron ring at its equilibrium position for five different values of beam current.

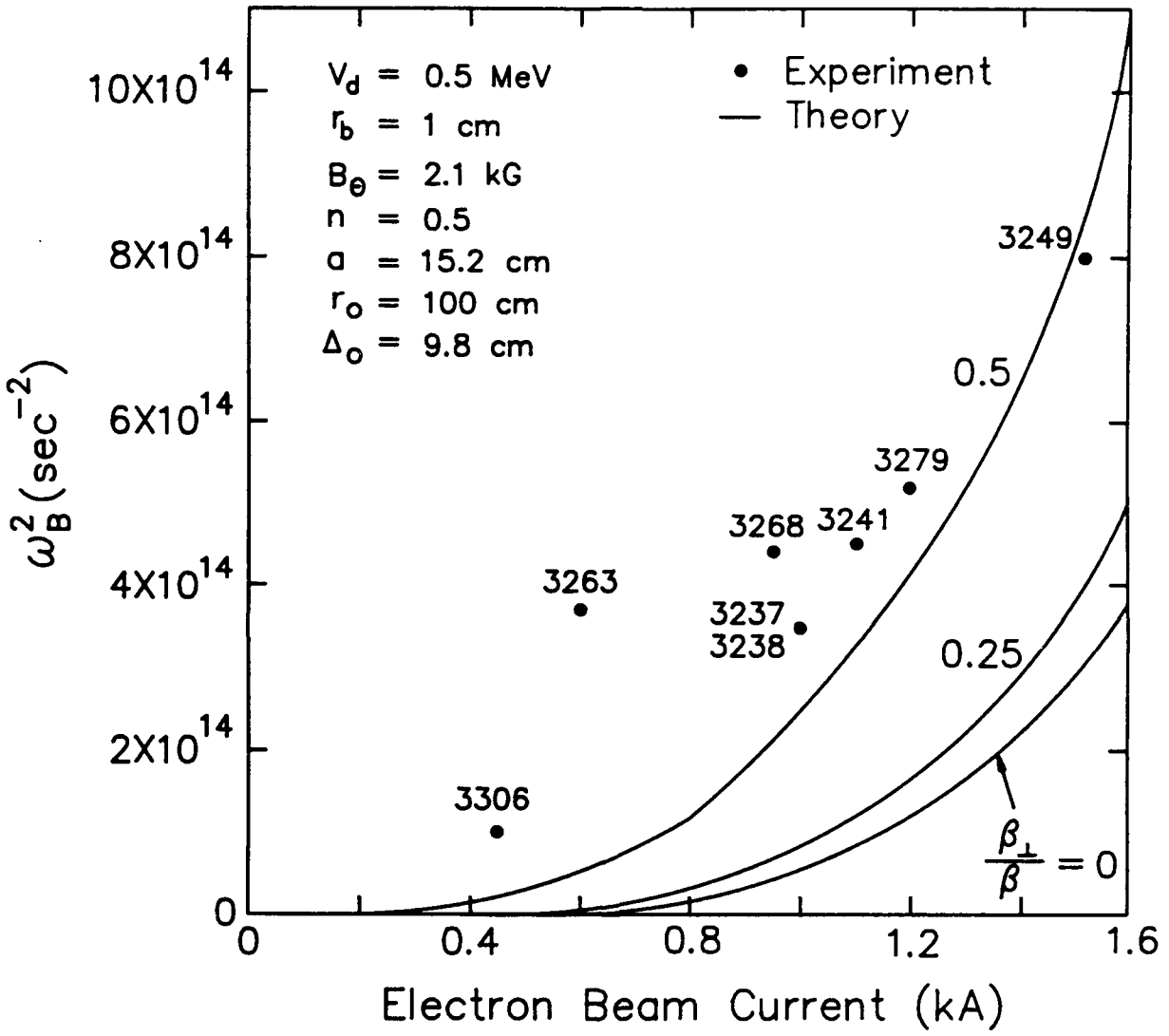

Fig. 7. Bounce frequency squared vs. electron beam current for three different values of transverse velocity.

Stellarator, Individual Particle and Centroid Indices

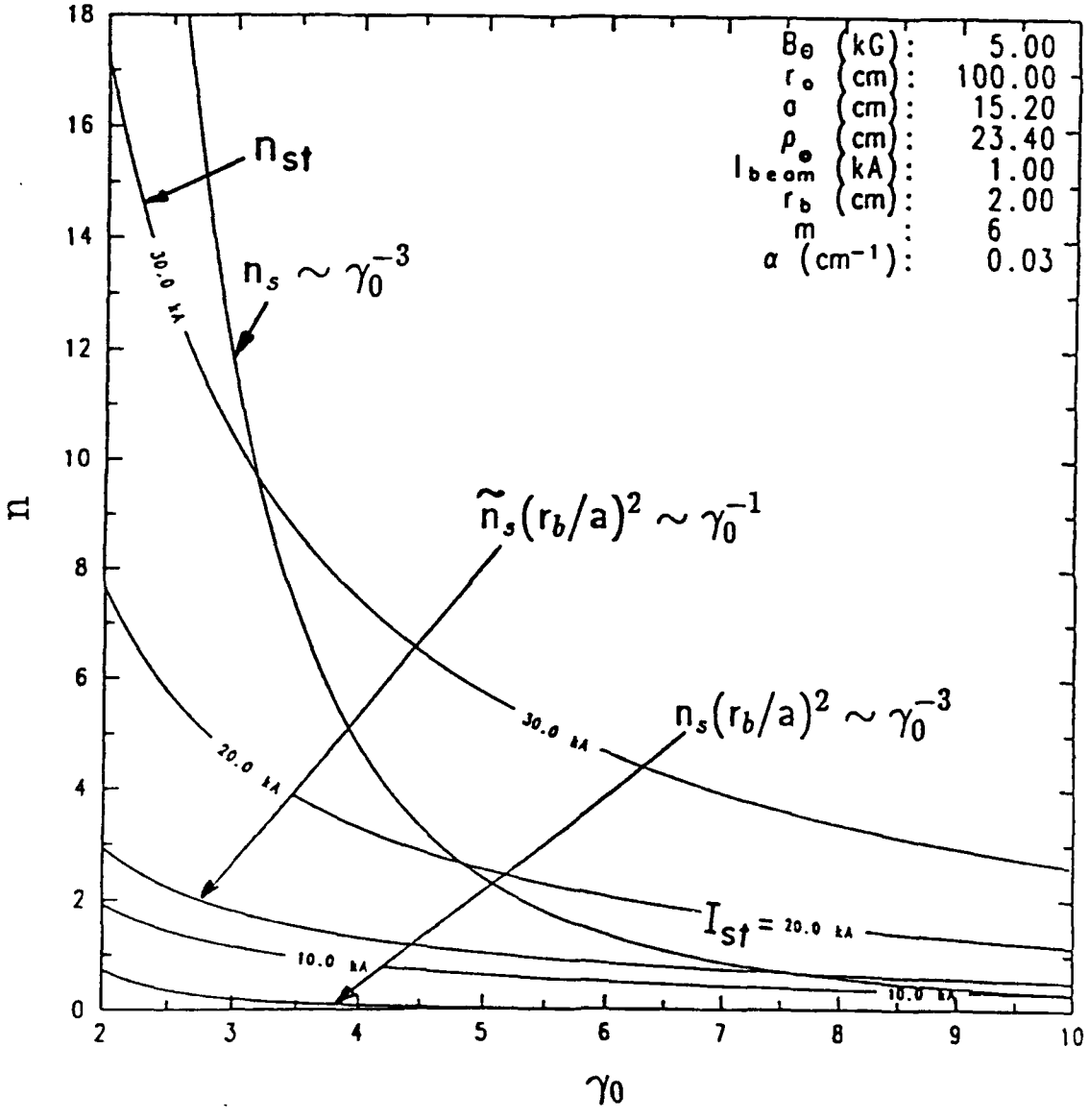

Fig. 8. Normalized ring lifetime vs. electron ring current for six different values of normalized beam energy γ_0. The parameter γ_0 is the normalized beam energy after the ring has been formed and it is smaller than the normalized electron energy in the diode γ_d.

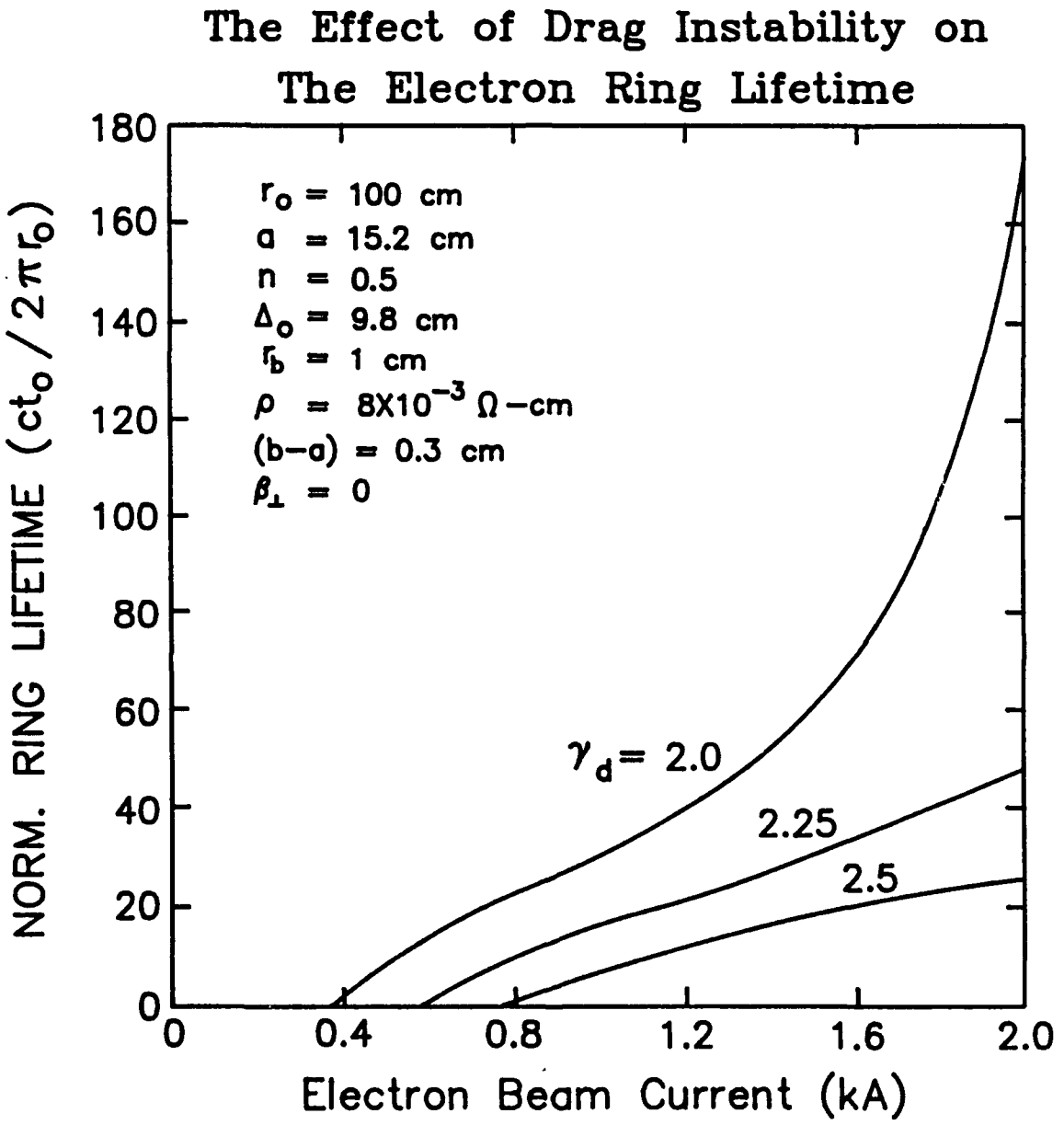

Fig. 9. Normalized ring lifetime vs. electron ring current for three values of the normalized electron energy at the diode γ_d. The beam is injected at the radial distance of $\Delta_0 = 9.8$ cm from the minor axis.

Modified Betatron with Stellarator Windings

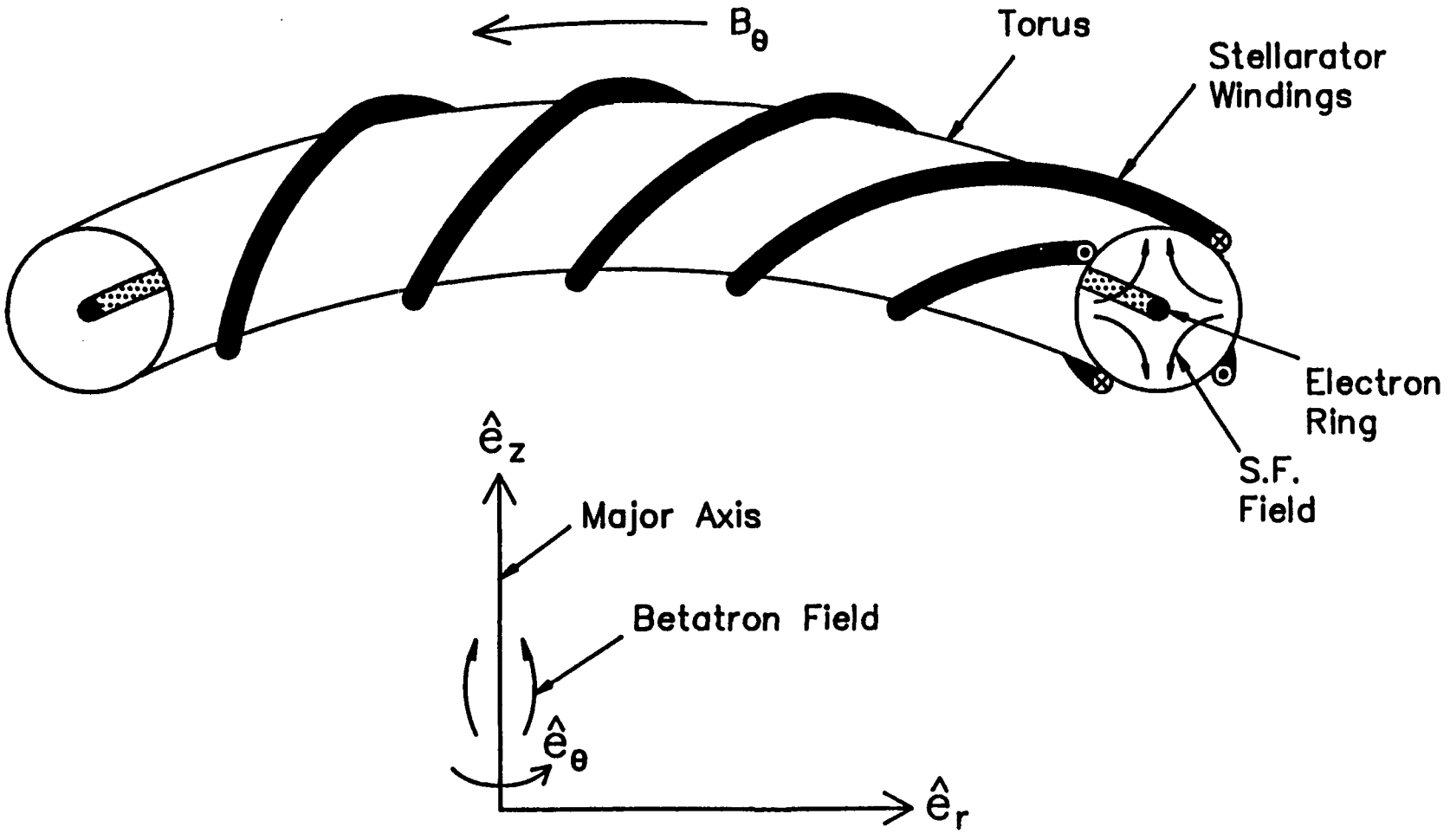

Fig. 10. Left-handed stellarator windings.

Modified Betatron with Torsatron Windings

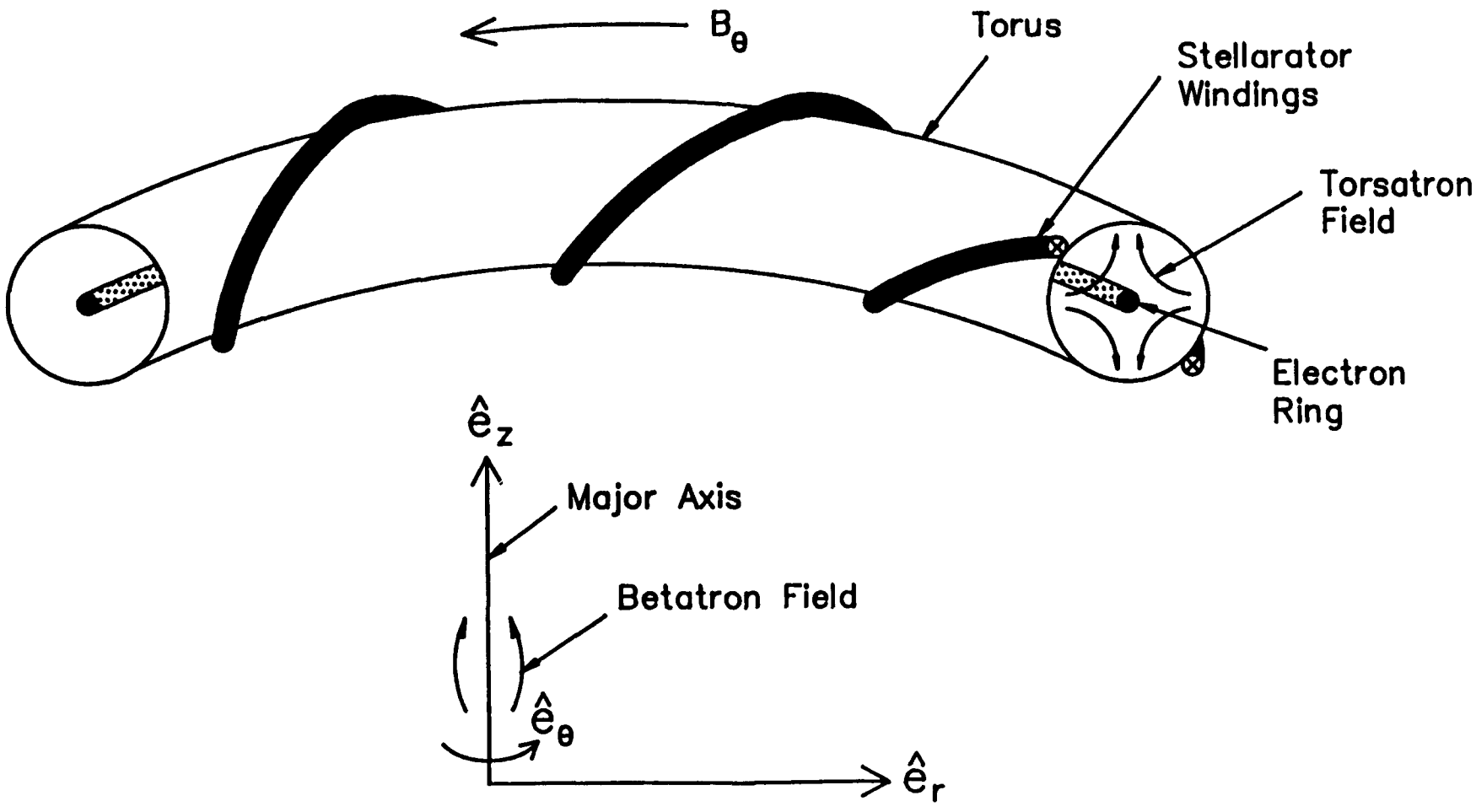

Fig. 11. Left-handed torsatron windings.

ORBITAL STABILITY DIAGRAM

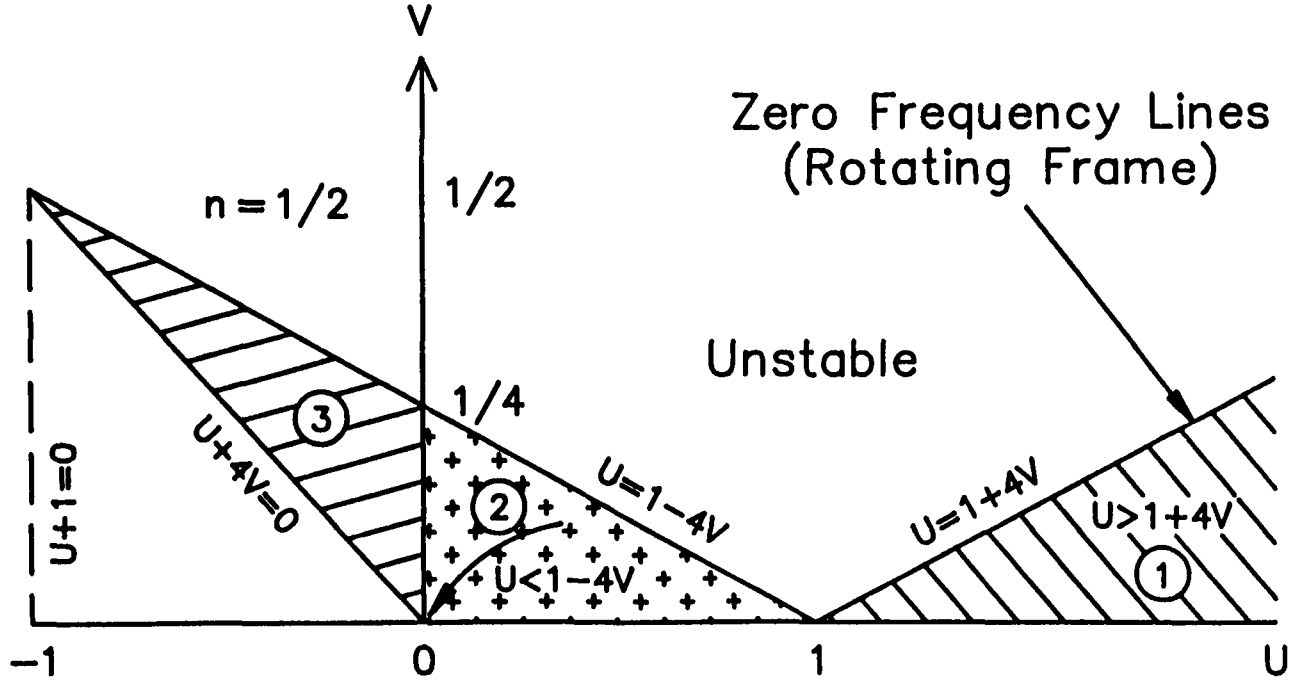

Fig. 12. Orbital stability diagram in the rotating frame from C.W. Roberson et al., Phys. Rev. Letts. **50**, 507 (1983).

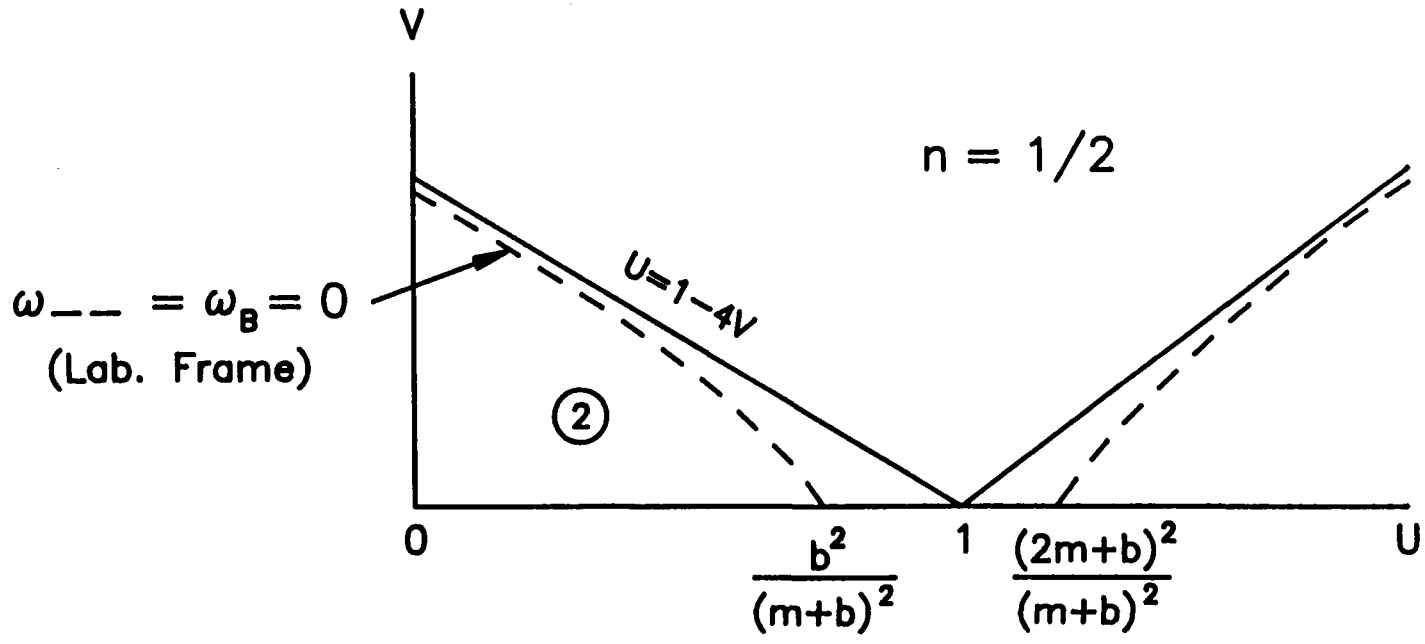

Fig. 13. Along the dashed lines the bounce frequency in the laboratory frame is equal to zero. At injection the values of U and V have to be selected to the right of the dashed line of region 2 for left-handed windings with B_θ and $v_\theta > 0$.

Stellarator, Individual Particle and Centroid Indices

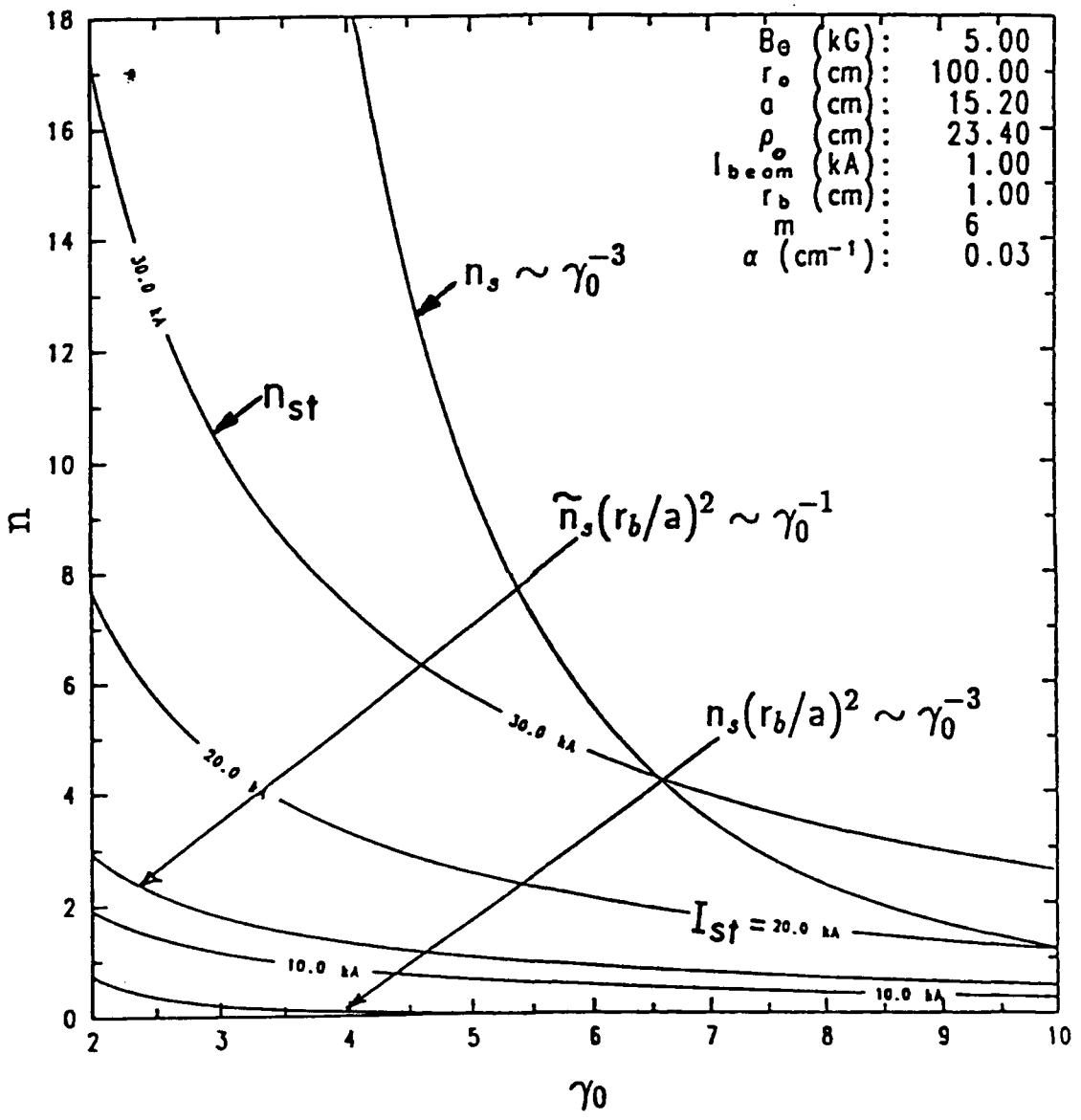

Fig. 14. Stellarator index n_{st}, individual particle self index n_s and centroid self indices for typical parameters of the NRL modified betatron.

Stellarator, Individual Particle and Centroid Indices

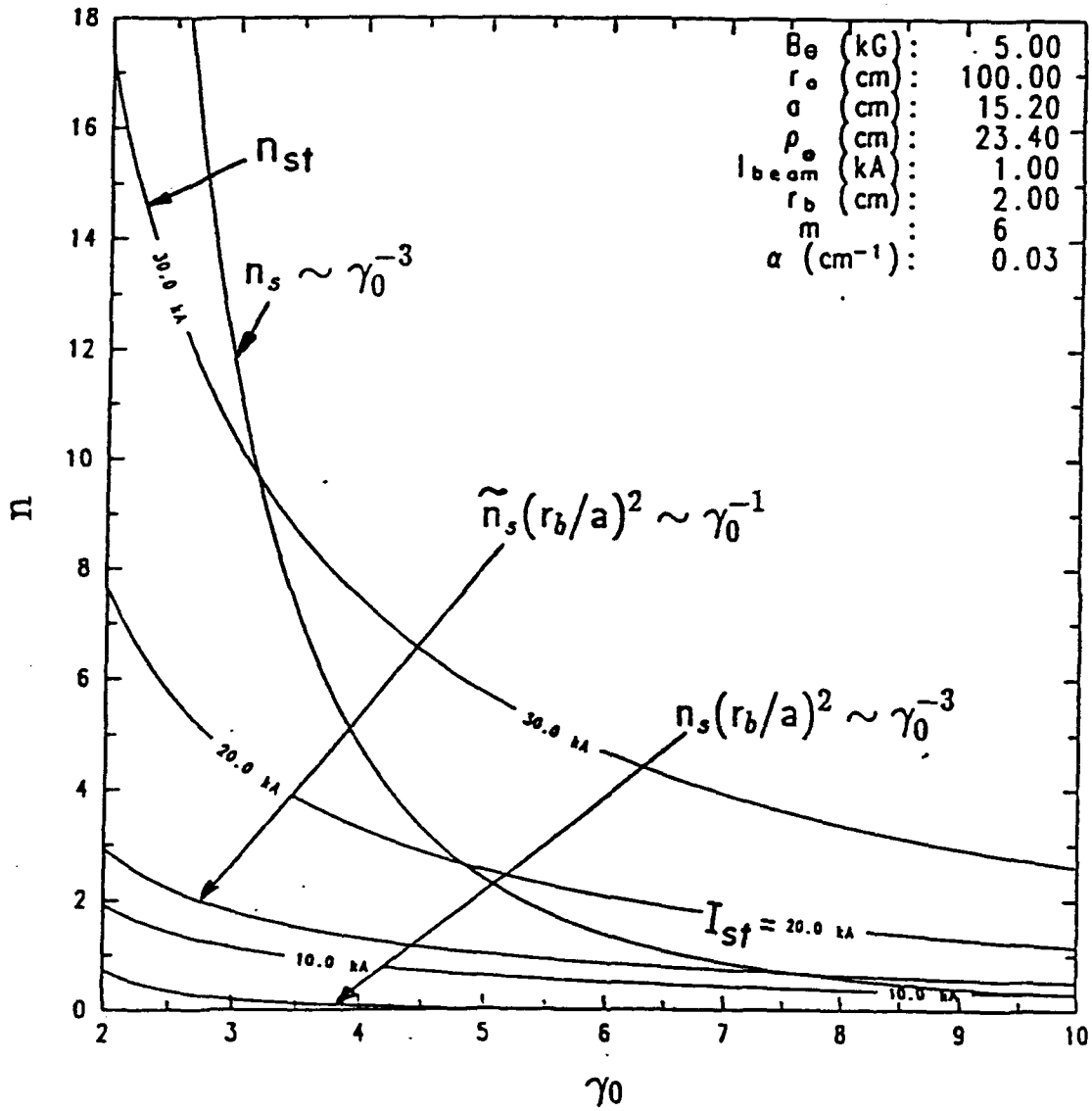

Fig. 15. As in Fig. (14) but with a beam radius of 2 cm instead of 1 cm.

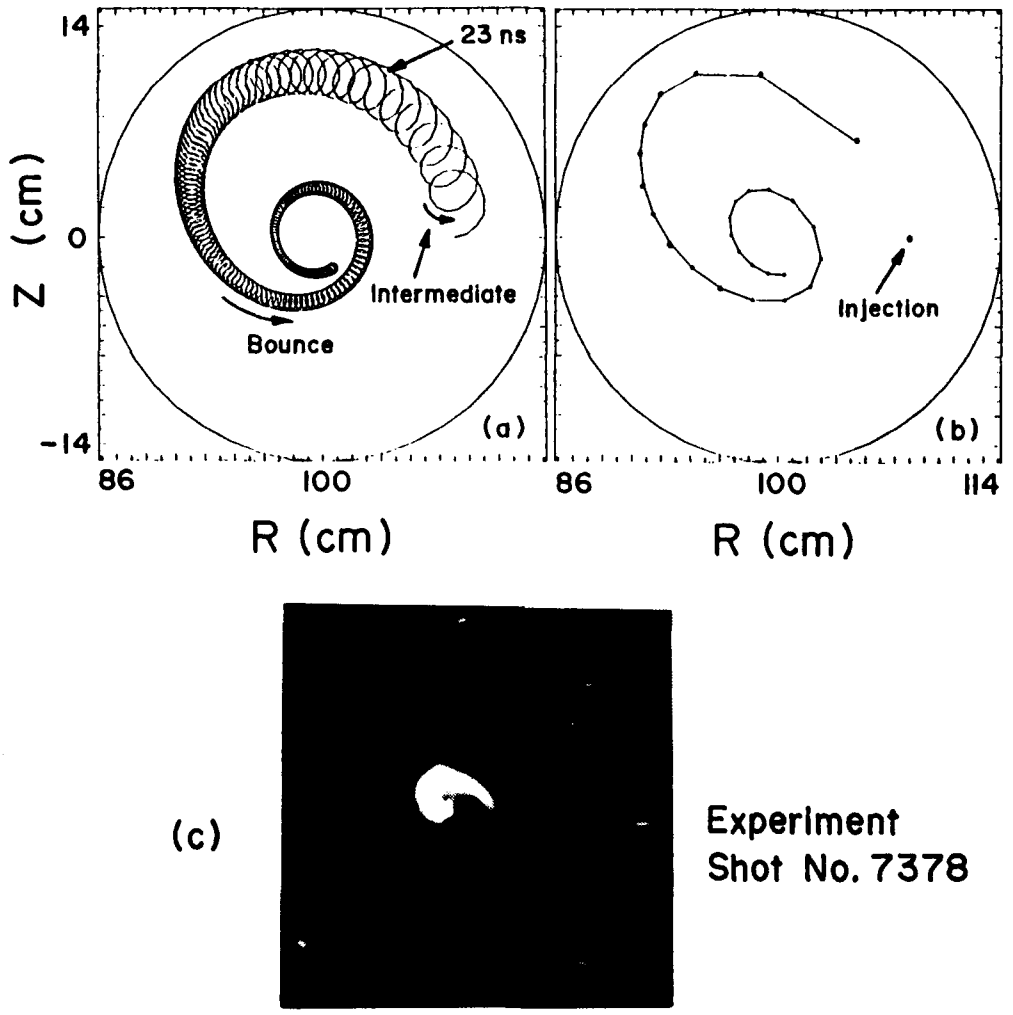

Fig. 16. Beam centroid orbit from the numerical integration of the equations of motion, using the image fields from the resistive shell model [(a) and (b)]. Results from the experiment (c).

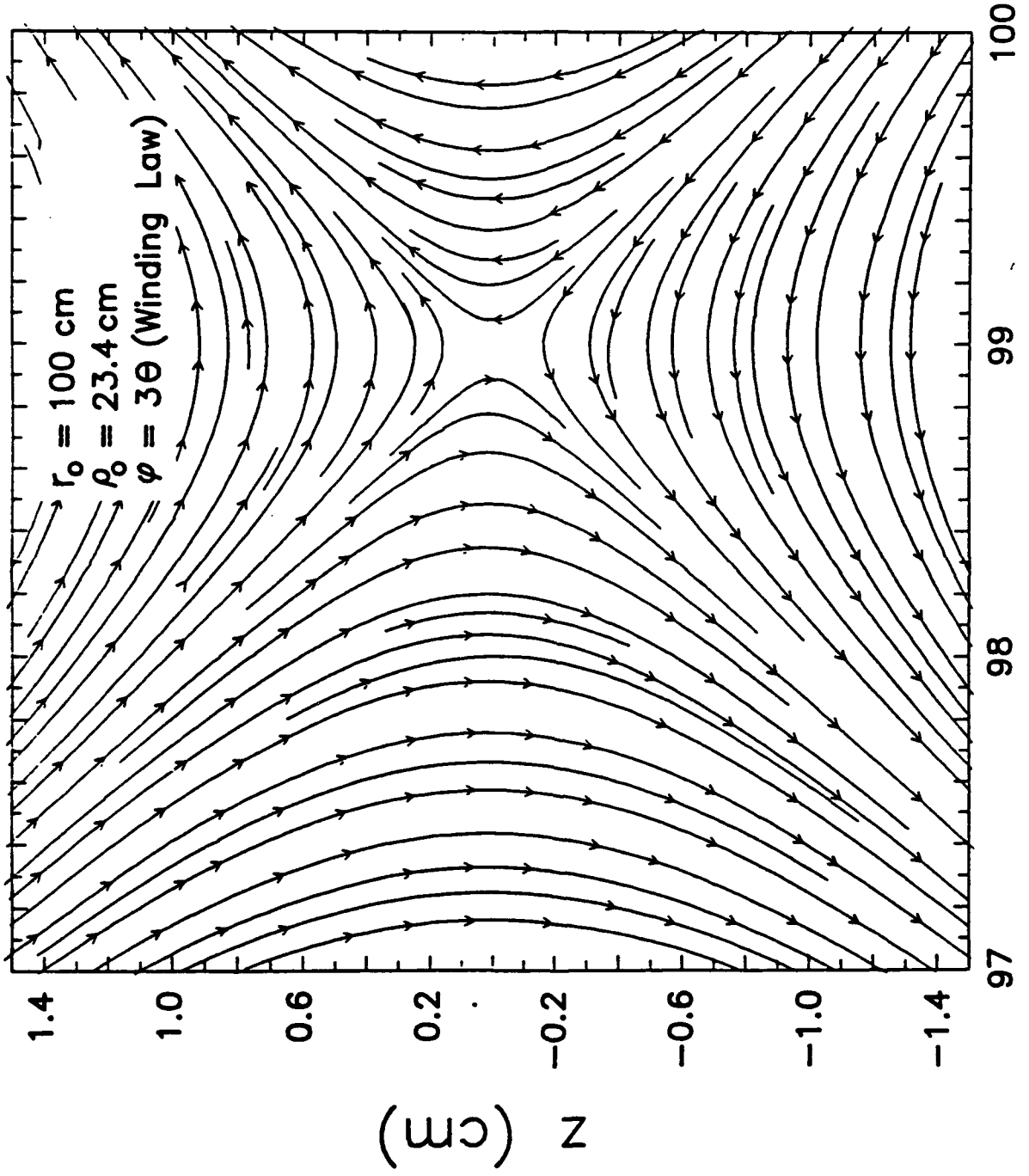

Fig. 17. Field lines in the vicinity of the magnetic axis (SF field).

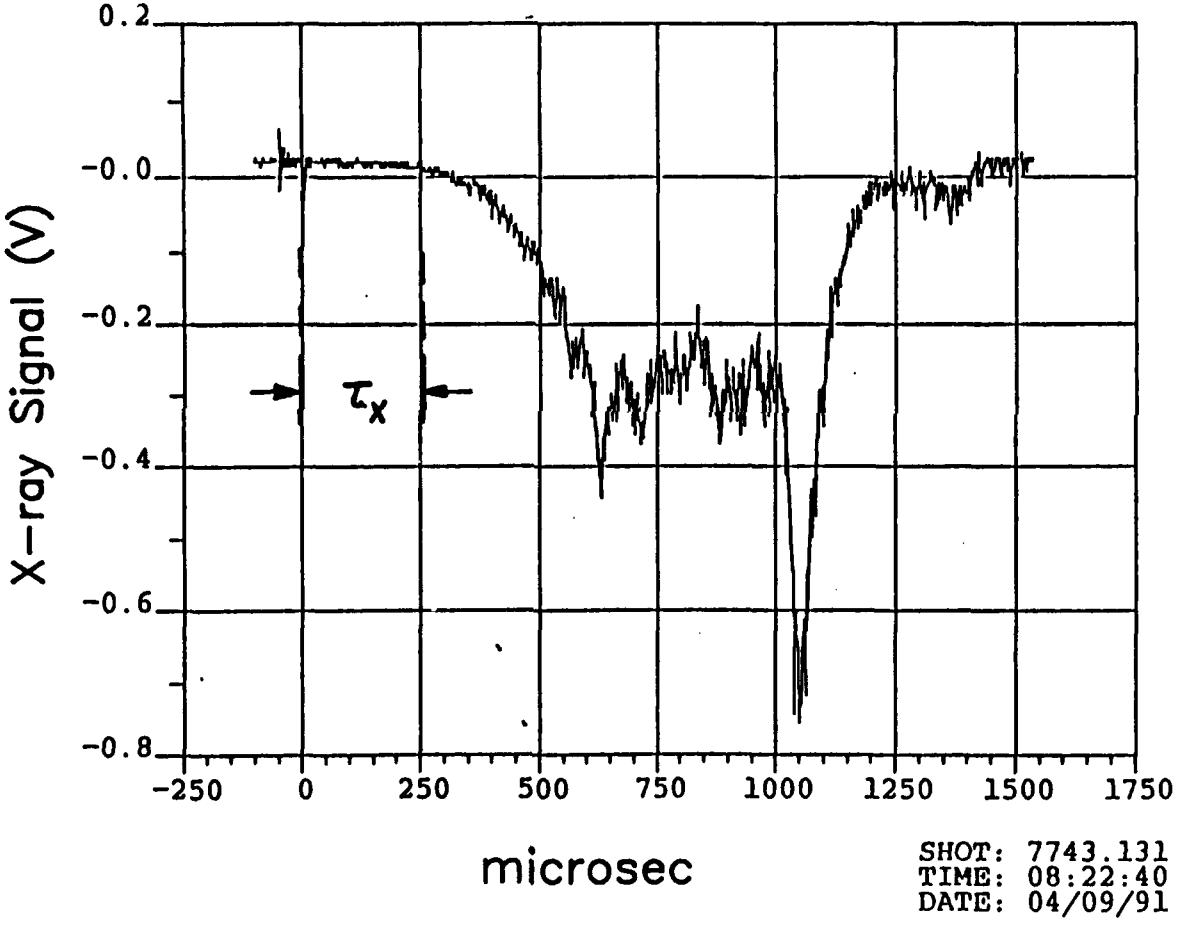

Fig. 18. X-ray signal as a function of time.

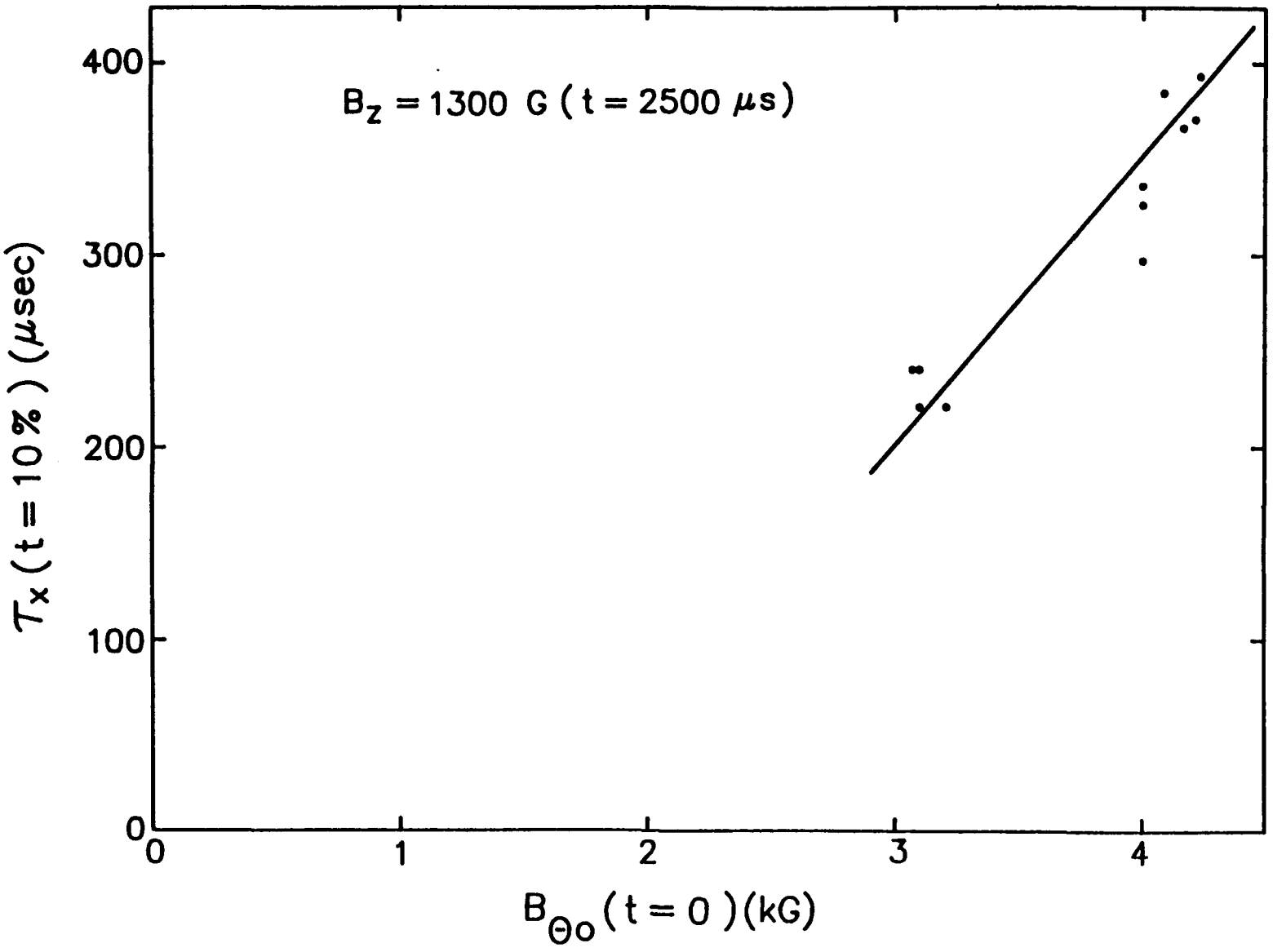

Fig. 19. The time the x-ray signal initially appears τ_x as a function of toroidal magnetic field for constant peak vertical field.

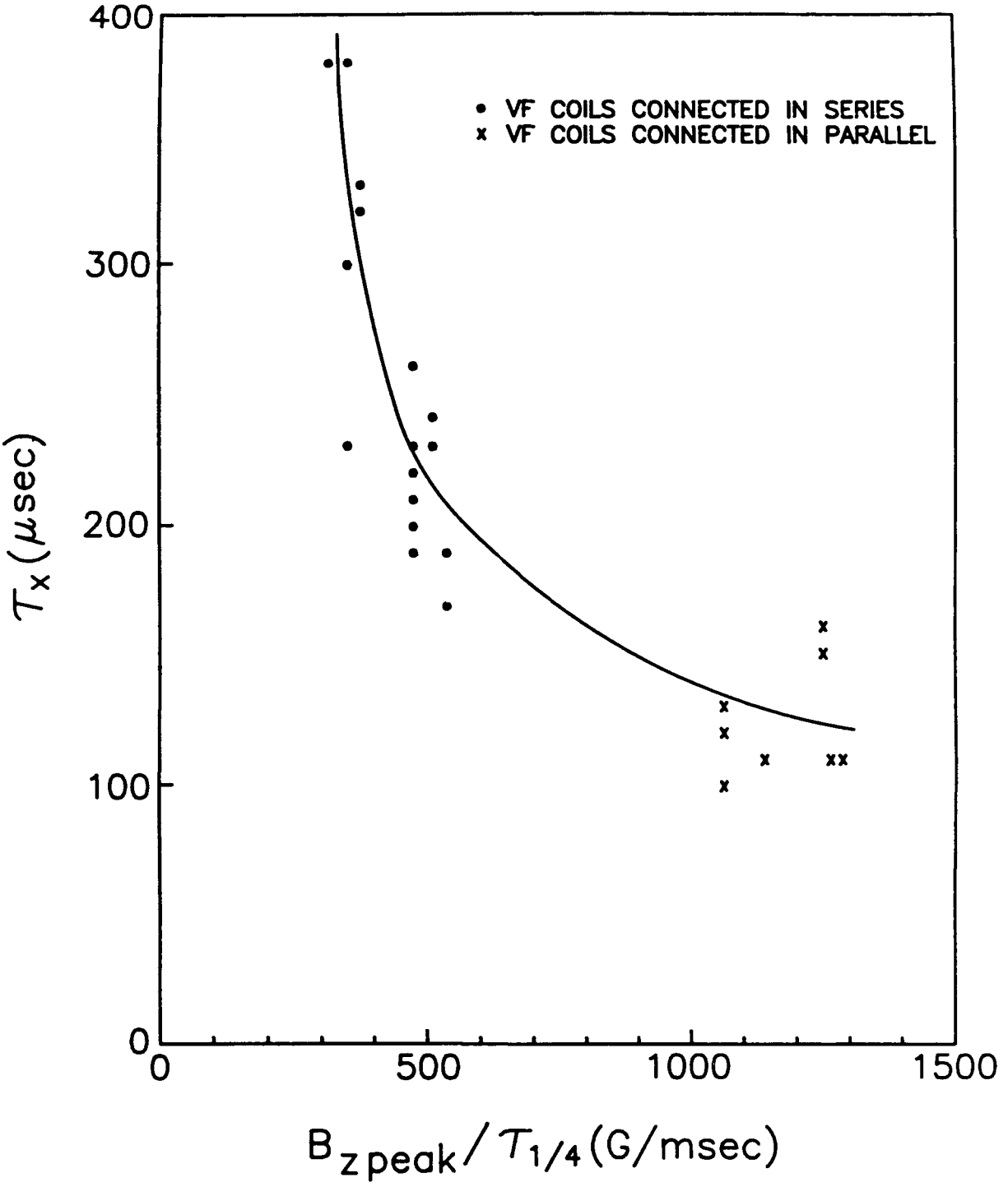

Fig. 20. The time τ_z as a function of the peak vertical magnetic field B_z peak divided by the risetime (quarter period) of the B_z waveform for $B_{\theta 0} \approx 4$ kG and a trapped beam current.

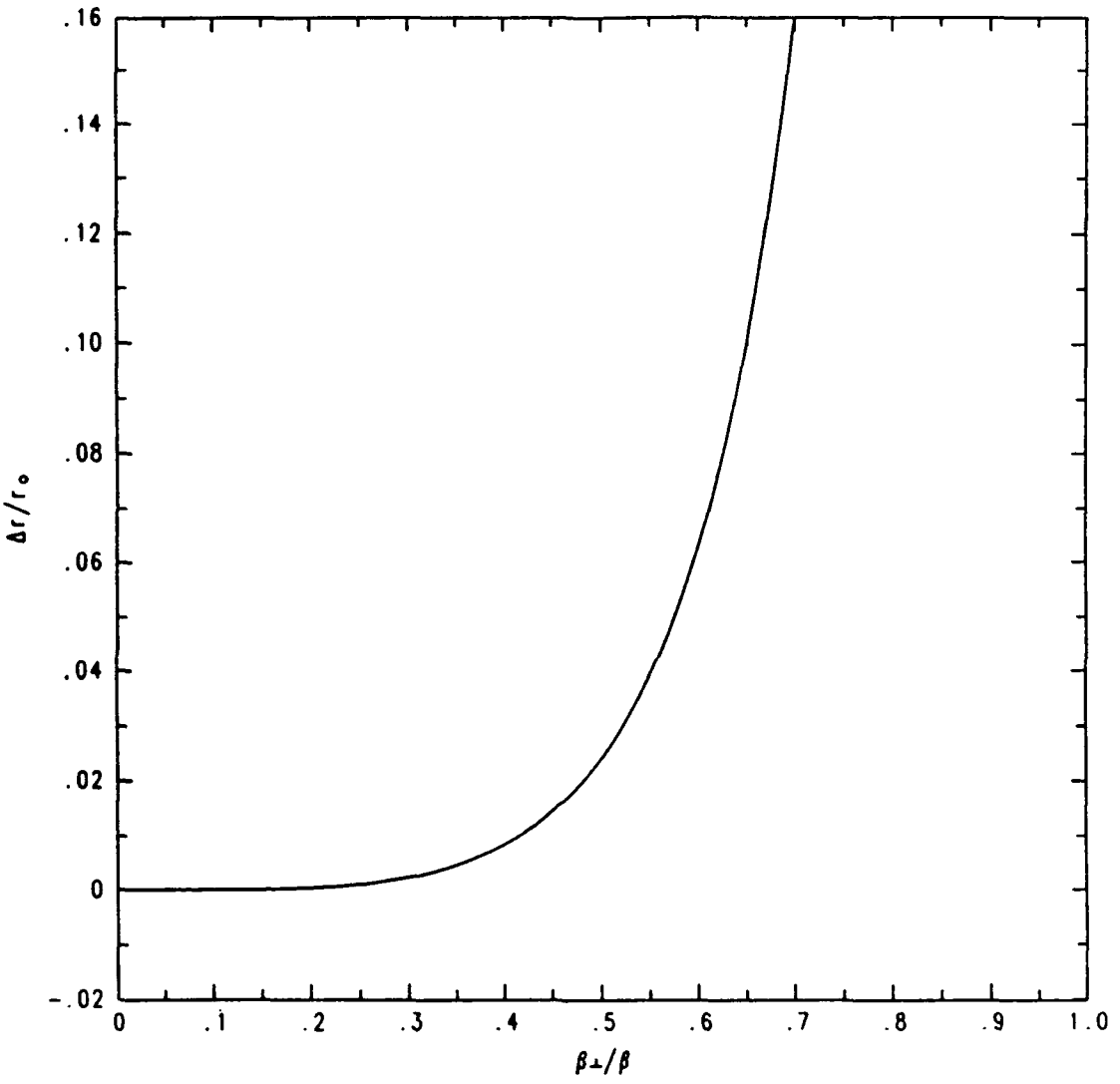

Fig. 21. Normalized radial displacement of the beam's equilibrium position vs. its normalized transverse velocity.

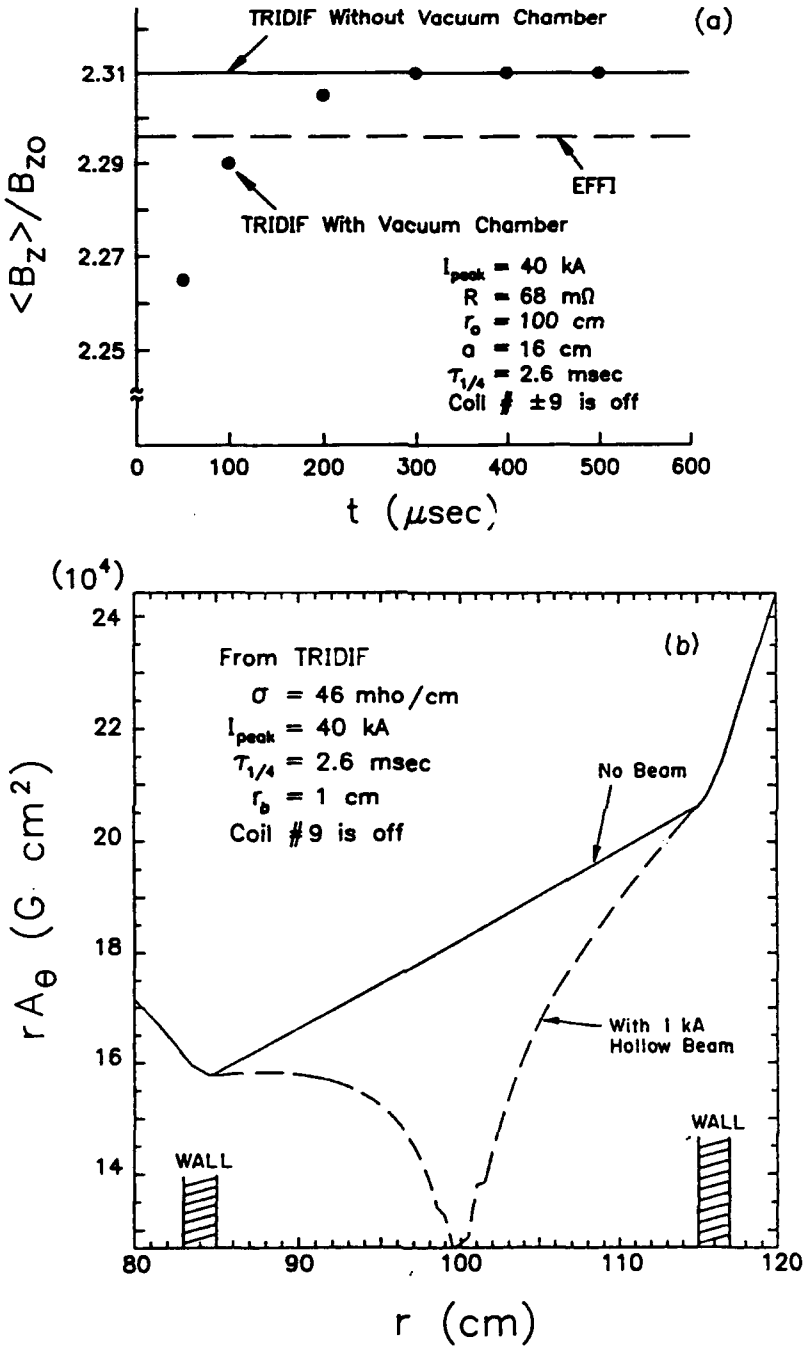

Fig. 22. (a) Betatron flux condition from TRIDIF and EFFI. The measured value of the betatron flux condition in the experiment is 2.3. (b) normalized magnetic flux vs. radial distance with and without the beam.

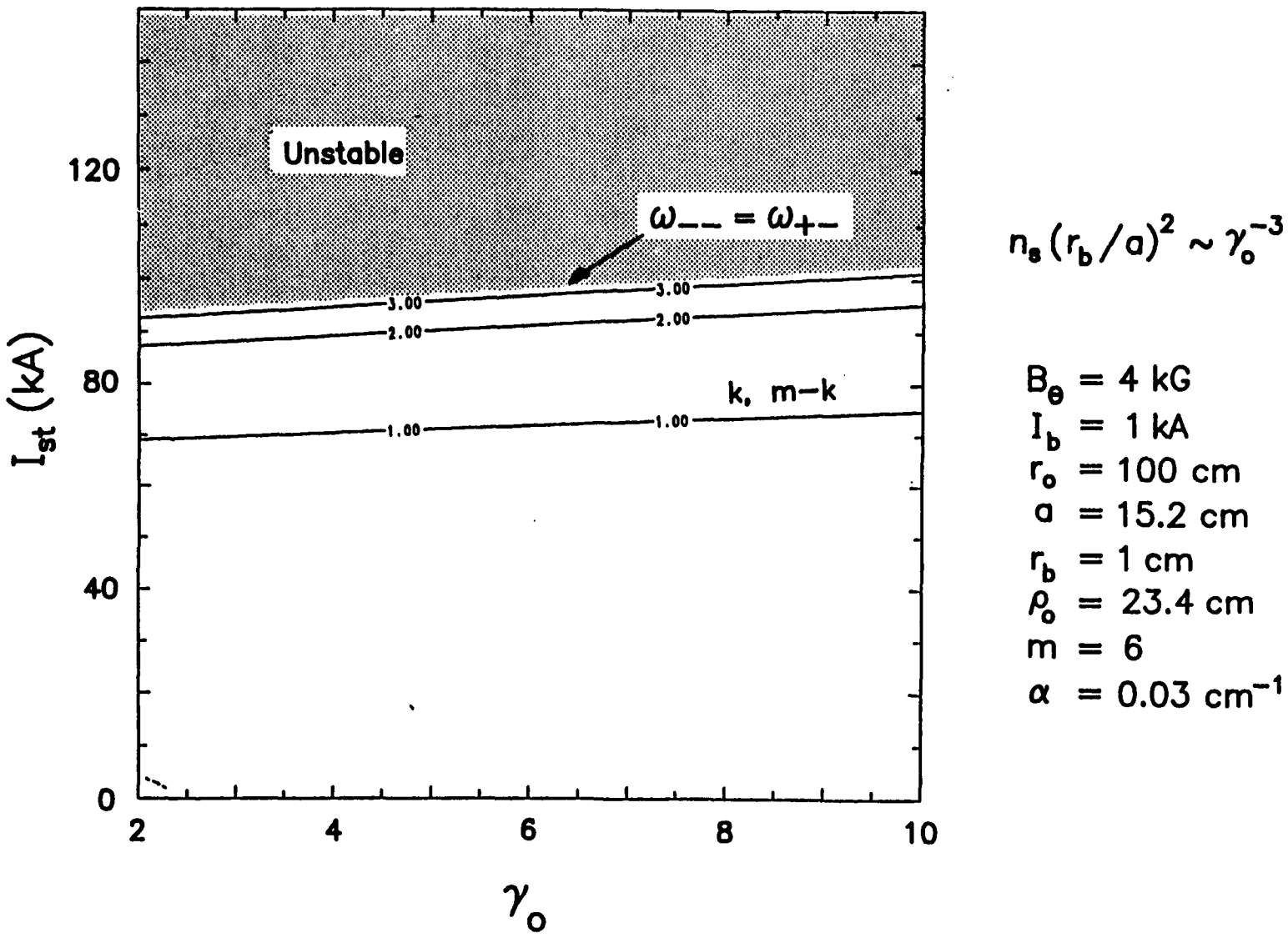

Fig. 23. Centroid integer resonances of the two low frequency modes ω_{--} (bounce) and ω_{+-} (SF mode) before the image magnetic field of the beam diffused out of the vacuum chamber $n(r_b/a)^2 \sim \gamma_0^{-3}$.

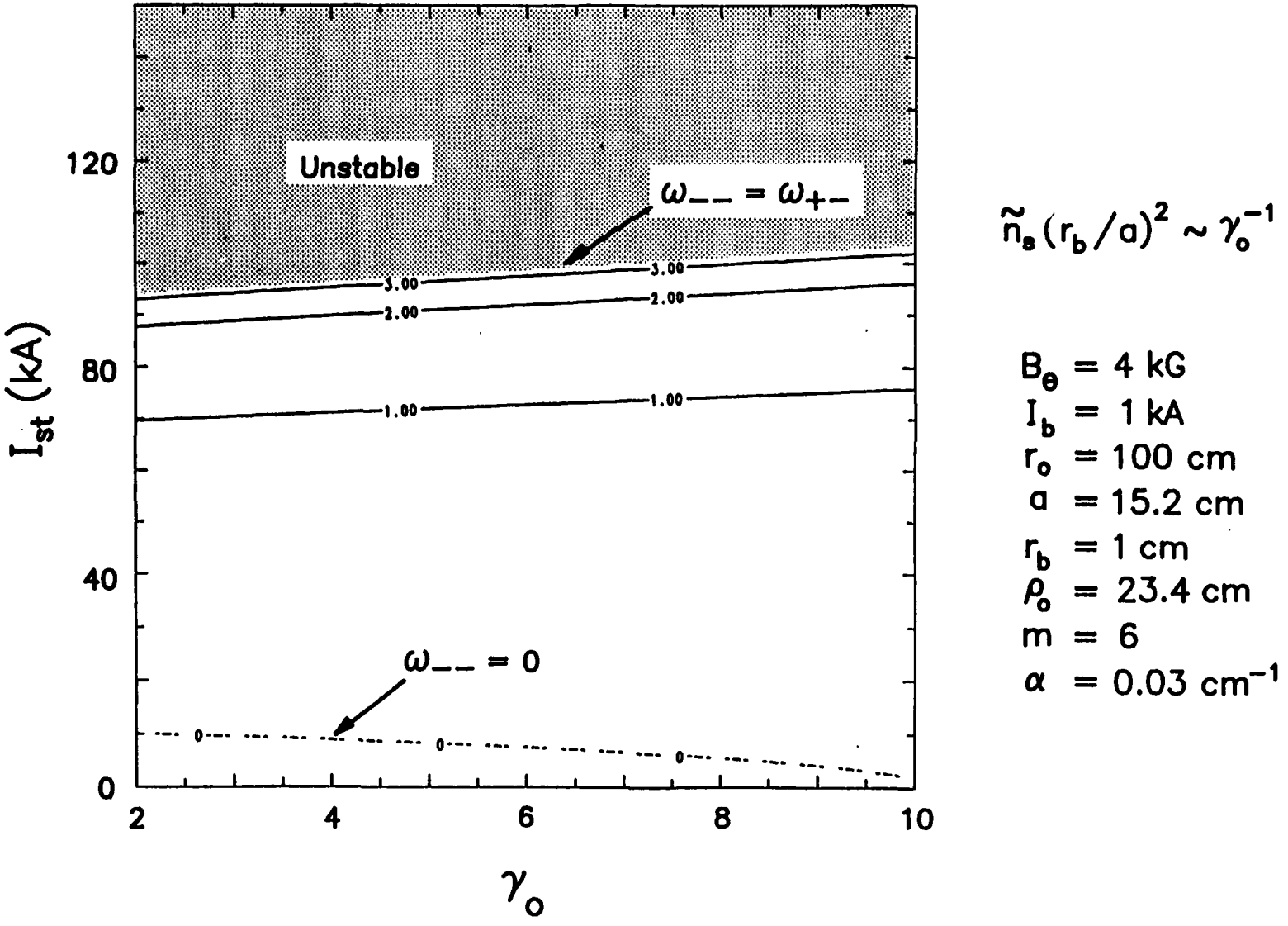

Fig. 24. As in Fig. (23) but after the image magnetic field of the beam diffused out of the vacuum chamber.

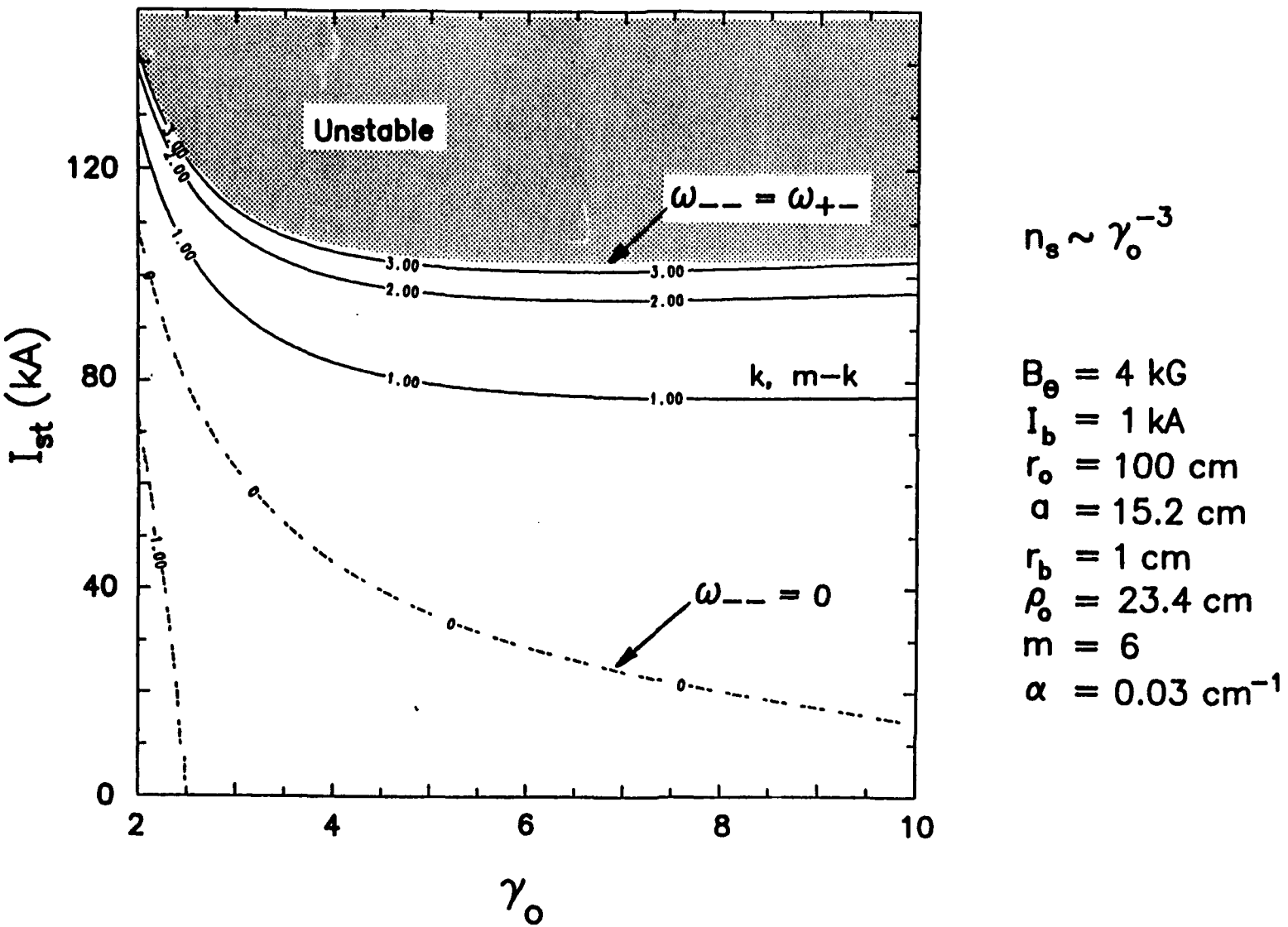

Fig. 25. Individual particle integer resonances of the two low frequency modes ω_{--} (bounce) and ω_{+-} (SF mode).

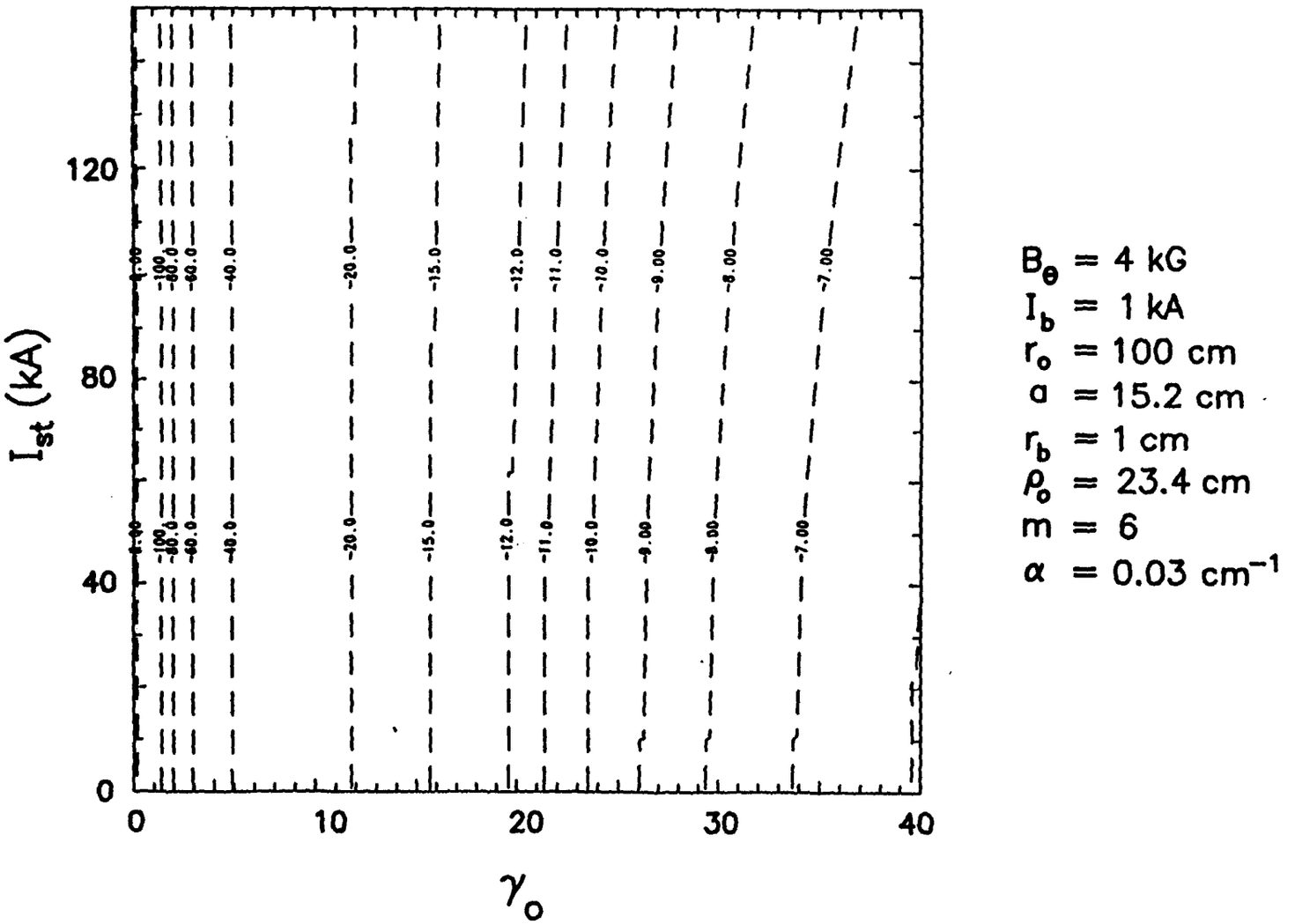

Fig. 26. Centroid integer resonances of the cyclotron mode ω_{-+}. For $\ell > 7$ and $I_{st} < 50$ kA these modes are independent of I_{st}.

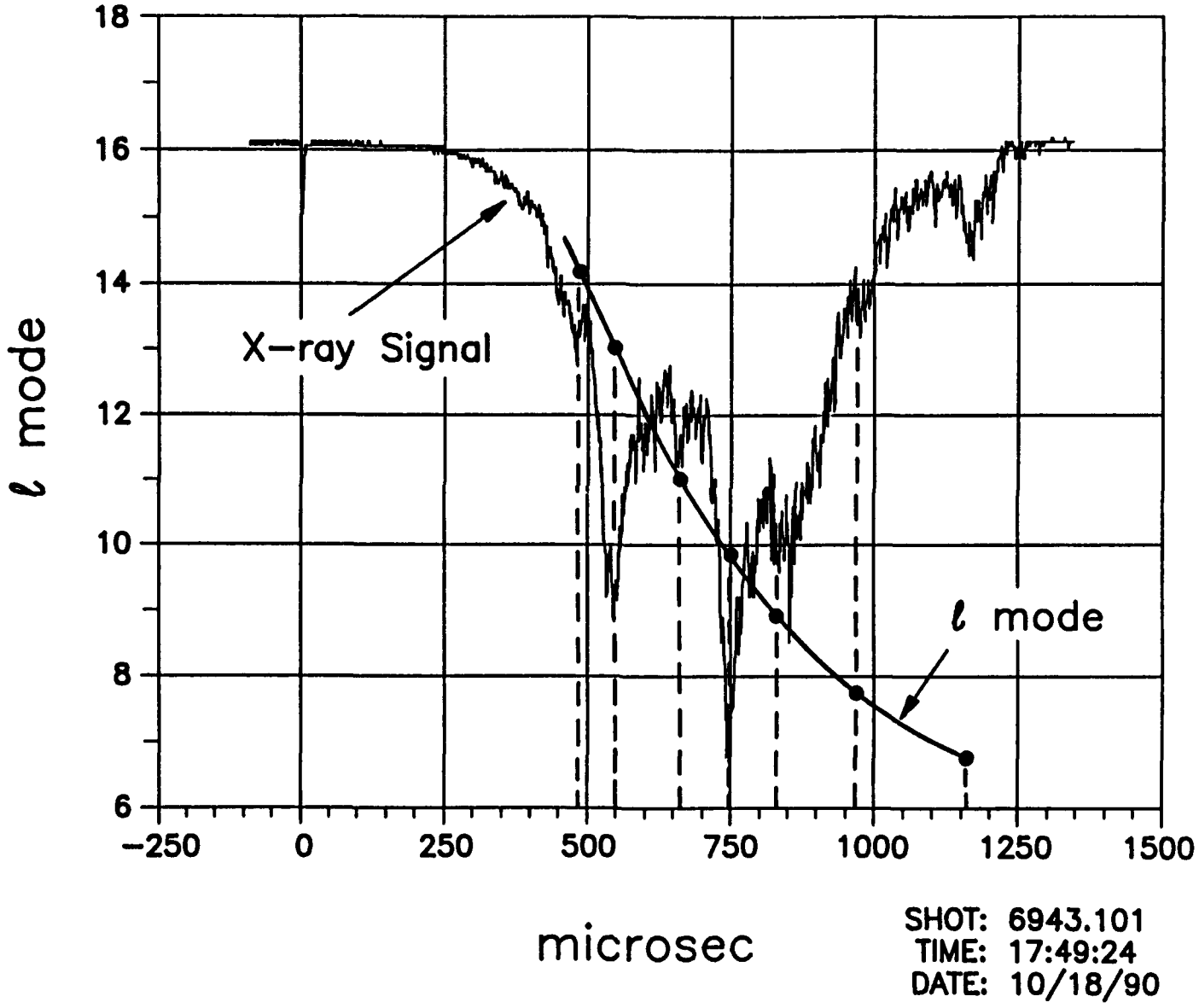

Fig. 27. X-ray signal as a function of time and ℓ from Eq. (49), after replacing $c\gamma\beta_\theta$ with $\Omega_{z0}r_0$.

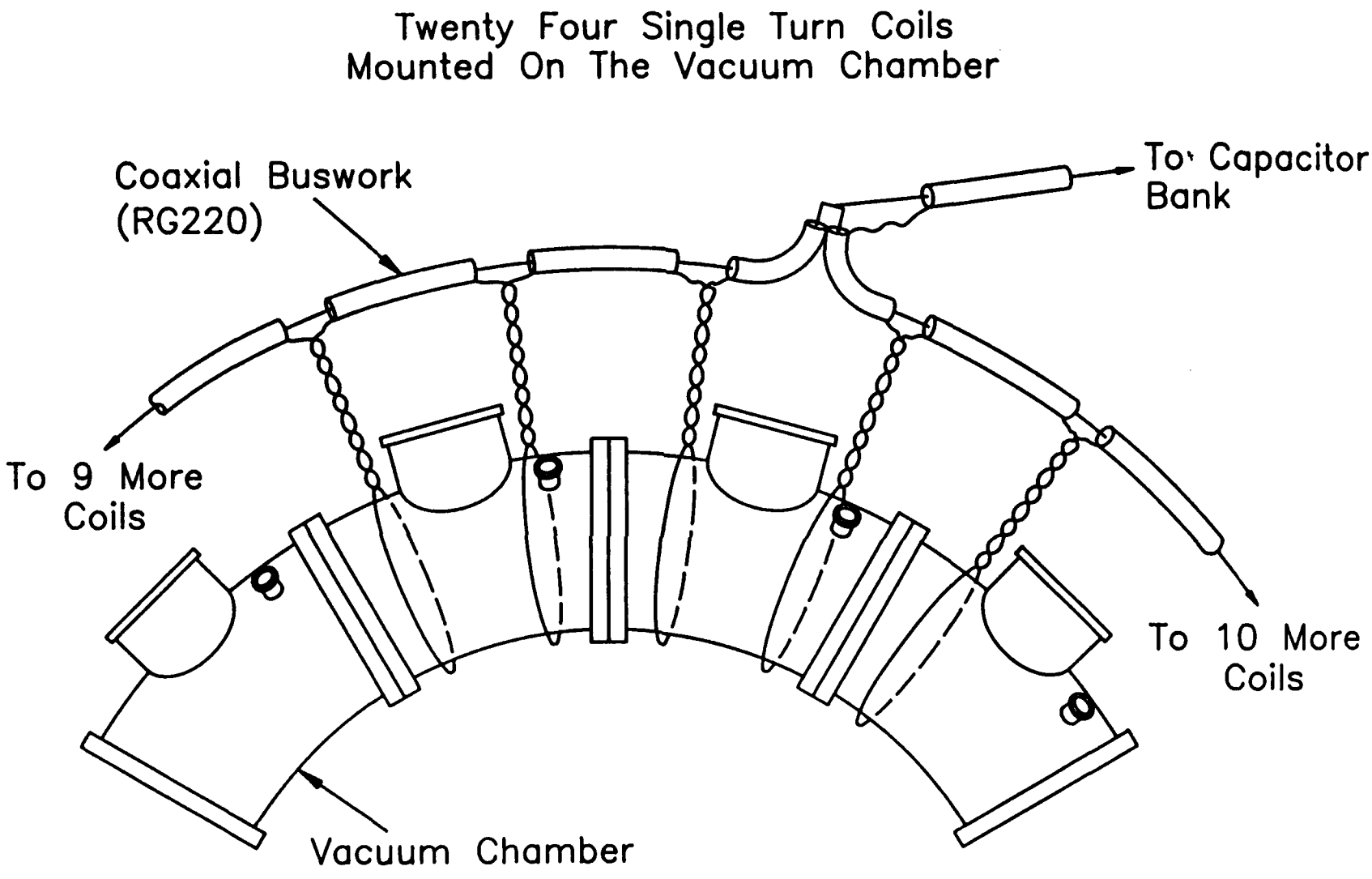

Fig. 28. Schematic of the initial twenty-four external resonant coils.

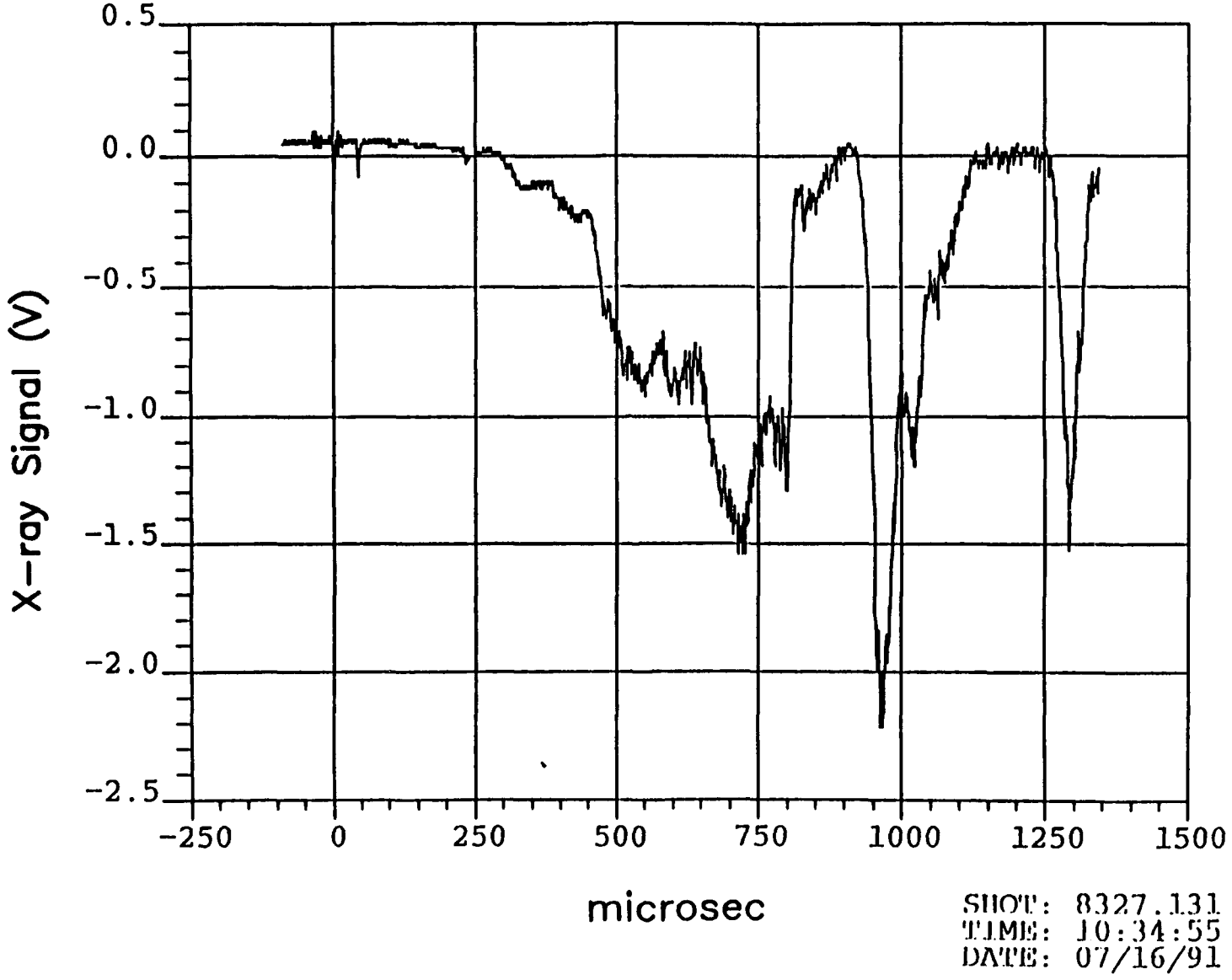

Fig. 29. X-ray signal vs. time. Between 800-900 μsec the ratio $B_{\theta 0}/B_{z0} \simeq$ constant $\neq$ interger.

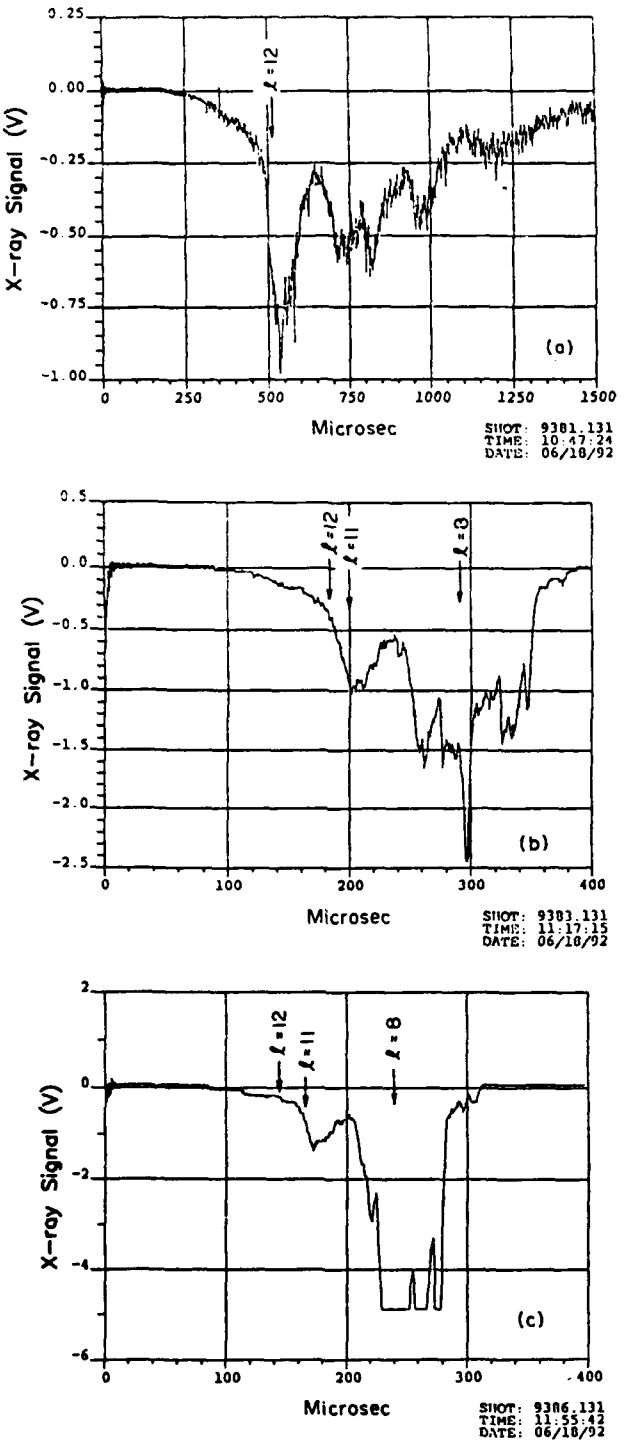

Fig. 30. X-ray signals as a function of time for three different acceleration rates: (a) $(\dot{B}_z)_{\mathbf{peak}} = 0.69\ G/\mu sec$, (b)1.69 $G/\mu sec$, and (c) 1.93 G/μsec. In all three runs $B_{\theta 0} \approx 4$ kG.

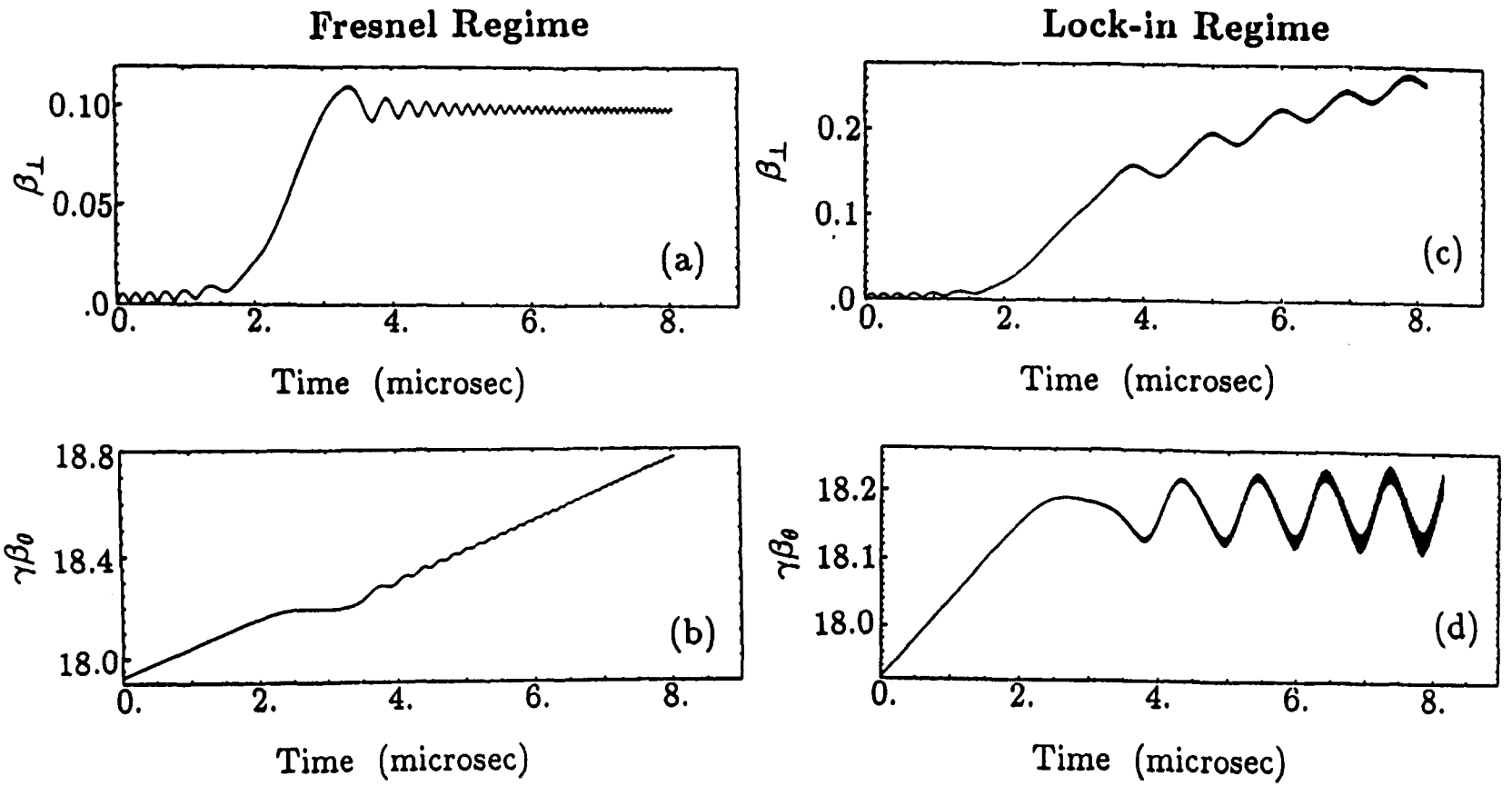

Fig. 31. Normalized transverse velocity $\beta_\perp$ and $\gamma\beta_\theta$ vs. time in the Fresnel and Lock-in regimes.

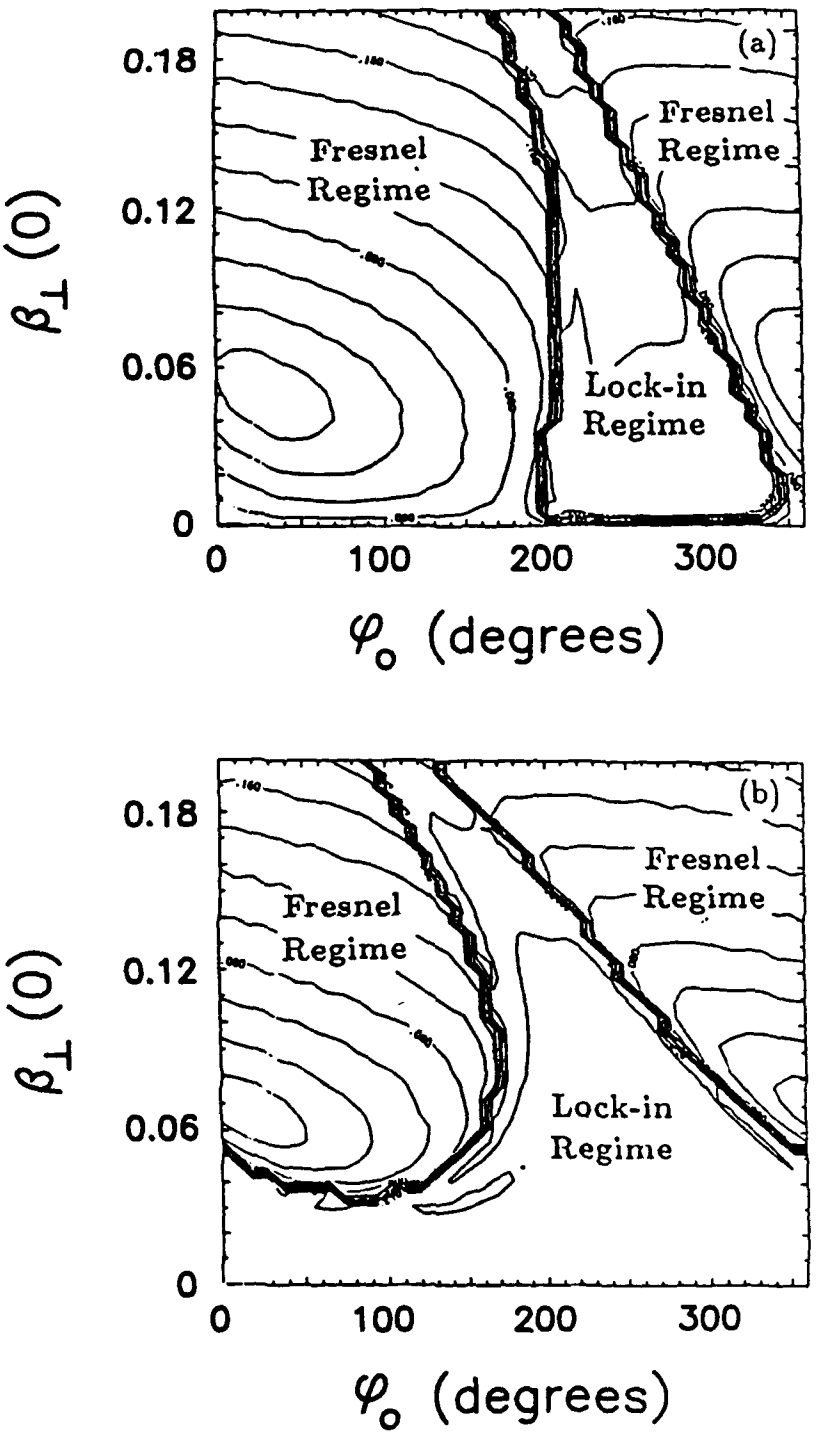

Fig. 32. Contour plots of the final $\beta_\perp$ in the $\beta_\perp^{(0)}, \varphi_o$ plane where $\beta_\perp^{(0)}$ and φ_o are the amplitude and phase of the initial value of transverse velocity and its phase. In (a) ΔB_{z0} = 0.2 G and in (b) ΔB_{z0} = 0.3 G.

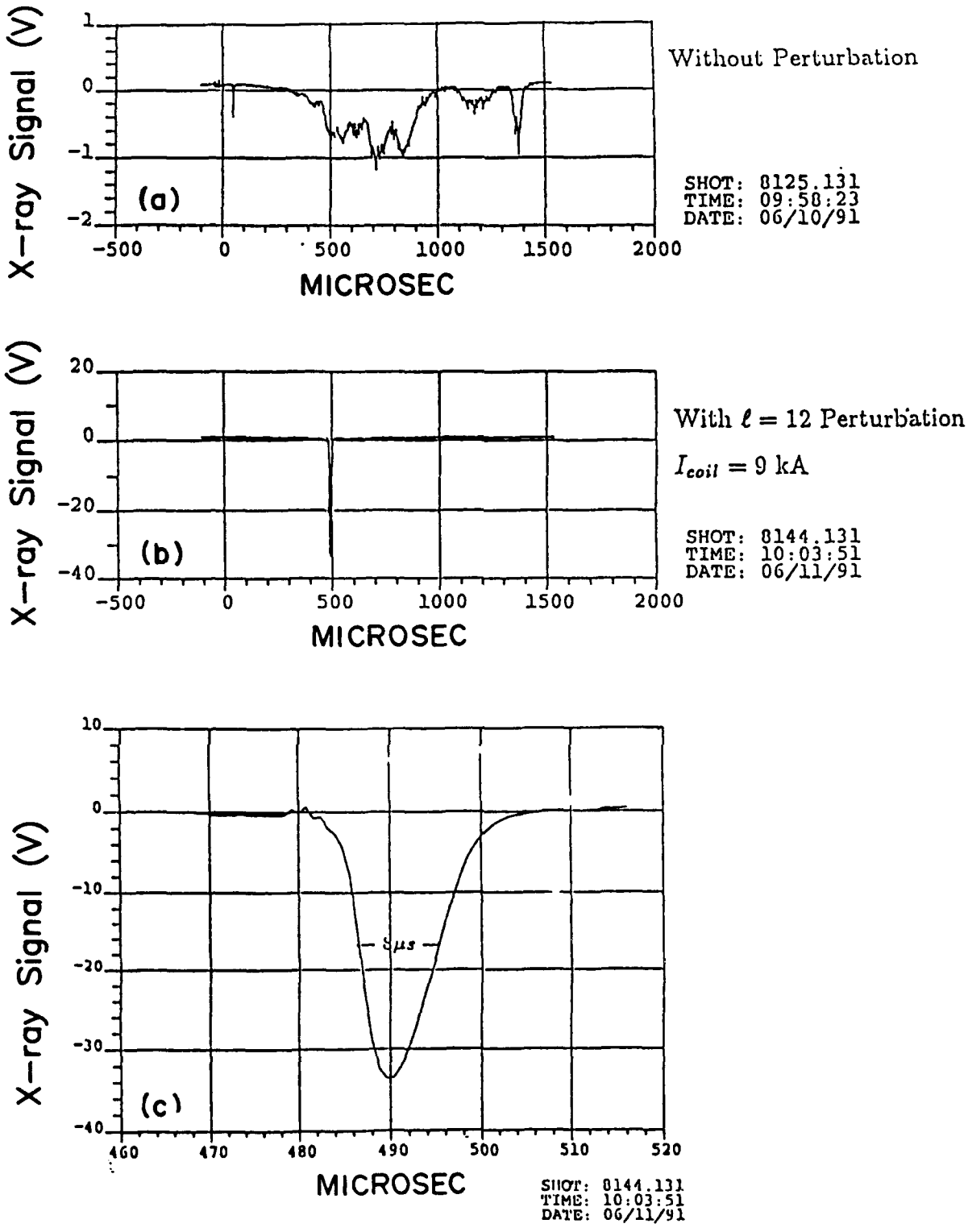

Fig. 33. X-ray signal vs. time: (a) Without the resonant coils, (b) when the resonant coils are activated and (c) the trace shown in (b) in a expanded time scale.

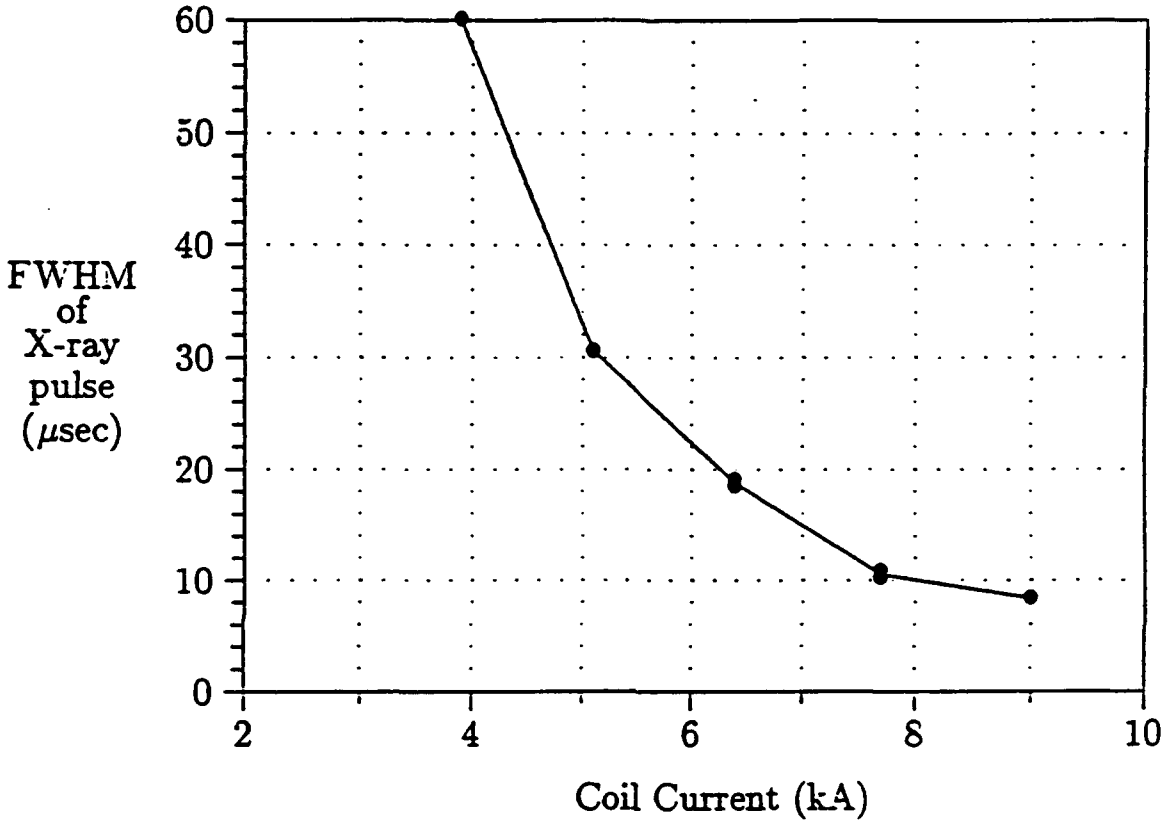

Fig. 34. Full width at half maximum (FWHM) of the x-ray pulse vs. resonant coil current when the coils are activated near the ℓ=12 resonance.

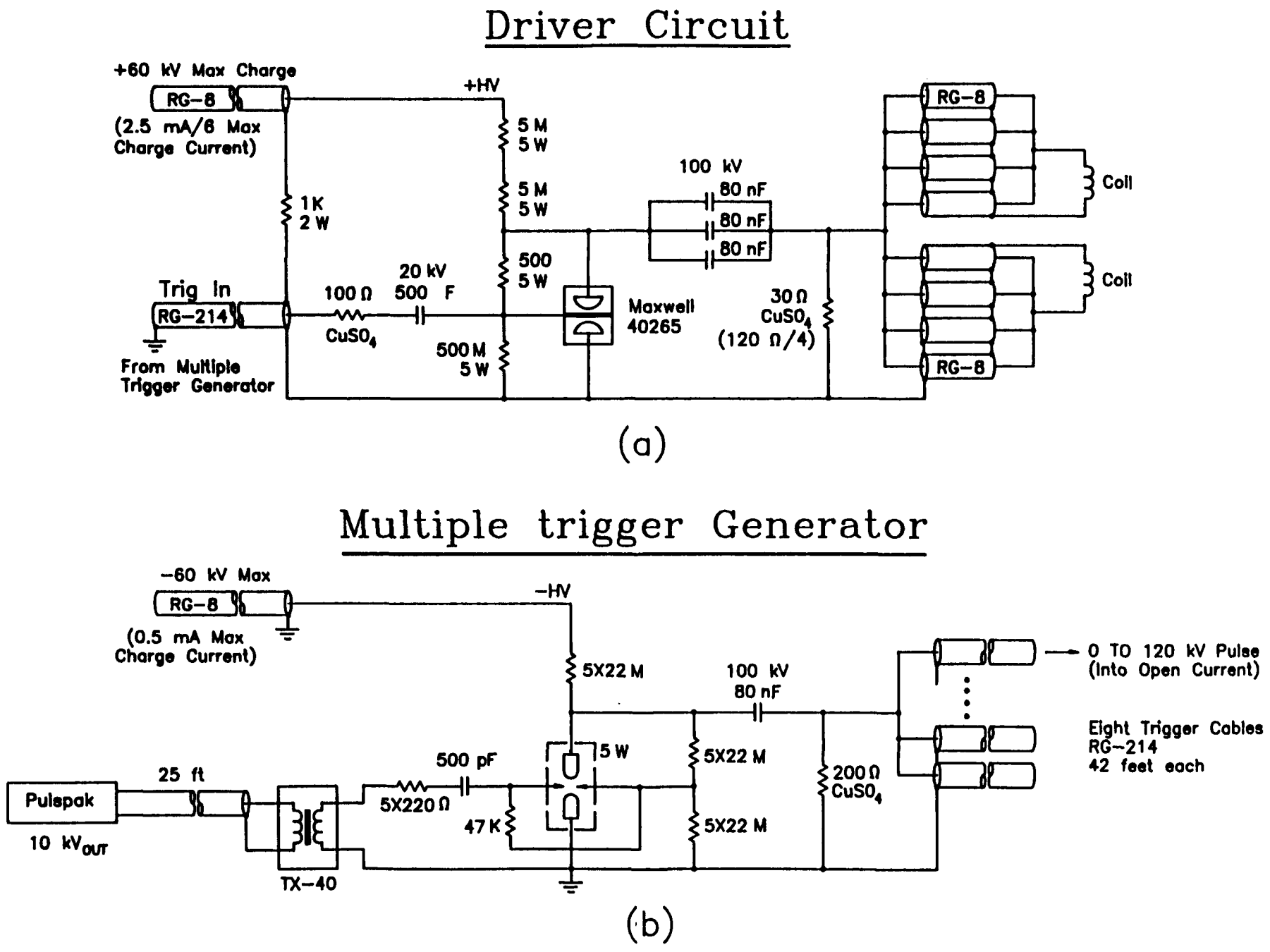

Fig. 35. Driver for the internal coils. (a) Driver circuit, (b) multitrigger generator circuit.

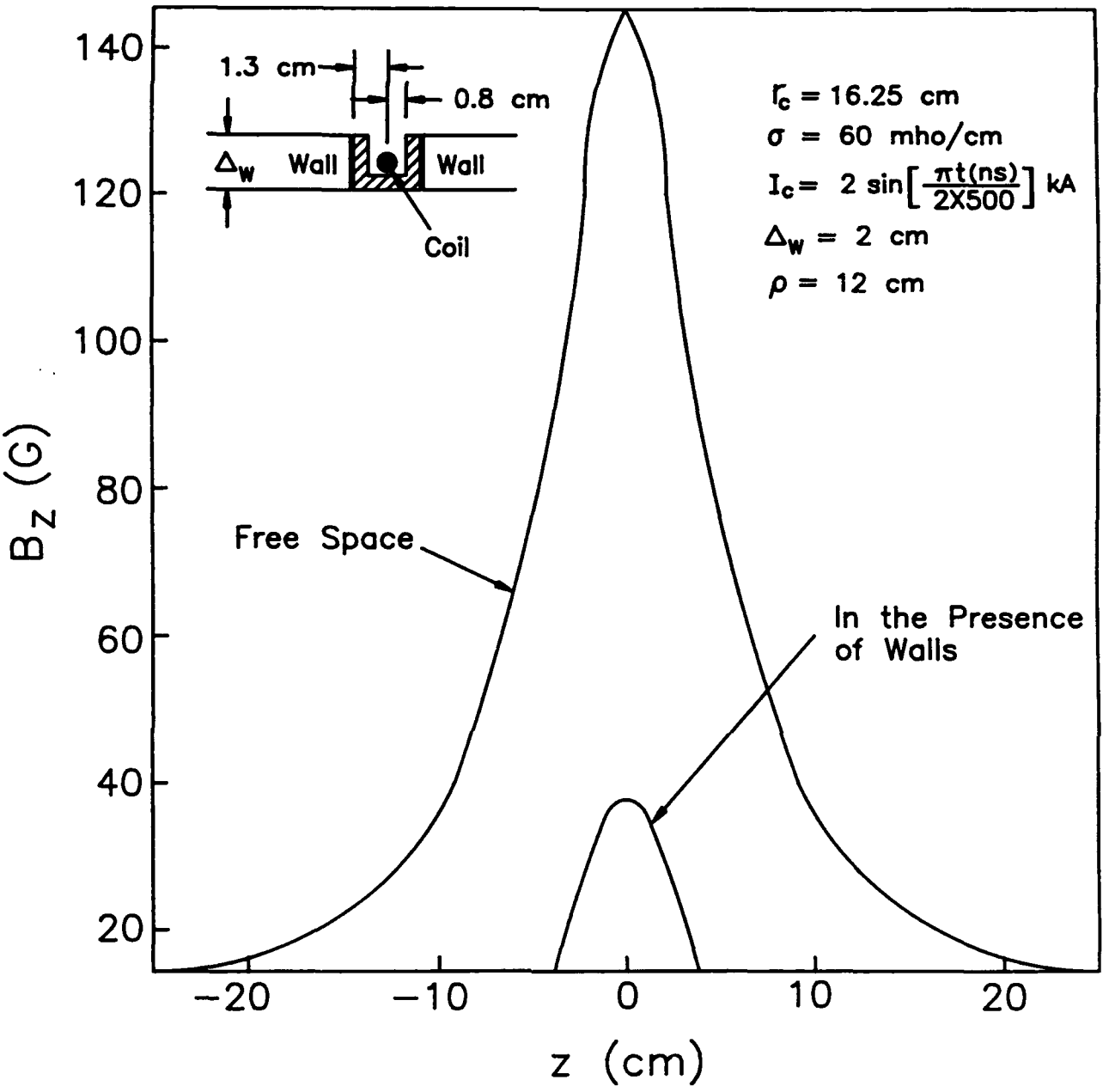

Fig. 36. Axial magnetic field at the radial distance of 12 cm from the minor axis in free space and in the presence of lateral walls.

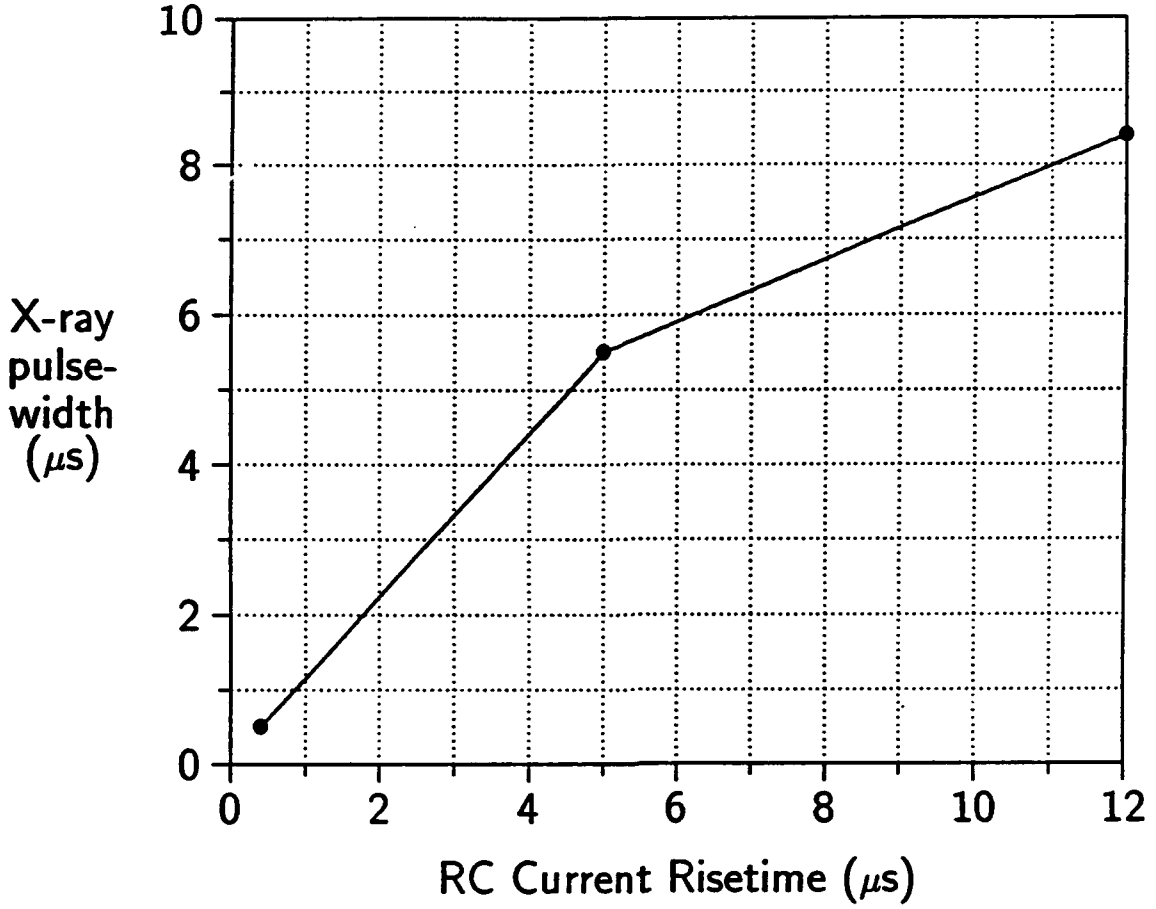

Fig. 37. FWHM of the x-ray signal vs. resonant coil current risetime.

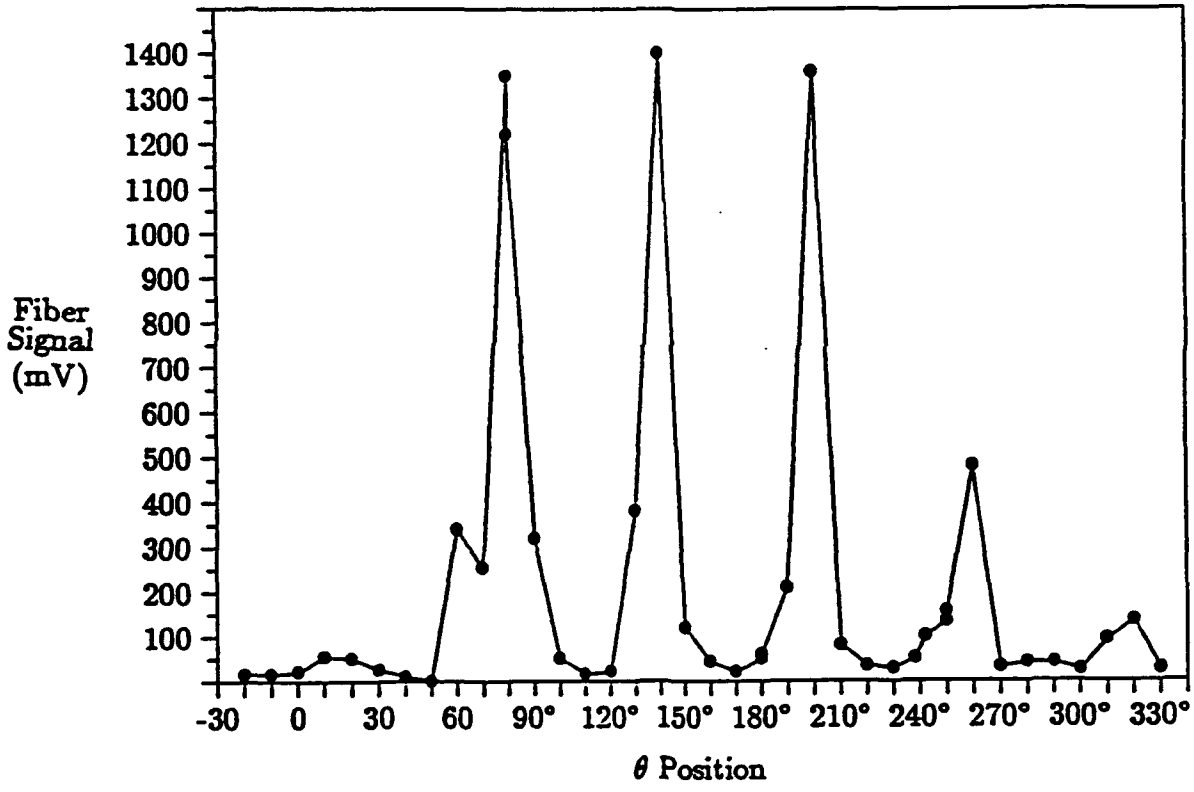

Fig. 38. Toroidal distribution of beam losses following the activation of the internal resonant coils.

From [pmt2.tex]

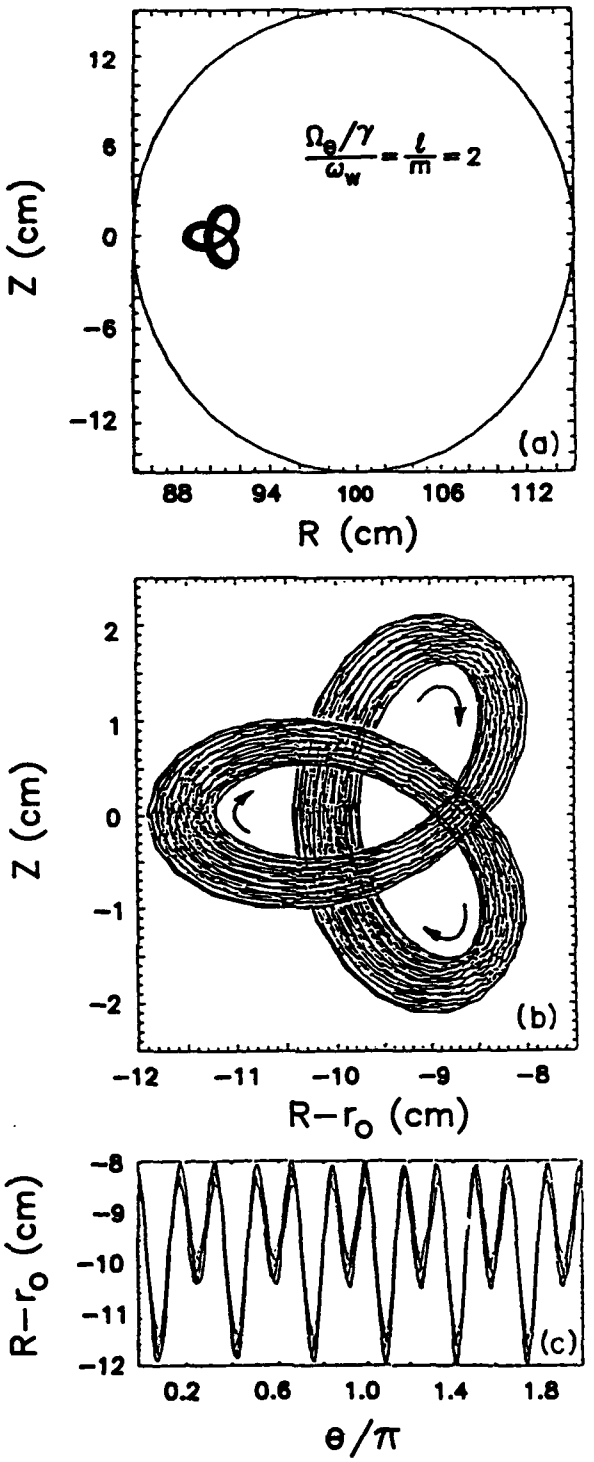

Fig. 39. Results from the numerical integration of orbit equations for the beam centroid near ℓ=12. (a) Projection of the orbit in the (R,Z) plane for 160 nsec, (b) as in (a) but in a expanded scale, (c) projection of the orbit in the $(R - r_o, \theta)$ plane.

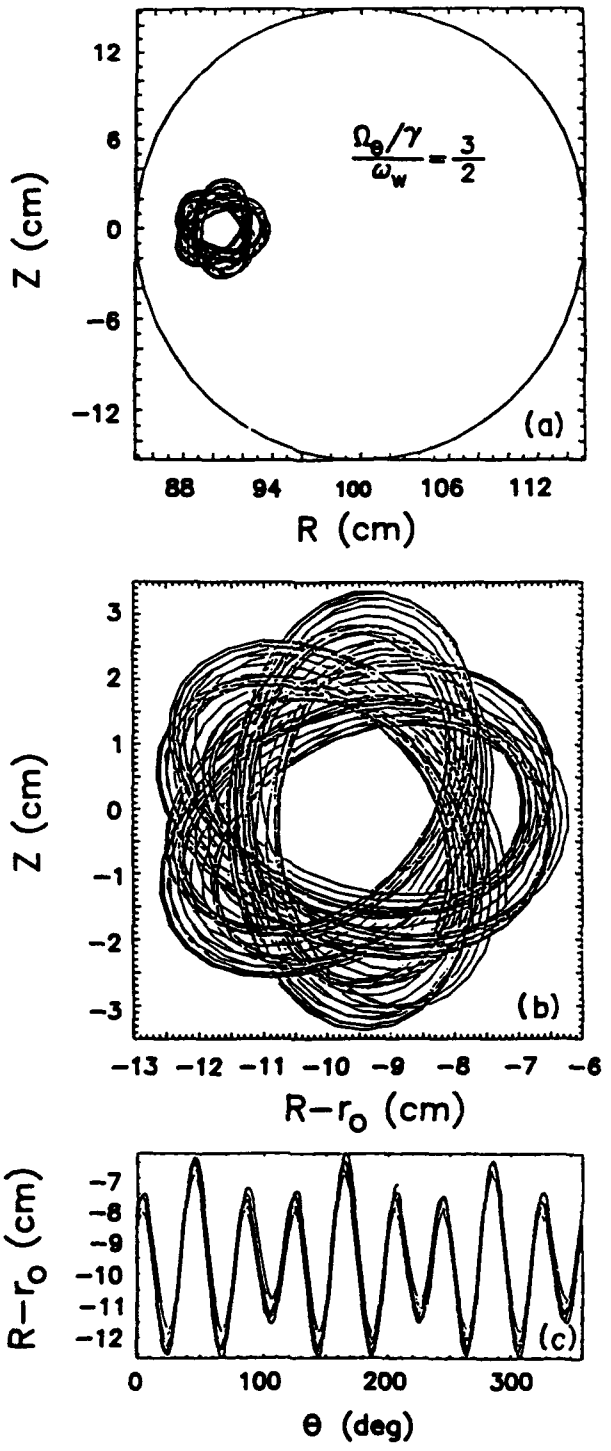

Fig. 40. Results from the numerical integration of orbit equations for the beam centroid near ℓ=9. (a) projection of the orbit in the R,Z plane for 160 nsec, (b) as in (a) but in a expanded scale, (c) projection of the orbit in the $(R - r_o, \theta)$ plane.

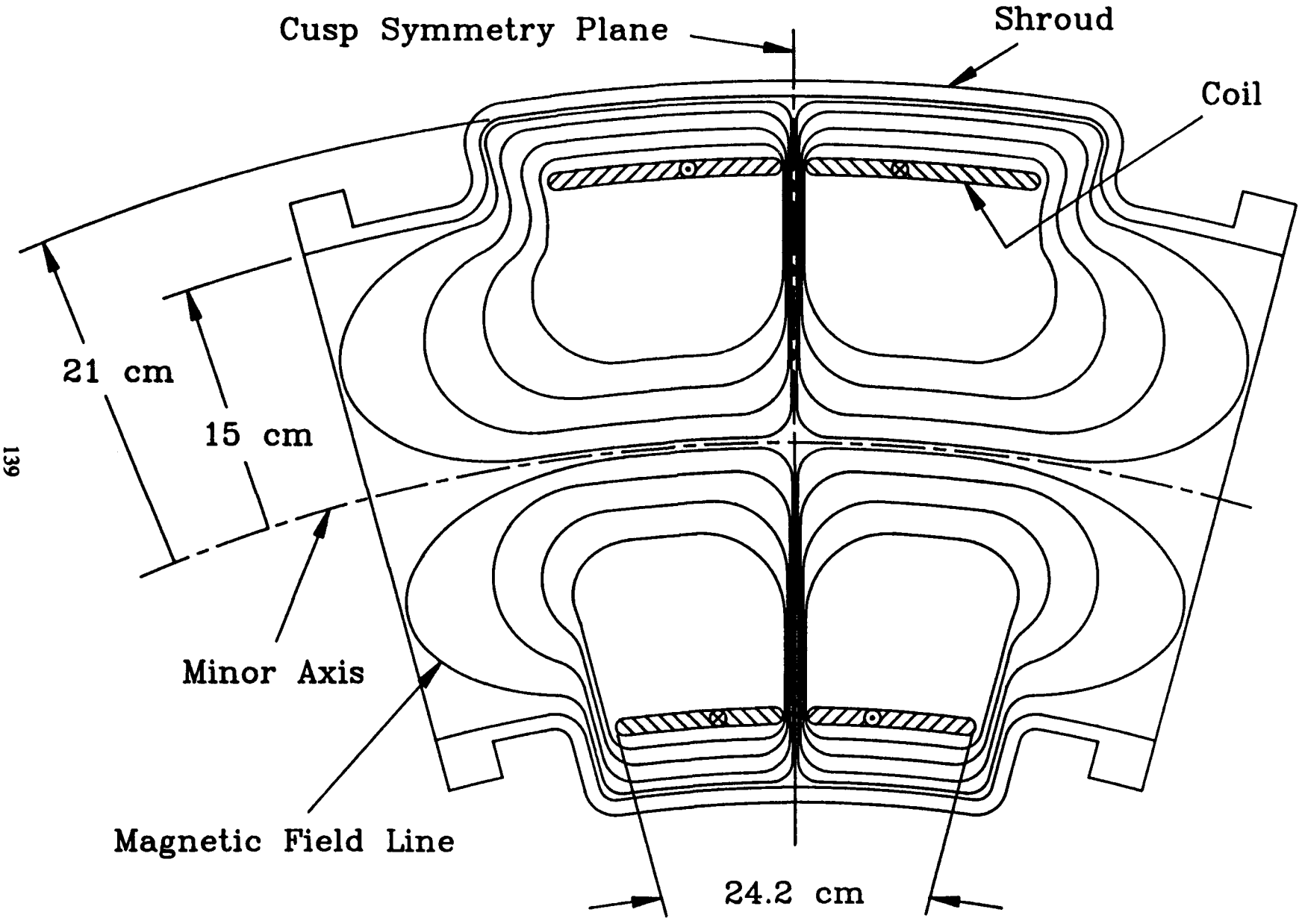

Fig. 41. Wide cusp and magnetic field lines.

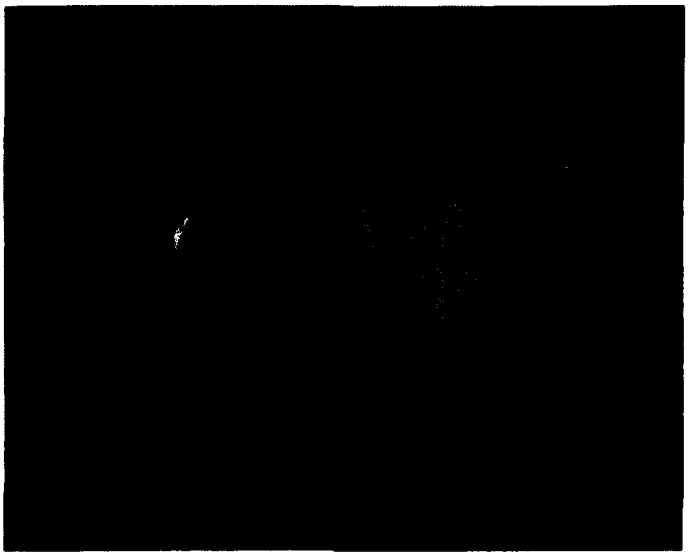

Fig. 42. Photograph of one of the double cusps.

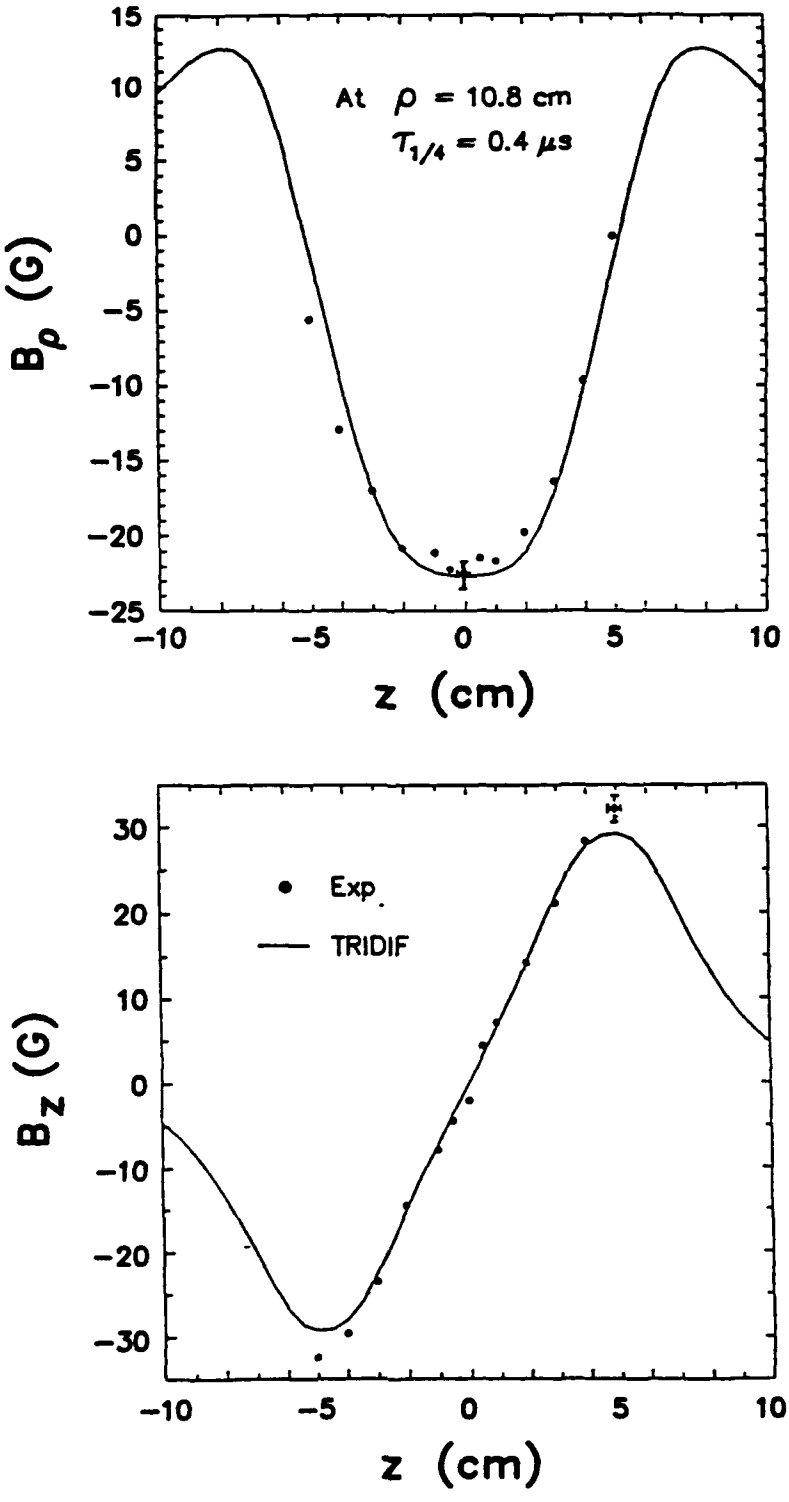

Fig. 43. Axial profile of radial (a) and axial (b) fields at ρ=10.8 cm from the minor axis. Solid lines are from TRIDIF and solid circles from the experiment.

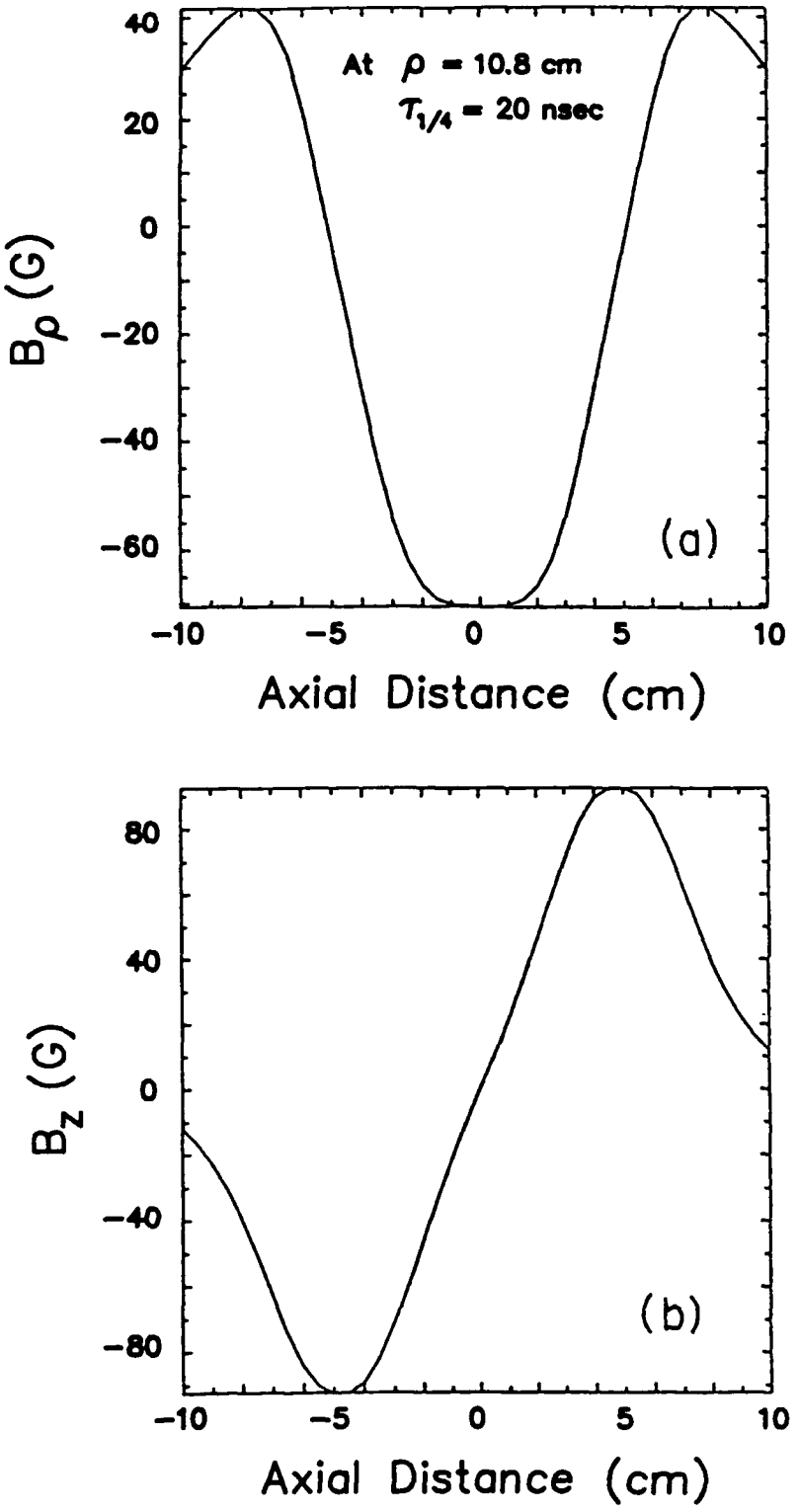

Fig. 44. Axial profile of radial (a) and axial (b) fields at ρ=10.8 cm from the minor axis.

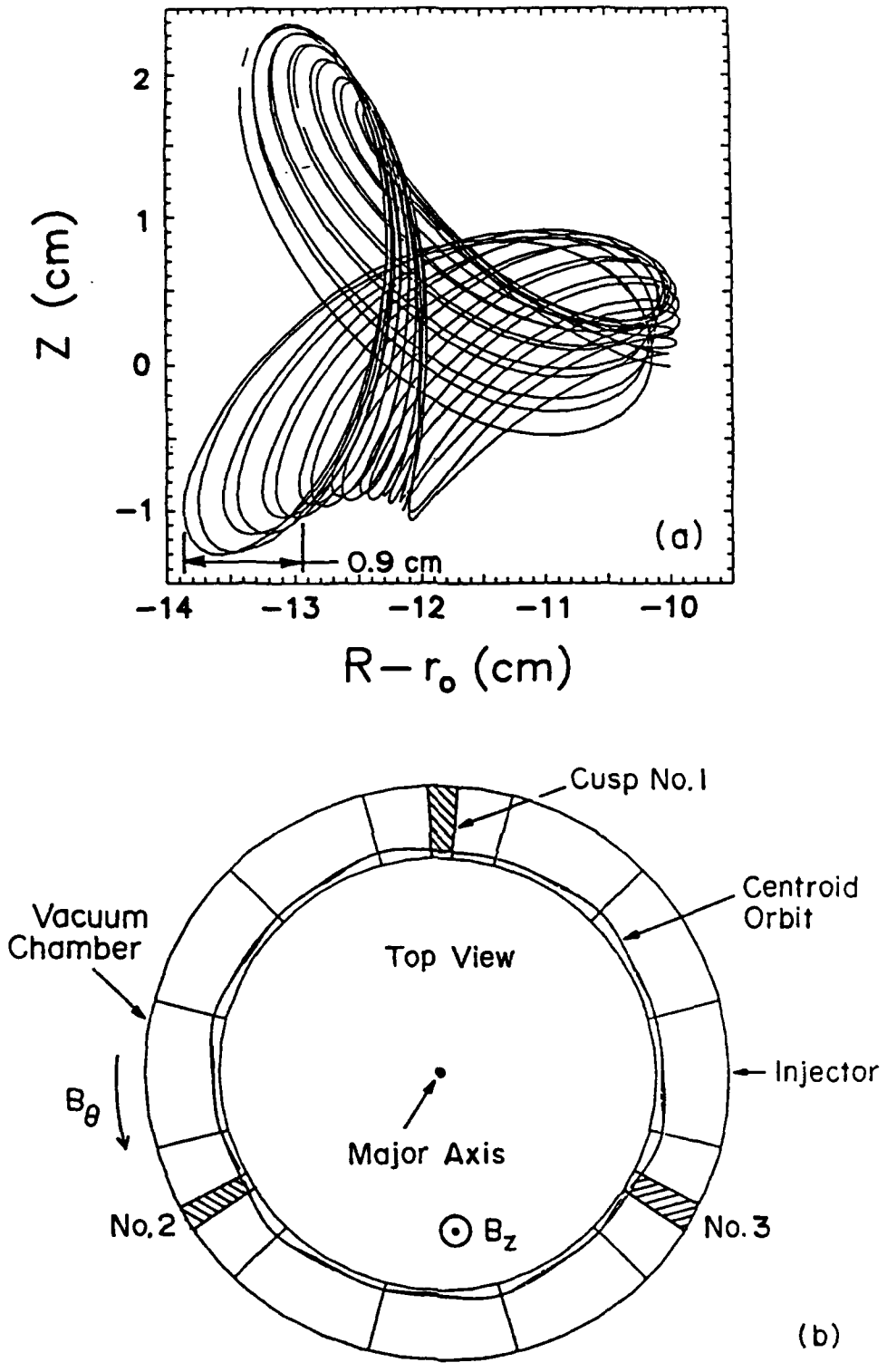

Fig. 45. (a) Projection of the beam centroid orbit in the transverse plane; (b) top view of the orbit.

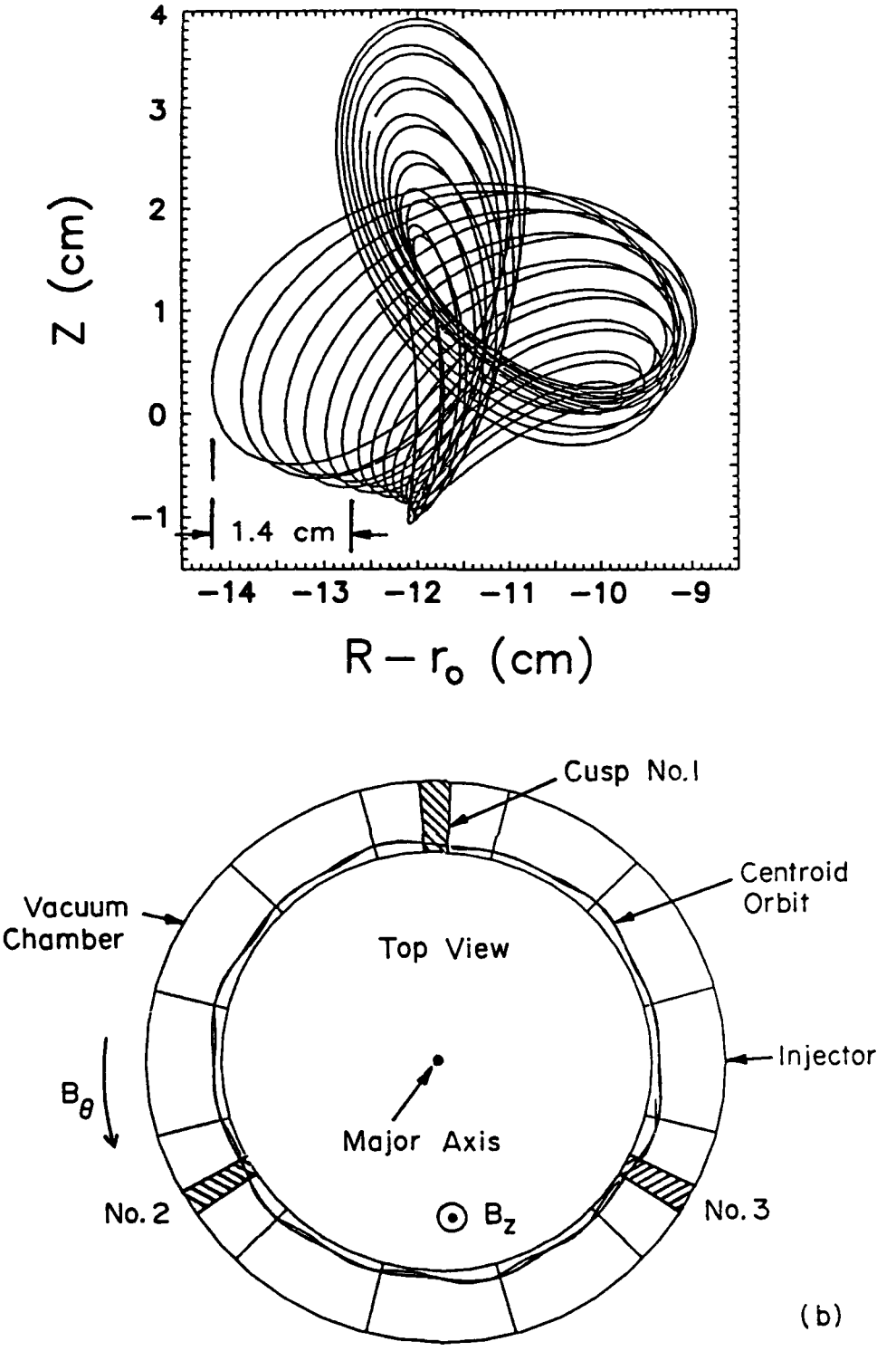

Fig. 46. (a) Projection of the beam centroid orbit in the transverse plane when B_ρ=0; (b) top view of the orbit.

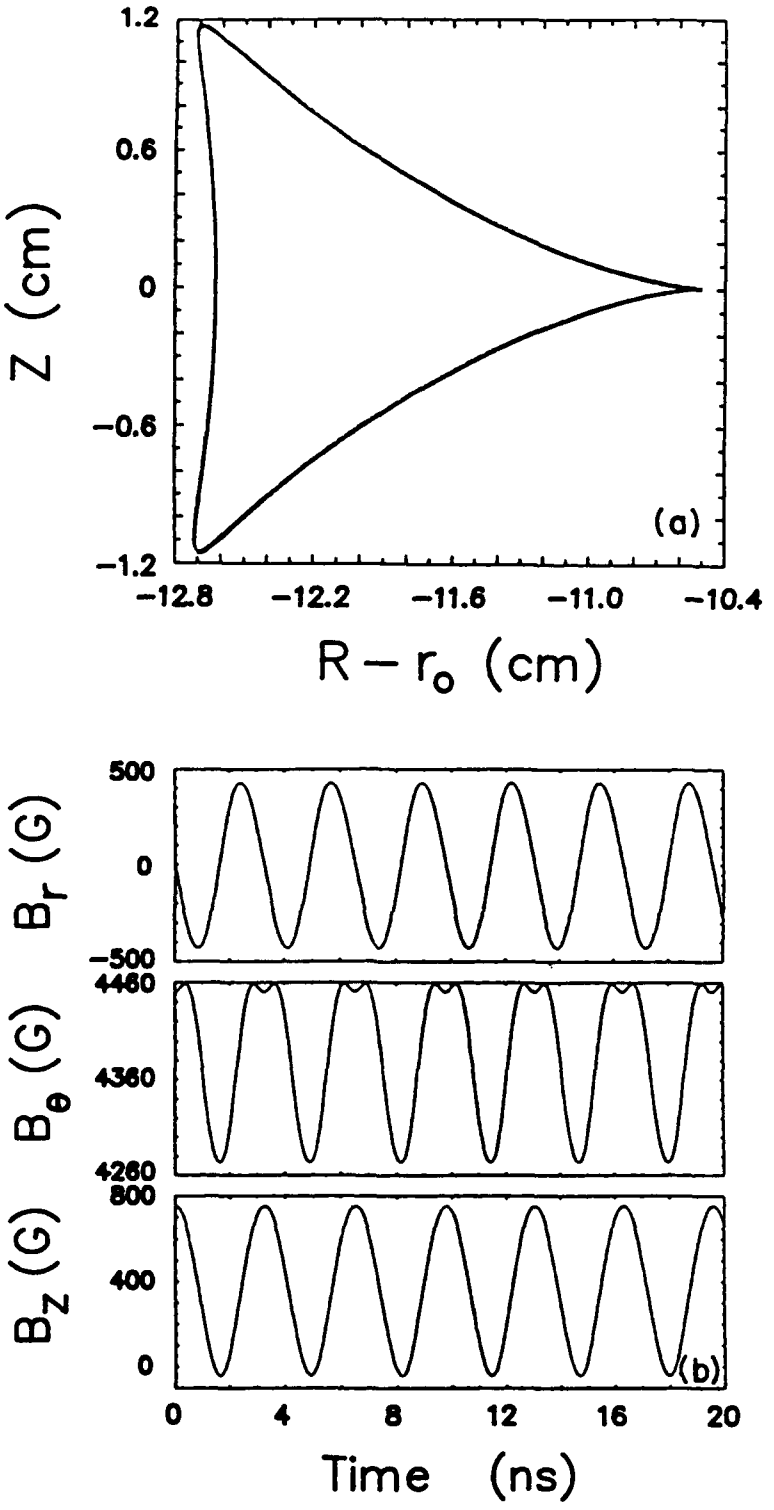

Fig. 47. (a) Projection of the beam centroid orbit in the transverse plane for 20 nsec when the cusps are off; (b) the three components of the magnetic field at the beam centroid.

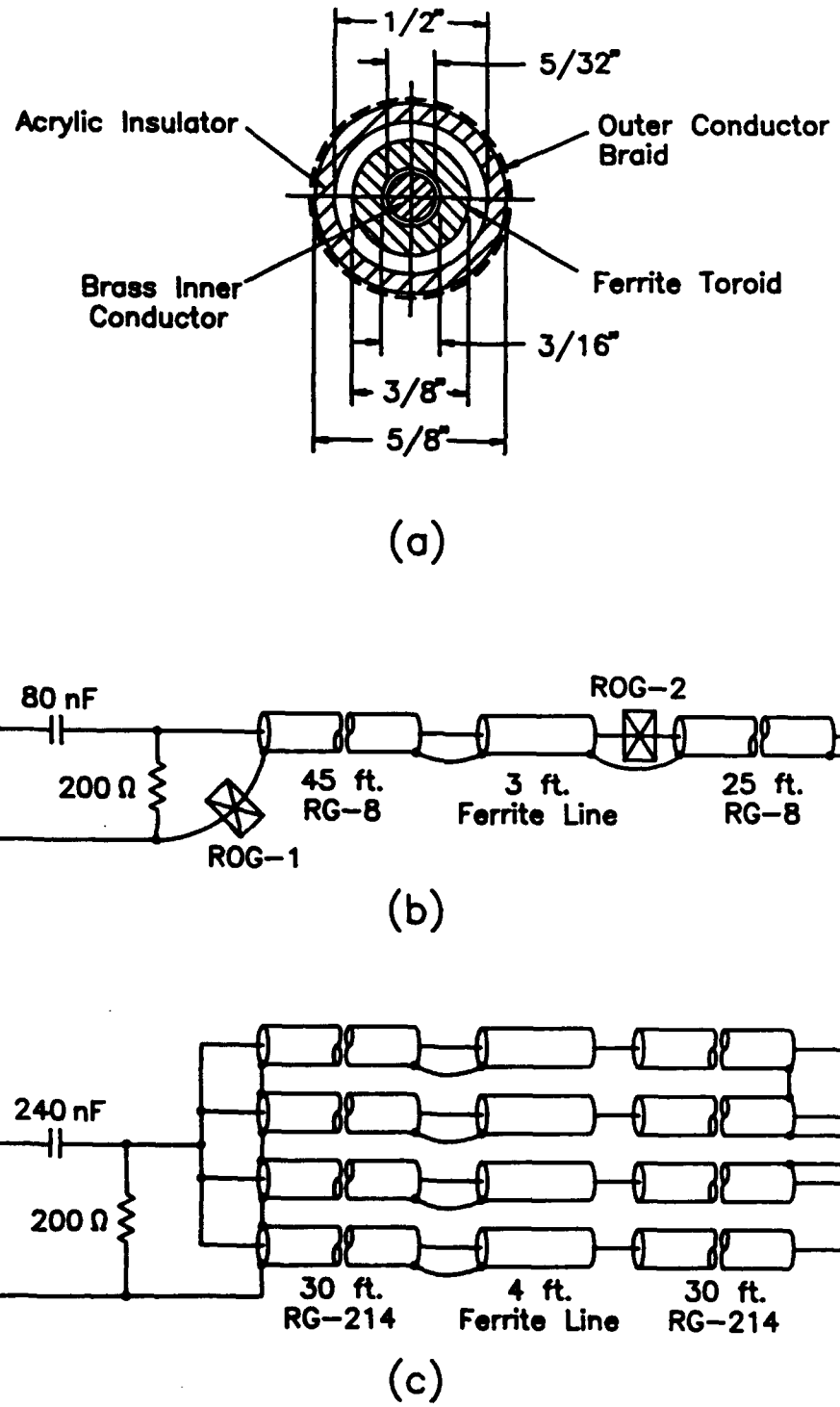

Fig. 48. (a) Cross sectional view of the pulse sharpener, (b) set-up to test the sharpener and (c) layout of the drivers to power the double cusps.

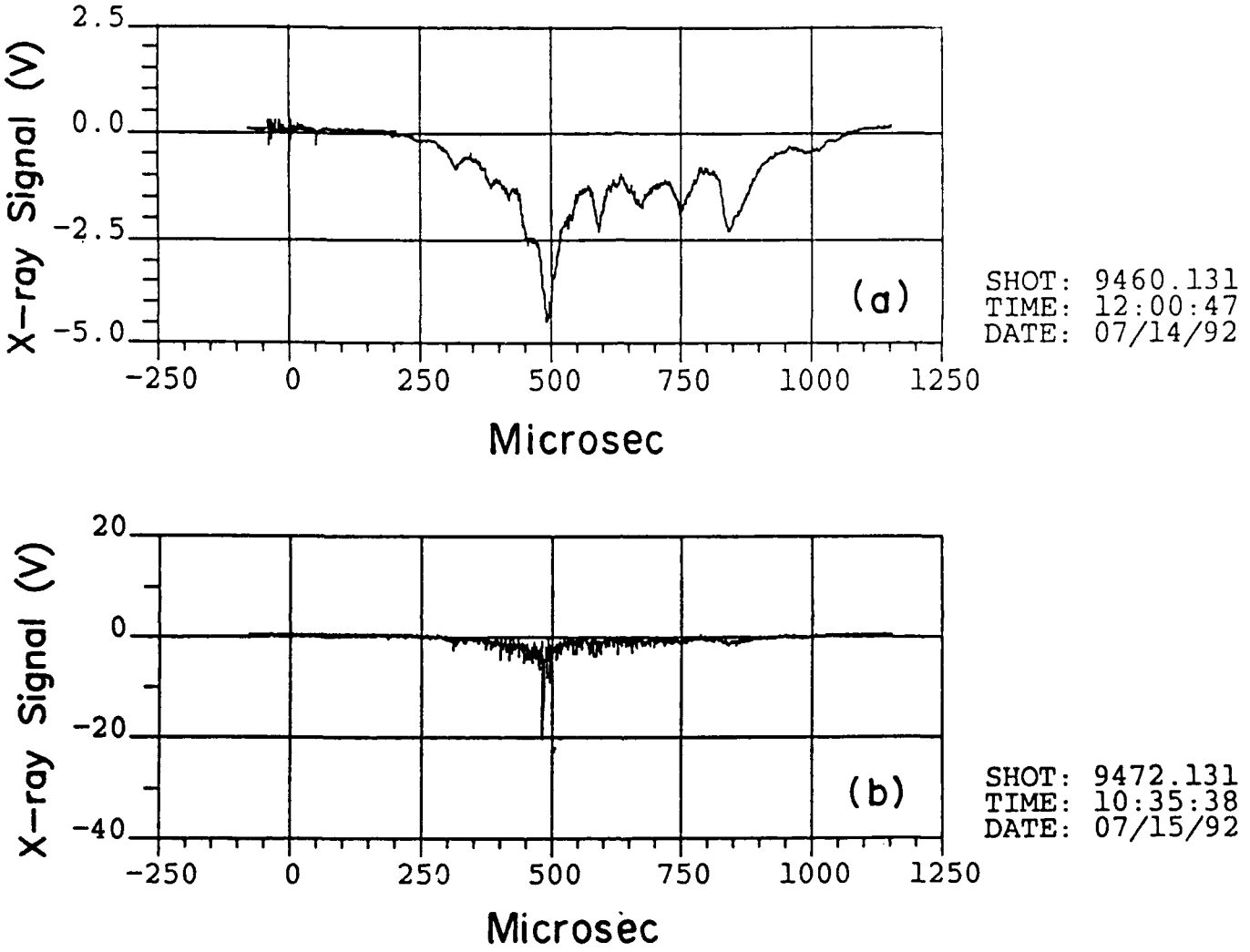

Fig. 49. X-ray signal vs. time: (a) With the double cusps off and (b) with the double cusps on. The amplitude of the signal in 49a is higher than that in Figs. 18 and 27 because of the copper wires in the double cusps.

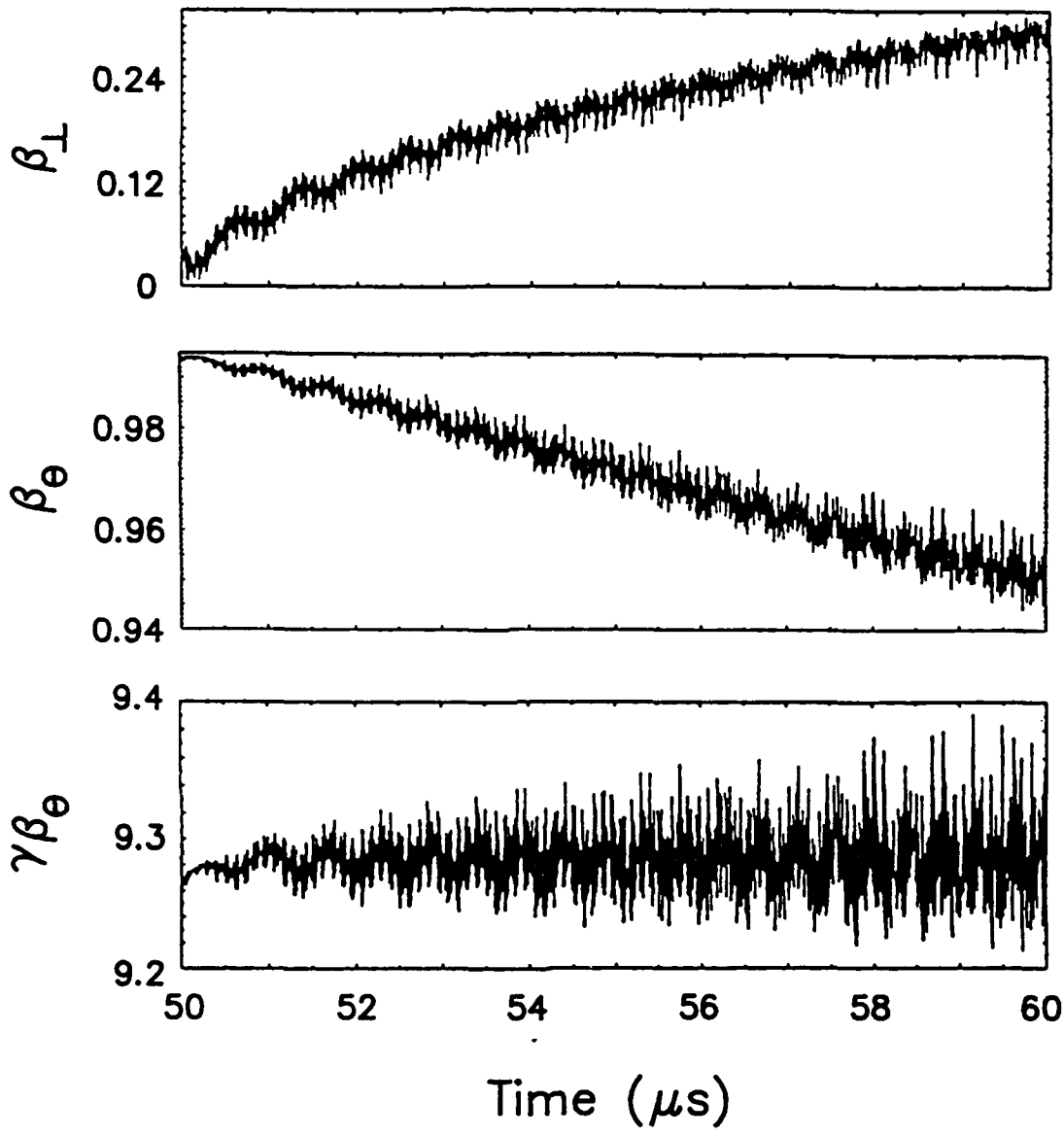

Fig. 50. Beam centroid transverse velocity $\beta_\perp$, axial velocity β_θ and $\gamma\beta_\theta$ between 50 and 60 μsec, immediately after the beam locks in the $\ell = 19$ mode. The assumed $\pm$ 2mm random spatial fluctuations in the stellarator windings are less than those in the experiment.

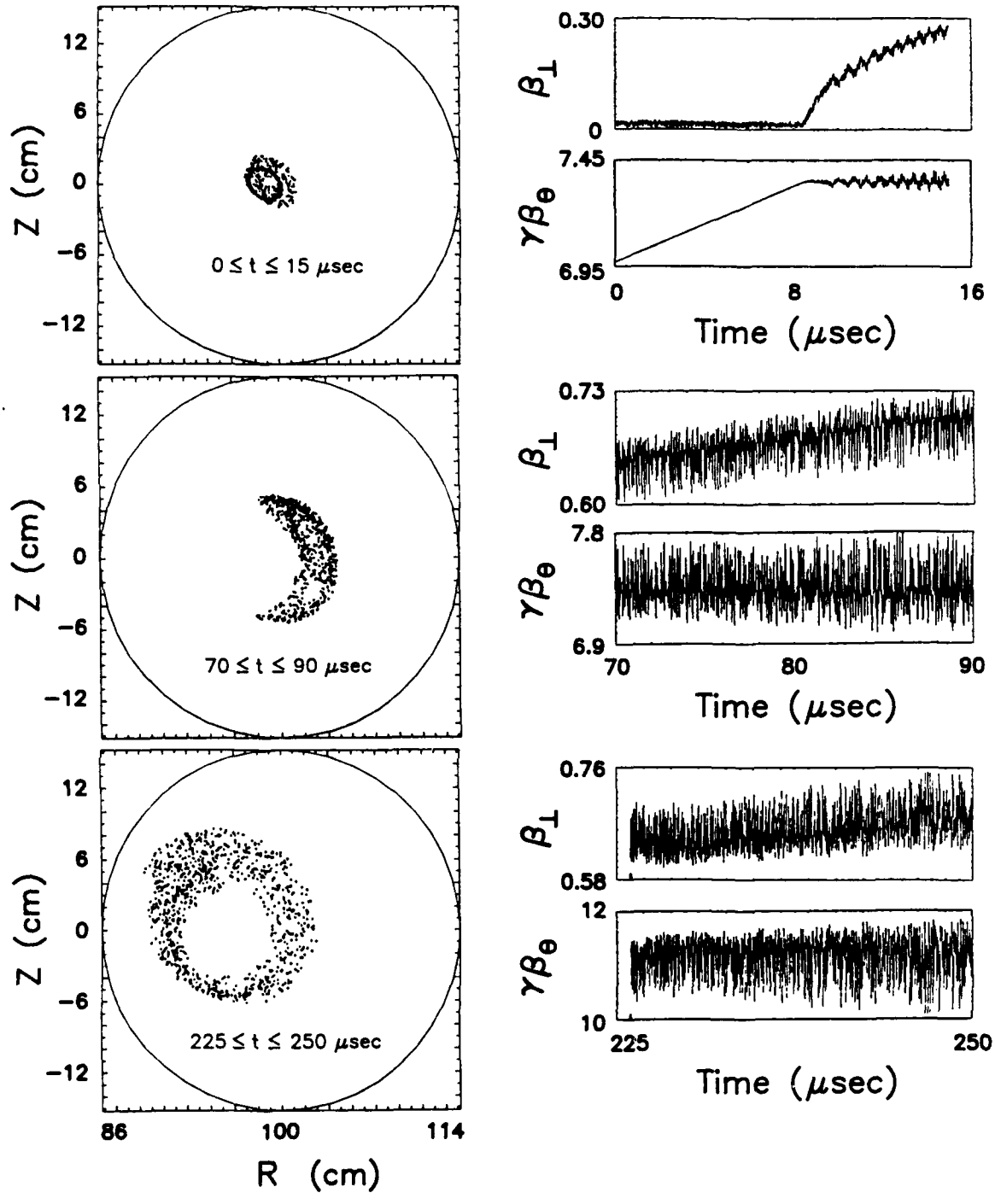

Fig. 51. The left column shows the positions the centroid crosses the $\theta = 0$ plane. The right column shows $\beta_\perp$ and $\gamma\beta_\theta$ in the time intervals of interest. The beam locks in the $\ell = 24$ mode at $\sim$ 8 μsec and unlocks at 150 μsec. During this time the equilibrium position remains still.